The ESCRT machinery at stress-induced ER-Golgi contact sites in *S. cerevisiae*:

A study of recruitment mechanism and function

Dissertation

Lis Albert

Ruprecht-Karls-Universität Heidelberg
2025

Inaugural dissertation

for

obtaining the doctoral degree

of the

Combined Faculty of Mathematics, Engineering and Natural Sciences

of the

Ruprecht - Karls – University

Heidelberg

Presented by

M. Sc. Lis Albert

Born in: Luxembourg, Luxembourg

Oral examination: 26.09.2025

The ESCRT machinery at stress-induced ER-Golgi contact sites in *S. cerevisiae*:

A study of recruitment mechanism and function

Referees: PD Dr. Axel Mogk
Prof. Dr. Sebastian Schuck

I. Summary

The endoplasmic reticulum (ER) forms an intricate network of sheets and tubules in eukaryotic cells. It is a highly dynamic organelle and can be remodeled upon demand. The ER for example undergoes extensive morphological changes upon ER stress, a condition caused by the accumulation of misfolded proteins within the ER lumen. Part of this stress-induced remodeling of the ER is mediated by a major ER stress response pathway, the Unfolded Protein Response (UPR). Apart from the UPR-induced ER expansion, membrane contact sites (MCSs) with other organelles are reorganized to maintain vital cellular functions.

A machinery that is involved in membrane remodeling at various cellular membranes is the endosomal sorting complex required for transport (ESCRT) machinery. This multi-subunit complex mediates membrane budding, repair and stabilization in different biological contexts. In *S. cerevisiae*, the ESCRT-III component Snf7 is recruited to specific regions of the ER, which we termed ER clusters, during ER stress. This recruitment requires the ESCRT-associated protein Bro1p.

In this study, I set out to determine how the ESCRT machinery is recruited to ER clusters and what role it plays at these sites. To identify proteins involved in this process, I used a proximity-dependent biotinylation approach coupled with mass spectrometry (PDB-MS). I showed that proper recruitment of Snf7 to ER clusters requires two Bro1 domain proteins, Bro1p and Rim20p, and that they act partially redundantly in this recruitment. I further found that the second hydrophobic patch and the TPR-like domain within the Bro1 domain of Bro1p are essential for recruitment of Bro1p and Snf7 to the ER, whereas they are dispensable for ESCRT function at multivesicular bodies (MVBs), highlighting a specific role of these features for stress-induced recruitment to the ER.

Furthermore, the hits of the PDB-MS experiment indicated that ER clusters are located at the ER-Golgi interface. I showed that several COPI coat components colocalize with ER clusters and established Cop1p as a suitable Golgi marker at these sites. I discovered that the ER-tether Nvj2p colocalized with Snf7 and Cop1p at ER clusters during stress and contributed to the finding that ESCRT recruitment to ER clusters was essential for the proper localization of another ER-tether, Tcb3p, to these sites. Nvj2p and Tcb3p were shown to play a role in non-vesicular ceramide transfer at stress-induced ER-Golgi contact sites, suggesting that ER clusters represent ER-Golgi contacts. As my findings showed that Nvj2p and Tcb3p were not essential for the establishment of these contacts, they possibly play a downstream role in ceramide transfer. The ESCRT machinery might further be involved in stabilization of these putative stress-induced ER-Golgi contact sites.

Taken together, I identified several determinants for ESCRT recruitment to ER clusters during ER stress and defined a novel site of action of the ESCRT machinery at stress-induced ER-Golgi contact sites. My study advances our understanding of the versatile ESCRT machinery, as well as the stress-induced remodeling of the ER in yeast.

II. Zusammenfassung

Das endoplasmatische Retikulum (ER) bildet ein komplexes Netzwerk aus tubulärem ER und flachen ER-Zisternen in eukaryotischen Zellen. Es ist ein äußerst dynamisches Organell und kann bei Bedarf umgestaltet werden. Das ER weist beispielsweise umfangreiche morphologische Veränderungen bei ER-Stress auf, einem Zustand der durch die Ansammlung fehlgefalteter Proteine im ER-Lumen verursacht wird. Diese stress-induzierte Umgestaltung des ER wird zum Teil durch einen wichtigen Stress-Signalweg, die ungefaltete Protein-Antwort (UPR), vermittelt. Neben der UPR-induzierten Erweiterung des ER, werden auch beispielsweise Membrankontaktstellen (MCS) mit anderen Organellen reorganisiert, um lebenswichtige Funktionen der Zelle aufrechtzuerhalten.

Eine Maschinerie, die an der Umgestaltung verschiedener Membranen in der Zelle beteiligt ist, ist die ESCRT-Maschinerie (Endosomal Sorting Complex Required for Transport). Dieser aus mehreren Untereinheiten bestehende Komplex vermittelt das Knospen, die Reparatur und die Stabilisierung von Membranen in verschiedenen biologischen Kontexten. In *S. cerevisiae* wird die ESCRT-III-Komponente Snf7 bei ER-Stress an bestimmte Regionen des ER, die wir als ER-Cluster bezeichnet haben, rekrutiert. Diese Rekrutierung erfordert das ESCRT-assoziierte Protein Bro1p.

In dieser Arbeit wollte ich herausfinden, wie die ESCRT-Maschinerie an ER-Cluster rekrutiert wird und welche Rolle sie an diesen Domänen spielt. Um Proteine zu identifizieren, die an diesem Prozess beteiligt sind, habe ich die Methode der Proximitäts-Biotinylierung gekoppelt mit Massenspektrometrie verwendet (PDB-MS). Ich konnte zeigen, dass zur effizienten Rekrutierung von Snf7 an ER-Cluster zwei Bro1-Domänenproteine, Bro1p und Rim20p, gebraucht werden und dass diese zum Teil redundant agieren. Ich habe außerdem herausgefunden, dass der zweite hydrophobe Bereich und die TPR-ähnliche Domäne innerhalb der Bro1-Domäne von Bro1 essenziell für die Rekrutierung von Bro1p und Snf7 ans ER sind, wobei sie für die ESCRT-Funktion an multi-vesikulären Körpern (MVBs) nicht benötigt werden, was auf eine spezifische Rolle dieser Merkmale für die stress-induzierte Rekrutierung ans ER hindeutet.

Darüber hinaus wiesen die Treffer des PDB-MS-Experiments darauf hin, dass sich ER-Cluster zwischen ER und Golgi befinden. Ich habe gezeigt, dass mehrere COPI-Mantel-Komponenten mit ER-Clustern kolokalisieren und habe Cop1p als geeigneten Golgi-Marker an dieser Domäne etabliert. Ich habe entdeckt, dass das ER-Tethering-Protein Nvj2p bei Stress mit Snf7 und Cop1p an ER-Clustern kolokalisiert und habe zu der Erkenntnis beigetragen, dass die Rekrutierung von ESCRT an ER-Cluster essenziell für die korrekte Lokalisierung eines anderen ER-Tethering-Proteins, Tcb3p, an diesen Domänen ist. Es wurde gezeigt, dass Nvj2p und Tcb3p eine Rolle bei nicht-vesikulärem Ceramid-Transfer an stress-induzierten ER-Golgi-Kontaktstellen spielen, was darauf hindeutet, dass ER Cluster ER-Golgi-Kontakte darstellen. Da meine Ergebnisse zeigten, dass Nvj2p und Tcb3p für die Bildung dieser Kontakte nicht essenziell waren, spielen sie möglicherweise eine Rolle beim Ceramid-Transfer. Die ESCRT-

Maschinerie könnte darüber hinaus an der Stabilisierung dieser mutmaßlichen stress-bedingten ER-Golgi-Kontaktstellen beteiligt sein.

Alles in allem habe ich mehrere Determinanten für die ESCRT-Rekrutierung an ER-Cluster während ER-Stress identifiziert und eine neue Zuständigkeit der ESCRT-Maschinerie an stress-induzierten ER-Golgi-Kontaktstellen definiert. Meine Studie verbessert somit unser Verständnis der vielseitigen ESCRT-Maschinerie sowie der stress-induzierten Umgestaltung des ER in Hefe.

Table of Contents

III. Contributions by co-workers

This study was part of a shared project with Oliver Pajonk, a fellow PhD student from the lab of Sebastian Schuck. We used complementary approaches to identify the recruitment mechanism of the ESCRT machinery to ER clusters upon stress, as well as their role. Oliver Pajonk, together with Carlos Martin de Hijas, Dimitris Papagiannidis, Peter Bircham, Jasmin Schäfer and Sebastian Schuck performed microscopy-based genetic screens to identify genes involved in this process.

Overall conceptualization of this project involved Sebastian Schuck and Oliver Pajonk. Unless otherwise stated, the experiments presented within this study were conceptualized, designed, performed and analyzed by me. Contributions by other people are stated here, as well as in the Results section, the Materials and Methods section, and in the figure legends. Strains generated by other people are marked in the strain list.

This project is based on the initial observation made by Jasmin Schäfer in the lab of Sebastian Schuck, showing the phenotype of Snf7 recruitment to the ER upon ER stress. The images of the phenotype in Figure 3 were acquired by Oliver Pajonk. Jasmin Schäfer determined that Bro1p is essential for Snf7 recruitment, whereas ESCRT-0, -I and -II were not required. She also gained first structural insight into ER clusters with correlative light and electron microscopy (CLEM), which inspired the schematic representation of ER clusters in Figure 14B.

Oliver Pajonk showed that Bro1p colocalized with Snf7 at ER clusters and that in a strain without tagged Snf7, Bro1p puncta at ER clusters were rare, which was used as a basis for the quantification performed by me in Figure 4E.

The GFP-binder beads for the co-IP in Figure 4D were generated by Natalie Friemel and me.

Carlos Martin de Hijas analyzed the Bro1 mutants expressed ectopically from the *LYP1* locus in a *BRO1* deletion background and found that the Bro1 domain is sufficient for Snf7 recruitment in this context, whereas the K246A and Y320D mutations disrupt recruitment. I used the plasmids he created with mutant Bro1 to introduce point mutants into endogenous Bro1.

The strain background and the protocol of the streptavidin pull-down for the PDB-MS experiment were established by myself during my Master thesis. For the PDB-MS in triplicates shown in Figure 8, sample preparation starting with the SDS-PAGE of eluate samples from the pull-down, as well as the mass spectrometry runs were performed by Sabine Merker, Thomas Ruppert and Marcin Luzarowski from the ZMBH Mass Spectrometry Facility. Initial data analysis with MaxQuant was done by Georg Borner.

Oliver Pajonk found that Rim20p-mNeonGreen colocalized with Snf7 at ER clusters during ER stress and showed that deletion of *RIM20* reduced recruitment of Snf7, as reproduced by me in Figure 9A and B. Carlos Martin de Hijas showed by RNA sequencing that there is no Bro1-dependent Rim101p signaling during ER stress.

Oliver Pajonk determined that Cop1p-mNeonGreen frequently colocalized with Snf7 at ER clusters

during ER stress. The spatial arrangement of Cop1p-mNeonGreen and Sec24p-Halo with Snf7 at ER clusters during ER stress was discovered by Oliver Pajonk and Chrysafenia Papavissarion and reproduced by me in Figure 13B.

Oliver Pajonk found that Nvj2p and Tcb3p colocalized with Snf7 at ER clusters during ER stress. He also showed that Tcb3p, Snf7 and Cop1p often coincided at ER clusters. The imaging experiment with Tcb3p-mNeonGreen and Snf7 in wildtype cells vs *bro1*^{Y320D} cells in Figure 14A and B was conceptualized and performed by Oliver Pajonk and me. I acquired images for one replicate, whereas he acquired the images for two replicates and quantified all three replicates.

IV. List of Abbreviations

BFP	Blue fluorescent protein
CLEM	Correlative light and electron microscopy
COPI	Coat protein complex I
COPII	Coat protein complex II
CPS	Carboxypeptidase S
CPY	Carboxypeptidase Y
DTT	Dithiothreitol
EM	Electron Microscopy
ER	Endoplasmic reticulum
ERAD	Endoplasmic reticulum-associated degradation
ERAS	Endoplasmic reticulum arrival sites
ERES	Endoplasmic reticulum exit sites
ERMES	ER-mitochondria encounter structure
ESCRT	Endosomal sorting complex required for transport
FDR	False discovery rate
GFP	Green fluorescent protein
GPI	Glycosylphosphatidylinositol
GPI-AP	Glycosylphosphatidylinositol-anchored protein
HTL	HaloTag ligand
ILV	Intralumenal vesicles
IPC	Inositol phosphoryl ceramide
LD	Lipid droplet
MCS	Membrane contact site
mNeon	mNeonGreen
mScarlet	mScarlet-i
MVB	Multivesicular bodies
NVJ	Nuclear-vacuolar junction
PDB	Proximity-dependent biotinylation
PDB-MS	Proximity-dependent biotinylation coupled to mass spectrometry
RESET	Rapid ER stress-induced export
SMP	Synaptotagmin-like mitochondrial lipid-binding protein
SPT	Serine palmitoyl transferase
Tm	Tunicamycin
TMD	Transmembrane domain
TPR	Tetratricopeptide repeat
UPR	Unfolded protein response
WT	Wildtype

V. List of Figures

VI. List of Tables

1. INTRODUCTION

Each eukaryotic cell contains a variety of different organelles: small, membrane-bound compartments that have developed over time and specialized to fulfil a certain task within the cell. They are tailored to the specific cell type; some are always present, others form when needed. Molecules, proteins and complexes work together within each organelle to perform their specialized job. Within the cell, each organelle plays their part while also coordinating with the other organelles via elegant communication strategies. Thus, they create a fine-tuned machinery that ensures the survival of the cell.

However, cells do not exist in isolation but are constantly in touch with their ever-changing environment. Proteins and organelles must adapt to changes in nutrient availability, temperature and pH by adjusting their jobs and redistributing resources. When faced with adverse conditions, cells employ stress response pathways to survive. These emergency strategies heavily rely on collaboration and communication between organelles.

1.1. The Endoplasmic Reticulum

The endoplasmic reticulum (ER) is the largest membrane-bound organelle within the cell and has essential functions in the synthesis, folding and secretion of soluble and membrane-associated proteins, calcium storage, as well as in lipid metabolism. The perinuclear ER forms the nuclear envelope, safeguarding the genetic material of the cell and providing an enclosed space for replication and transcription of DNA. The peripheral ER further constitutes the entry point to the secretory pathway and communicates with other organelles via membrane contact sites (MCSs).

1.1.1. ER morphology

The architecture of the ER is complex and dynamic. It makes up the nuclear envelope interspersed with nuclear pore complexes and extends into the periphery as an interconnected network of sheets and tubules. ER sheets play a role in protein production, whereas ER tubules are involved for example in lipid metabolism or contact site formation. Different ER shaping proteins are involved in the formation or stabilization of sheets and tubules. Curvature-stabilizing proteins of the reticulon family for example localize to ER tubules or sheet edges, whereas sheets are stabilized by proteins like Climp63 and SigmaR1 (Voeltz et al., 2006; Shibata et al., 2010; Sawyer et al., 2024).

ER morphology can vary largely between different cell types, depending on their specific needs (G. E. Palade & Porter, 1954; Porter & Palade, 1957). Whereas Leydig cells in testes, responsible for testosterone production, show a huge amount of smooth, tubular ER, acinar cells in the pancreas contain many ER stacks for digestive enzyme production (Fawcett, 1981). Furthermore, the ER can be remodeled upon internal cues or changes in the environment, for example for antibody production during the differentiation of plasma cells or upon accumulation of misfolded proteins during ER stress (Fawcett, 1981; Federovitch et al., 2005; Schuck et al., 2009).

Apart from tubules and sheets, the peripheral ER can adopt various other morphologies, such as tubular matrices, fenestrated sheets and nanoholes (Nixon-Abell et al., 2016; G. E. Palade, 1956; Schroeder et al., 2019). Within these morphological features of the ER, distinct ER subdomains related to specific functions can be defined, such as ER-exit sites (ERES), membrane contact sites (MCS) with other organelles and de-novo organelle biogenesis domains, e.g. for lipid droplets or autophagosomes (Jang & Haucke, 2024).

1.1.2. ER exit sites

Proteins which are destined for residence in the endomembrane system or at the plasma membrane, as well as for secretion, are synthesized at the ER and transported to their destination via the secretory pathway. Translation of these proteins takes place at the ER by ER-bound ribosomes. The polypeptide chain is translocated into the ER lumen via the translocon, its signal sequence for ER targeting is cleaved and initial modifications, like N-glycosylation, take place for some proteins (Rapoport et al., 2017; Milstein et al., 1972; Yan & Lennarz, 1999; Chen et al., 2001). Once the proteins have adopted their correct fold with the help of chaperones within the ER, they can be exported from the ER via ERES (C. Barlowe & Helenius, 2016).

At these sites, COPII vesicles form by sequential binding of COPII components. In *S. cerevisiae*, the process is initiated by activation and membrane binding of the small GTPase Sar1p (Nakano & Muramatsu, 1989). Sar1p recruits the heterodimeric complex of the inner coat proteins Sec23p and Sec24p and in turn, they recruit the heterotetrameric complex of outer coat proteins Sec13p and Sec31p (Matsuoka et al., 1998). Eventually, COPII-coated vesicles bud off the ER and deliver their cargo to the Golgi by fusion with the Golgi membrane.

To sustain continuous ER to Golgi export, cargo receptors and membrane are returned to the ER via retrograde COPI-mediated Golgi to ER transport. COPI-coated vesicles travel to the ER, are tethered by the ER-localized Dsl1 complex and fuse with the ER membrane (C. K. Barlowe & Miller, 2013).

ER export can be adapted for different kinds of cargoes. While proteins can leave the ER to some extent in a non-specific manner via bulk flow, they can also be sorted into ER-exit sites by specific export receptors. Some ERES are specialized for a certain type of cargo. In *S. cerevisiae*, this is the case for GPI-anchored proteins (GPI-APs; (Muñiz et al., 2001)). Since they are anchored within the inner leaflet of the ER membrane and thus invisible from the cytosol, they rely on an export receptor, the p24 complex, bridging them with the COPII coat (Muñiz et al., 2000; Castillon et al., 2011). Furthermore, they use a Sec24p homologue, Lst1p, as part of the COPII coat (Miller et al., 2002; D'Arcangelo et al., 2015).

In *S. cerevisiae*, the morphology of ERES ranges from slightly curved ER regions to regions portraying single or multiple budding events, induced by the COPII coat (Melero et al., 2022). In animal cells, COPII-coated vesicular carriers at ERES, as well as more elaborate structures, coexist (Nair et al., 2025). Export of large procollagen fibers is mediated by larger tubular structures from ERES requiring TANGO1 (Saito

et al., 2009; Raote et al., 2020). In mammalian cells, ERES consisting of large tubular networks have been described as well (Shomron et al., 2021; Weigel et al., 2021). In this case, the COPII machinery has been proposed to remain associated with the neck region, whereas COPI components localize more distally at the ER (Weigel et al., 2021).

1.1.3. Membrane contact sites

The ER forms contacts with many other organelles of the cell including the plasma membrane, endosomes, the Golgi and mitochondria (Fig. 1). These tight contacts bringing membranes as close as 10 nm in distance facilitate processes like lipid or calcium transfer, but also have effects on organelle maturation, dynamics and localization (Phillips & Voeltz, 2016; Wu et al., 2018). They are established by tethering proteins bridging the two membranes. At the ER, many MCSs are established by the VAP family proteins, which are tail-anchored membrane proteins at the ER, interacting with proteins of the partner membrane via their FFAT motives. The latter can act as mere tethers or fulfil additional functions like lipid transfer (Wu et al., 2018).

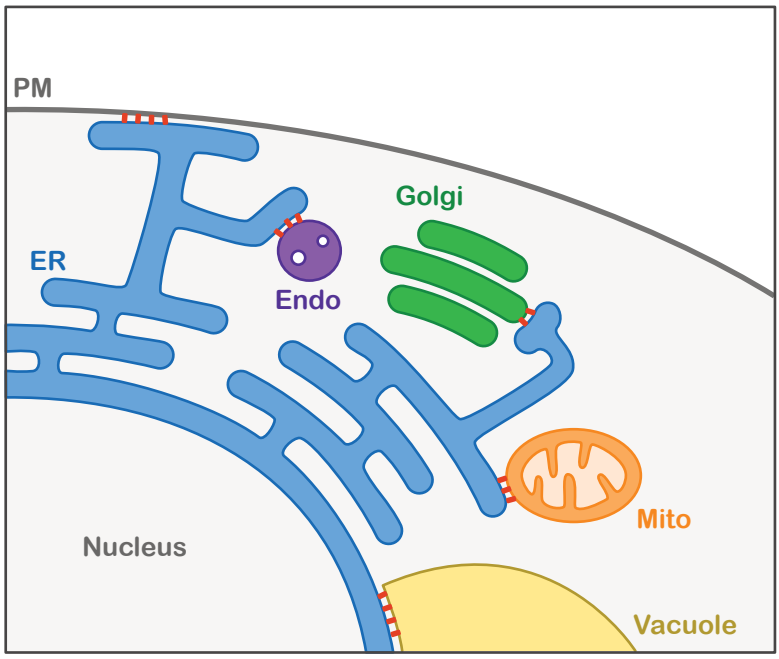

Figure 1: Membrane contact sites between the ER and other organelles.
Schematic representation of the endoplasmic reticulum and some of the organelles it establishes membrane contact sites with: the plasma membrane (PM), mitochondria (mito), the Golgi, endosomes (endo) and the vacuole (in yeast and plant cells). Contact sites are established by tethering proteins that differ between sites and have been indicated here as red rods.

Many lipids are synthesized at the ER and need to be transferred to other organelles. In part, this transport is mediated via vesicles, but MCSs facilitate rapid non-vesicular lipid transfer. Both phosphatidylserine and phosphatidic acid are synthesized at the ER and need to be transported to

mitochondria to be further converted into phosphatidylethanolamine or cardiolipin, respectively (Dennis & Kennedy, 1972; Osman et al., 2011). In *S. cerevisiae*, the ERMES complex between the ER and mitochondria appears to mediate transfer of certain lipid species (Kornmann et al., 2009; Kojima et al., 2016; Jeong et al., 2017). In mammalian cells, the nature and function of ER-mitochondria contact sites are less clear (Larrañaga-SanMiguel et al., 2025). At ER-plasma membrane contact sites, Osh3p, together with VAP proteins, controls PI metabolism in yeast (Stefan et al., 2011). Moreover, extended synaptotagmin-like proteins (E-Syts) in mammalian cells and tricalbins in yeast regulate ER-PM contact formation and possibly also lipid transfer (Manford et al., 2012; Toulmay & Prinz, 2012). Transfer of ceramide and cholesterol from the ER to the Golgi involves the lipid transfer proteins CERT and OSBP respectively in mammalian cells (Hanada et al., 2003; Mesmin et al., 2013). These interact with VAPs at the ER and bind the Golgi via their PI4P sensing PH domain (Kawano et al., 2006; Hanada et al., 2003; Levine & Munro, 2002; Loewen et al., 2003). In *S. cerevisiae*, non-vesicular ceramide transfer is mediated at MCSs by the shuttling protein Svf1p at steady state (Limar et al., 2023).

Besides enabling non-vesicular lipid transfer, MCSs between the ER and other organelles can affect maturation and dynamics of organelles. ER-mitochondria contact sites are for instance involved in fission of mitochondria and mark division sites on mitochondria in mammalian cells and *S. cerevisiae* (Friedman et al., 2011). Mobility of peroxisomes and distribution within cells depend on contacts with the ER as well (Costello et al., 2017). Thus, communication between the ER, as the largest organelle in the cell, and other organelles, is essential for the coordination of many cellular processes.

1.2. Endoplasmic Reticulum Stress

Cells are exposed to external stimuli and constantly need to adapt to changing conditions in their environment. Increases in temperature or nutrient scarcity are some of the factors that can lead to disruption of cellular processes. The ER is particularly affected by conditions that lead to protein misfolding, as the accumulation of misfolded proteins in the ER lumen is causing ER stress (Walter & Ron, 2011). Experimentally, ER stress can also be chemically induced, e.g. by inhibiting N-linked glycosylation with tunicamycin (Tm) or by inhibiting disulfide bridge formation with the reducing agent dithiothreitol (DTT) (Braakman et al., 1992; Tkacz & Lampen, 1975). Cells have developed various stress response pathways to monitor and restore ER homeostasis. The major and best studied ER stress response pathway in cells is the Unfolded Protein Response (UPR) (Walter & Ron, 2011). In *S. cerevisiae*, the UPR is mediated by a single branch involving the kinase and endonuclease Ire1p at the ER, whereas it comprises two more branches involving ATF6 and PERK1 in higher eukaryotes (J. S. Cox et al., 1993; Harding et al., 1999; Haze et al., 1999). Upon accumulation of misfolded proteins in the ER, the ER-luminal Hsp70 chaperone Kar2p (BiP in mammalian cells) is titrated away from its binding partner Ire1p and binds to the misfolded polypeptide chains (Bertolotti et al., 2000; Okamura et al., 2000). Removal of Kar2p allows Ire1p to dimerize and form higher oligomeric assemblies (Bertolotti et al., 2000; Shamu

& Walter, 1996; C. Y. Liu et al., 2000). An alternative model describes the importance of direct binding of unfolded proteins to Ire1p for stabilization of oligomers (Credle et al., 2005; Gardner & Walter, 2011). More recently, it has been found that the UPR can also be activated by lipid bilayer stress, which is caused by perturbations of ER membrane properties and presumably increases membrane stiffness and thus drives Ire1p oligomerization (Ho et al., 2020; Volmer et al., 2013; Radanović & Ernst, 2021). Dimerization and further oligomerization of Ire1p induces trans-autophosphorylation of Ire1p and activation of its endonuclease activity (Shamu & Walter, 1996; Welihinda & Kaufman, 1996). Activated Ire1p, together with the tRNA ligase Trl1p then mediates splicing of *HAC1* mRNA (XBP1 in mammalian cells) (Mori et al., 1996; Sidrauski et al., 1996; J. S. Cox & Walter, 1996; Sidrauski & Walter, 1997). Spliced *HAC1* mRNA can be translated and acts as a transcription factor in the nucleus, activating ER stress response genes (Mori et al., 1996; Travers et al., 2000). This transcriptional response induces the upregulation of folding capacity within the ER, an increase of protein degradation through ER-associated degradation (ERAD) and the upregulation of membrane lipid biosynthesis (Travers et al., 2000; J. S. Cox et al., 1997; Walter & Ron, 2011).

ER stress and the UPR also lead to prominent morphological changes of the ER. Expansion of the ER, mediated by the UPR-dependent upregulation of lipid synthesis genes can be observed in yeast (Schuck et al., 2009). This expansion is mediated by an increased amount of ER sheets, thus providing more space to accommodate misfolded proteins and chaperones (Papagiannidis et al., 2021; Schuck et al., 2009). ER size can be further influenced by stress-dependent selective autophagy of the ER activated by the UPR, which mediates degradation of misfolded proteins and controls ER size under stress conditions in mammalian cells (Ogata et al., 2006). In yeast, ER stress induces micro-ER-phagy, which entails the formation of multilamellar ER whorls and their uptake into the vacuole by invagination and scission of the vacuolar membrane mediated by the ESCRT machinery (Schuck et al., 2014; Schäfer et al., 2020).

Apart from the morphology and size of the ER, its communication with other organelles via membrane contact sites is also affected by ER stress. The degree of association between organelles, as well as the functions mediated by MCSs can be adapted. For instance, the number of contacts between the ER and mitochondria in mammalian cells increases upon ER stress to promote mitochondrial respiration (Bravo et al., 2011). Similarly, in *S. cerevisiae*, the extent of contact between the ER and the Golgi increases by formation of stress-induced ER-Golgi contact sites. The ER-tethering protein Nvj2p was shown to be involved in formation of these contacts upon DTT treatment, by partially re-localizing from its steady-state location at nuclear-vacuolar junctions (NVJs) (Pan et al., 2000; L.-K. Liu et al., 2017). Another ER-tethering protein, the tricalbin Tcb3p, which at steady state mediates contacts between the ER and the plasma membrane, partially localizes to ER-Golgi contacts in cells treated with tunicamycin (Manford et al., 2012; Ikeda et al., 2020). Both tethers seem to facilitate non-vesicular ceramide transfer during

ER stress (Ikeda et al., 2020; L.-K. Liu et al., 2017).

Thus, the remodeling of the ER and the rearrangement of its subdomains strongly contributes to restoring ER homeostasis and it is conceivable that additional pathways are involved to regulate these processes.

1.3. The ESCRT machinery

One of the machineries that mediates remodeling of various cellular membranes is the endosomal sorting complex required for transport (ESCRT) machinery. The machinery comprises four hetero-oligomeric complexes, ESCRT-0, ESCRT-I, ESCRT-II and ESCRT-III, as well as the AAA+ - ATPase Vps4p. ESCRT-III and Vps4, as well as the mechanism of membrane remodeling by this machinery, are highly conserved from archaea to metazoan (Makarova et al., 2024; Schlösser et al., 2023; Souza et al., 2025). ESCRTs were first described to be involved in the formation of multivesicular bodies (MVBs) by mediating the budding of intralumenal vesicles (Katzmann et al., 2001). Since then, a variety of different cellular functions have been ascribed to this versatile machinery, such as the abscission step during cytokinesis, budding of HIV from the plasma membrane, repair of nuclear pore complexes (NPCs) and plasma membrane repair (Fig. 2A; (Morita et al., 2007; Carlton & Martin-Serrano, 2007; Garrus et al., 2001; Webster et al., 2016; Scheffer et al., 2014; Jimenez et al., 2014)).

1.3.1. Recruitment mechanisms for ESCRT-III

Membrane remodeling is mediated by the ESCRT-III complex of the ESCRT machinery. Given the various roles of the ESCRT machinery in cells, ESCRT-III can be recruited in different location- and process-specific manners. Recruitment can be mediated in distinct, but not mutually exclusive ways: by upstream ESCRT complexes, ESCRT-0 to ESCRT-II; by Bro1 domain proteins; or by other location-specific recruitment factors (Fig. 2B).

In MVB sorting, ESCRT-0, -I and -II constitute a hierarchical recruitment cascade for ESCRT-III (Katzmann et al., 2001; Raiborg & Stenmark, 2009). The ESCRT-0 complex in yeast consists of a heterotetramer of two subunits of Vps27p and Hse1p each and interacts with ESCRT-I protein Vps23p via Vps27p (Mayers et al., 2011; Bache et al., 2003). Vps23p forms the ESCRT-I heterotetramer together with Vps28p, Vps37p and Mvb12p (Kostelansky et al., 2007). This in turn interacts with the ESCRT-II complex, a heterotetramer of Vps36p, Vps22p and two Vps25p proteins (Babst, Katzmann, Snyder, et al., 2002; Teo et al., 2006; Hierro et al., 2004). All three complexes can interact with ubiquitinated cargoes (Hofmann & Falquet, 2001; Katzmann et al., 2001; Slagsvold et al., 2005; Alam et al., 2004). ESCRT-0 and ESCRT-II additionally interact with PI3P and thus target the ESCRT machinery to endosomal membranes (Teo et al., 2006; Raiborg et al., 2001).

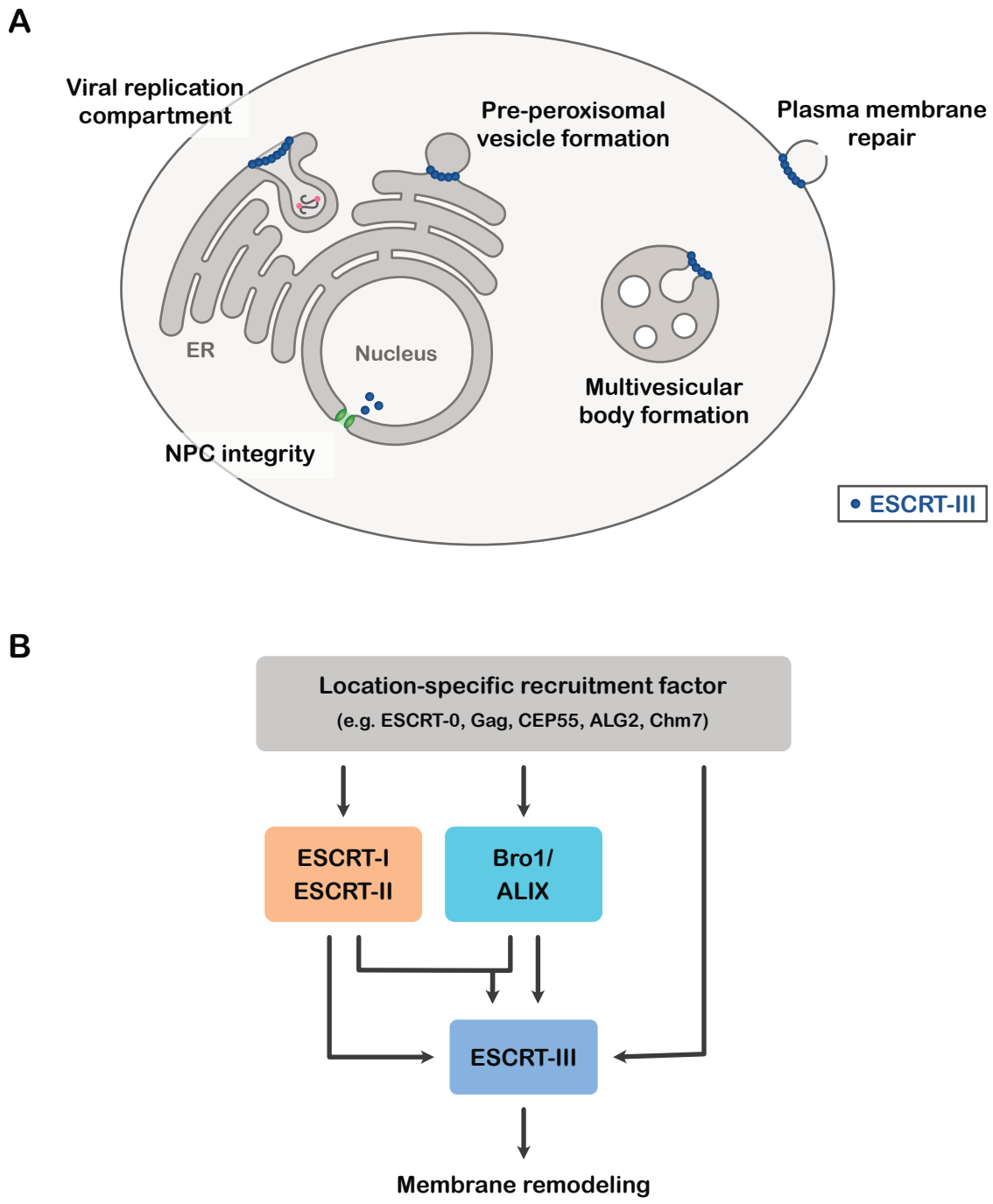

Figure 2: Cellular functions and recruitment mechanisms of the ESCRT machinery.
A: Schematic representation of some of the functions mediated by the ESCRT machinery within the cell. ESCRT-III subunits forming spiral-like assemblies on different membranes are shown as blue spheres. The ESCRT machinery plays a role in budding events such as the formation of intralumenal vesicles in multivesicular body formation (reverse topology) or budding of pre-peroxisomal vesicles from the ER (classical topology). They also mediate membrane repair by shedding off damaged membrane at the plasma membrane or by sealing off aberrant nuclear pore complexes (NPCs). In some cases, membrane remodeling is not followed by scission and the ESCRT machinery has a stabilizing role, e.g. at membrane necks of viral replication compartments. I based this schematic on the following reviews: (Hurley, 2015; Vietri et al., 2020).
B: Flow chart of different mechanisms recruiting ESCRT-III to membranes. Recruitment of the ESCRT machinery is initiated by specific recruitment factors that vary depending on the location and role played by the ESCRTs. Examples are ESCRT-0 interacting with ubiquitinated cargo at MVBs, Gag for HIV budding, CEP55 in cytokinesis, ALG2 for plasma membrane repair and Chm7p for NPC quality control. These factors either recruit ESCRT-III

directly or they interact with ESCRT-I and ESCRT-II and/or Bro1 proteins (Bro1p in yeast, ALIX in mammalian cells) that in turn recruit ESCRT-III. I based this schematic on section 1.3.1 and (Schöneberg et al., 2017).

Bro1 domain proteins, such as Bro1p in yeast or ALIX or HD-PTP in mammalian cells, serve as ESCRT-associated proteins. They contain an N-terminal Bro1 domain, followed by a V domain and a C-terminal PRD domain (Kim et al., 2005; Lee et al., 2007). The boomerang-shaped Bro1 domain is highly conserved and contains a TPR-like domain as well as two hydrophobic patches (Kim et al., 2005). The first hydrophobic patch in yeast Bro1p mediates its interaction with ESCRT-III component Snf7p (Bowers et al., 2004; Kim et al., 2005). Bro1p has been proposed to recognize ubiquitinated cargo at MVBs via its V-domain and mediate deubiquitination of cargo by recruiting the deubiquitinase Doa4 via the PRD domain (Pashkova et al., 2013; Luhtala & Odorizzi, 2004). In other ESCRT-mediated processes, Bro1 domain proteins are directly involved in the recruitment of ESCRT-III. Viral budding of HIV from the plasma membrane of mammalian cells for instance requires ESCRT-I, -II, ubiquitinated viral Gag protein, as well as ALIX to recruit ESCRT-III (VerPlank et al., 2001; Garrus et al., 2001; Carlton & Martin-Serrano, 2007). Cytokinesis requires the specific recruitment factor CEP55 at the midbody ring, leading to the recruitment of ESCRT-III via ESCRT-I, ESCRT-II and ALIX (Morita et al., 2007; Carlton & Martin-Serrano, 2007; Christ et al., 2016). ALIX can also recruit ESCRT-III on its own, as is the case for plasma membrane repair in mammalian cells, which is triggered by influx of calcium bound by ALG2, which in turn interacts with ALIX and recruits ESCRT-III component CHMP4B (Jimenez et al., 2014; Scheffer et al., 2014).
The quality control of nuclear pore complexes is an example for ESCRT-III recruitment that is independent of Bro1 domain proteins and upstream ESCRTs. Here, the nucleus-specific factor Chm7p directly recruits Snf7p to defective NPCs to seal off the membrane (Webster et al., 2016).

1.3.2. Membrane remodeling by the ESCRT machinery

The ESCRT-III subcomplex is responsible for the actual membrane remodeling step by assembling into large polymers on membranes. The ESCRT-III complex includes Vps2p, Vps20p, Vps24p and Snf7p as core subunits, as well as Vps60p, Did2p and Ist1p (Babst, Katzmann, Estepa-Sabal, et al., 2002; Rue et al., 2008; Pfitzner et al., 2023). The most abundant subunit, Snf7p, consists of six α-helices and exists as soluble subunit in its closed, inactive form in the cytosol (Tang et al., 2015; Teis et al., 2008). The folding of α-helix 5 onto helices α1-4 mediates this auto-inhibition and it can be released by interaction with binding partners, such as Bro1p via α6 or Vps20p via α1 and α2 (Tang et al., 2015, 2016). In its open conformation, Snf7p can assembly into high-order polymers forming spiral-like assemblies on membranes (Cashikar et al., 2014; Chiaruttini et al., 2015; Shen et al., 2014).
It was proposed that Vps20p nucleates oligomer assembly of Snf7p, whereas Vps24p and Vps2p are involved in termination of these assemblies and recruitment of the AAA+ - ATPase Vps4p (Teis et al., 2008; Tang et al., 2016). Activation of Snf7p can additionally or in parallel be mediated by Bro1p (Tang

et al., 2016). Vps4p, together with its activator Vta1p, is responsible for disassembly and recycling of ESCRT subunits (Babst, 1998). It is recruited by interaction with the MIM domains of ESCRT-III subunits, such as Snf7p and acts as a hexamer, which disassembles ESCRT polymers by unfolding and threading them through its central pore (Obita et al., 2007; Stuchell-Brereton et al., 2007; Caillat et al., 2015; Yang et al., 2015). More recently, ESCRT-III assembly has been described as a polymerization sequence in which different subunits are progressively exchanged. The sequence starts off with Snf7 polymers stabilizing wider spirals and ends up with Did2-Ist1 polymers stabilizing tighter spiral assemblies. The exchange of subunits, mediated by Vps4, leads to membrane constriction (Pfitzner et al., 2020). ESCRT-III filament buckling leads to membrane deformation, which can eventually entail scission of the membrane (Pfitzner et al., 2020; Schöneberg et al., 2017).

The ESCRT machinery can facilitate membrane remodeling resulting in different topologies (Fig. 2A). In most processes known to date, the ESCRT machinery mediates membrane budding away from the cytosol, leading to so-called reverse-topology budding. However, more processes are emerging in which the ESCRTs mediate so-called classical topology budding events towards the cytosol. ESCRT-III proteins for instance drive the budding of pre-peroxisomal budding from the ER in yeast and the fission of recycling tubules from endosomes in mammalian cells, processes in which they assemble on the outside of the membrane neck (Allison et al., 2013; Mast et al., 2018).

In many instances, the ESCRT machinery eventually induces membrane scission and budding of vesicles such as intralumenal vesicles at MVBs or HIV viruses at the plasma membrane. Membrane scission also constitutes the basis for membrane repair processes by the ESCRT machinery (Jimenez et al., 2014; Skowyra et al., 2018). Nevertheless, not all ESCRT-mediated processes require scission. During infection of yeast cells with brome mosaic virus, ESCRT proteins mediate the formation of protected replication compartments at the ER by invagination of the membrane and stabilization of the membrane neck (Diaz et al., 2015). Moreover, in the fungal Rim/Pal pathway for sensing of extracellular pH, the ESCRT machinery stabilizes Rim proteins at the plasma membrane, acting as a scaffold for Rim signaling rather than inducing membrane remodeling or scission (Xu et al., 2004; Calcagno-Pizarelli et al., 2011; Peñalva et al., 2014).

All in all, membrane association of the ESCRT machinery can mediate a variety of morphological and functional outputs.

1.4. Previous work

A former PhD student in the lab of Sebastian Schuck, Jasmin Schäfer, observed that the ESCRT-III component Snf7 formed bright puncta at the ER when yeast cells were experiencing ER stress caused by treatment with tunicamycin (Fig. 3). Snf7-mNeonGreen localized to the cytosol and endosomes at steady state and massively re-localized to bright ER patches upon ER stress. CLEM imaging by Jasmin Schäfer further revealed a complex architecture for the Snf7-positive ER regions, with tubular

extensions reaching into the cytosol. These structures, that we later termed ER clusters, occurred both at the nuclear envelope and at the cortical ER to a similar degree, as judged by fluorescence microscopy by Oliver Pajonk. As for the recruitment of Snf7, Jasmin Schäfer showed that upstream ESCRT components of the ESCRT-0, -I or -II complexes were not required, but the ESCRT-associated protein Bro1p was essential. Deletion of *BRO1* almost completely abolished Snf7 recruitment.

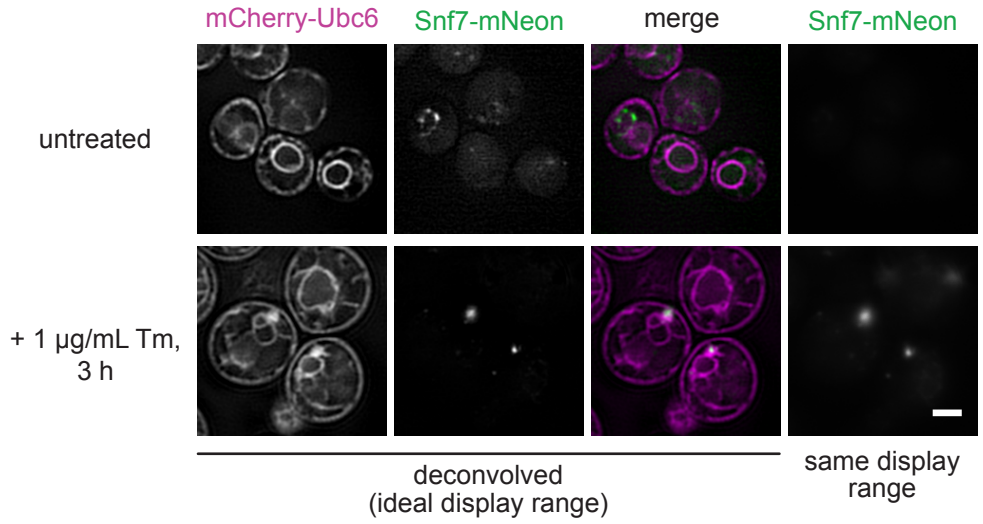

Figure 3: Recruitment of the ESCRT-III component Snf7 to ER clusters upon ER stress.
Fluorescence microscopy images of cells stably expressing the general ER marker mCherry-Ubc6 and Snf7-mNeonGreen from the *VPS24* promoter. Exponentially growing cells were treated with tunicamycin (Tm) (1 µg/mL) for 3 h or left untreated. Images of all channels were deconvolved with the Wiener filter algorithm. Deconvolution leads to the appearance of some saturated pixels on the images and prevents quantitative comparison between genotypes. The Snf7 signal is additionally shown prior to deconvolution with the same display range between untreated and treated cells to allow for comparison of signal intensities between the conditions. The scale bar indicates 2 µm. This observation was originally made by Jasmin Schäfer. Images were acquired by Oliver Pajonk. The strain was generated by Jasmin Schäfer.

To investigate which genes are involved in the recruitment of the ESCRT machinery to ER clusters during stress, Oliver Pajonk, together with Jasmin Schäfer, Dimitris Papagiannidis, Carlos Martin de Hijas, Peter Bircham and Sebastian Schuck, performed microscopy-based genetic screens of the ER deletion collection and the temperature-sensitive allele collection of essential genes. Genes that were required for Snf7 recruitment to the ER were identified and included the following categories: ER export and ER-Golgi trafficking, GPI-anchor remodeling, the GET machinery, ER structural genes, lipid metabolism genes, ribosome or proteasome-related genes (Pajonk, PhD dissertation, 2025).
During my Master Thesis, I set up a proximity-dependent biotinylation approach coupled to mass spectrometry (PDB-MS) as a complementary method to ask which proteins are enriched at ER clusters during stress and thus possibly involved in ESCRT recruitment or function at these sites. This preliminary work served as a basis for the study described in this thesis.

2. AIMS OF THIS THESIS

The occurrence of the ESCRT machinery, as a major membrane remodeling machinery, at specific stress-induced ER regions raised the question whether the ESCRT machinery is involved in formation or remodeling of these sites. During my PhD, I aimed to shed light on the role of the ESCRT machinery at stress-induced ER clusters in *S. cerevisiae*.

In particular, I aimed to:

1) determine how the ESCRT machinery is recruited to the ER during ER stress.
2) elucidate the function of the ESCRT machinery at stress-induced ER clusters.

Addressing these aims will lead to a better understanding of the versatile ESCRT remodeling machinery, as well as its putative role in the cellular ER stress response in budding yeast.

3. RESULTS

3.1. Bro1p-dependent recruitment of Snf7 to ER clusters

3.1.1. Effect of tagging of Snf7 on Bro1p localization and Snf7-Bro1p interaction

Before further characterizing the recruitment mechanism of Snf7 to ER clusters during ER stress, I set out to test the effect of tagged Snf7 on ESCRT function at MVBs and in stress-dependent recruitment to ER clusters. Tagging Snf7p has been shown to interfere with its function, whereas expressing tagged Snf7 version alongside endogenous, untagged Snf7p does not impair MVB formation (Teis et al., 2008; Adell et al., 2017). Thus, within this study, I used strains expressing fluorescently tagged Snf7 from the *VPS24* promoter, which is weaker than the *SNF7* promoter, alongside the endogenous Snf7p to follow Snf7 localization within cells. This same strain background did not affect ESCRT function in micro-ER-phagy (Schäfer et al., 2020).

As a read-out for one of the major ESCRT-mediated processes at multivesicular bodies, I used the Mup1-pHluorin assay for MVB cargo sorting throughout this study (Prosser et al., 2016). This assay uses the methionine transporter Mup1 C-terminally tagged with a pH sensitive fluorophore, pHluorin, which is quickly internalized by endocytosis upon addition of methionine, sorted into MVBs with the help of the ESCRT machinery and subsequently reaches the vacuole (Fig. 4B). The decrease of Mup1-pHluorin fluorescence over time reports on the fraction of Mup1-pHluorin that was sorted into the vacuole where quenching of the fluorescence occurs due to the low vacuolar pH.

To assess the effect of tagged Snf7 on ESCRT function at MVBs, I applied this assay to strains stably expressing cytosolic BFP and Mup1-pHluorin in a wildtype or *SNF7* deletion background in presence or absence of Snf7-mScarlet-i expressed from the *VPS24* promoter. Mup1-pHluorin and BFP fluorescence were measured by flow cytometry during a timeframe of 90 minutes after addition of methionine. Cytosolic BFP fluorescence was used to normalize Mup1-pHluorin fluorescence to the size and translational capacity of the cells. Deletion of *SNF7* reduced the loss of relative Mup1-pHluorin fluorescence over time, thus confirming impaired MVB sorting (Fig. 4A). Expression of tagged Snf7 in a *SNF7* deletion background mimicked the effect of the *SNF7* deletion, showing that Snf7-mScarlet was not functional on its own. Expression of Snf7-mScarlet-i from the *VPS24* promoter alongside the endogenous Snf7 did not affect MVB sorting efficiency. Thus, expression of tagged Snf7 alongside endogenous Snf7 was indeed neutral in the case of MVB sorting, as shown before (Adell et al., 2017).

Next, we addressed whether tagged Snf7 is also functionally neutral in the stress-induced ESCRT recruitment to ER clusters. Oliver Pajonk could show that Bro1p-mNeonGreen colocalized with Snf7-mScarlet at ER clusters upon ER stress (Pajonk, PhD dissertation, 2025). He also found that in strains without tagged Snf7, Bro1p-mNeonGreen puncta could only rarely be observed at ER clusters.

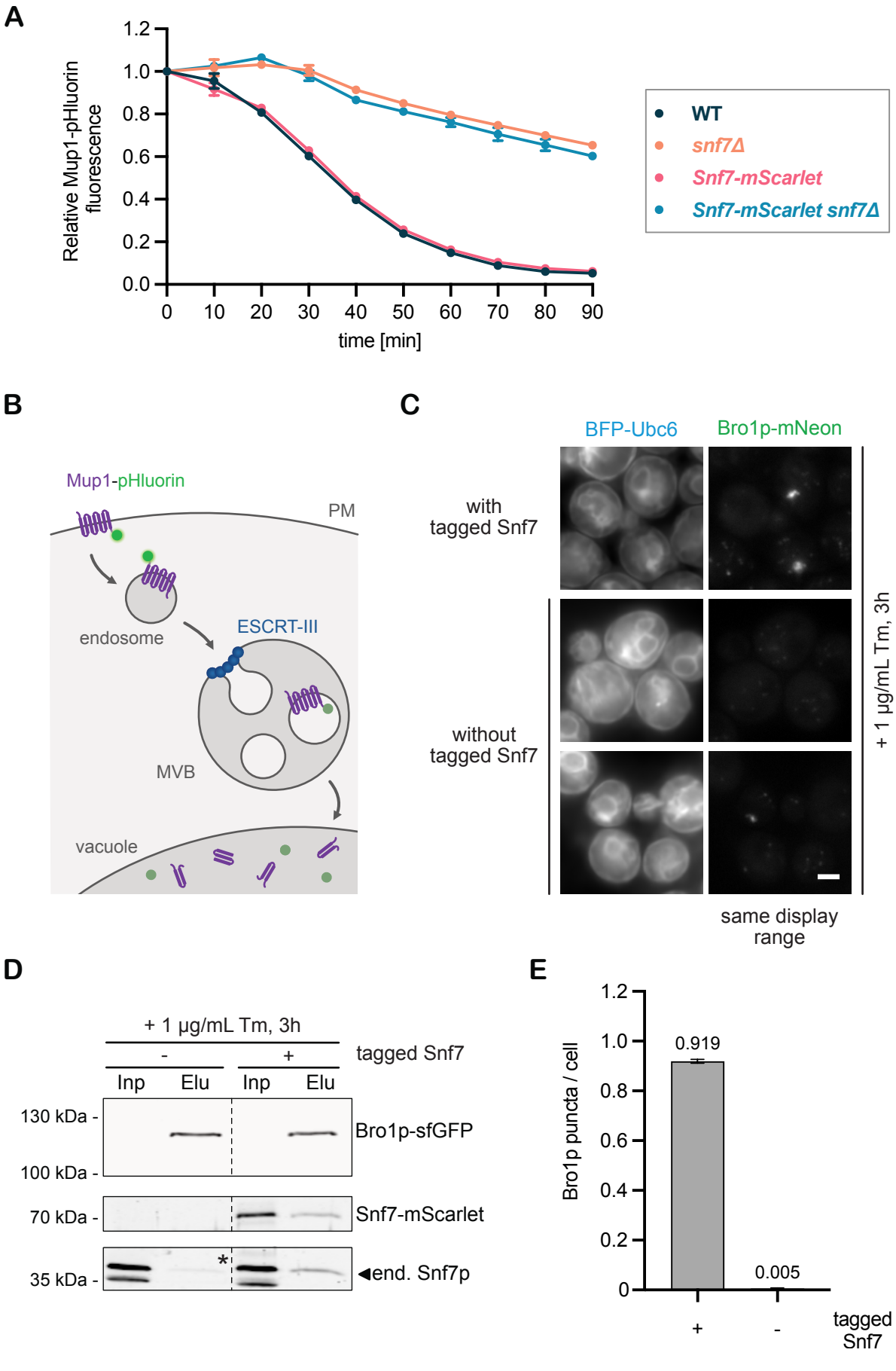

Figure 4: Effect of tagged Snf7 on the Bro1p-Snf7 interplay at ER clusters and on MVB sorting efficiency.

A: Mup1-pHluorin assay of cells with and without Snf7-mScarlet-i expressed from the *VPS24* promoter in a wildtype or *SNF7* deletion background. Cells were all expressing Mup1-pHluorin and cytosolic BFP and were grown to exponential growth phase in absence of methionine. At t = 0 min, one set of cultures was supplemented with methionine inducing endocytosis of Mup1-pHluorin and its vacuolar degradation via MVBs. The graph shows the relative Mup1-pHluorin fluorescence intensity of cells supplemented with methionine compared to cells growing in absence of methionine for the entire timeframe of the experiment. GFP autofluorescence was subtracted and Mup1-pHluorin intensities were normalized to the cytosolic BFP signal to adjust for cell size and translational capacity. Results from independent biological replicates are shown (n=3). The error bars indicate the standard error of the mean. The strains were generated by Petra Hubbe, Oliver Pajonk, Sebastian Schuck and me.
B: Schematic representation of the Mup1-pHluorin assay for MVB sorting. The methionine transporter Mup1 tagged with pHluorin, a pH-sensitive fluorophore, is used as a reporter for MVB sorting. Upon addition of methionine, Mup1-pHluorin is internalized via endocytosis into endosomes, then sorted into multivesicular bodies with the help of the ESCRT machinery, particularly ESCRT-III mediating the scission of intralumenal vesicles (ILV). Upon fusion with the vacuole, the ILVs and their cargo are degraded, leading to degradation of Mup1-pHluorin. pHluorin is quenched upon arrival in MVBs and further in the vacuole, thus the decrease of fluorescence intensity reports on MVB sorting efficiency. Figure adapted from (Prosser et al., 2016). PM: plasma membrane, MVB: multivesicular body.
C: Fluorescence microscopy images of cells stably expressing the general ER marker BFP-Ubc6 and Bro1p-mNeonGreen in a background with or without Snf7-mScarlet-i expressed from the *VPS24* promoter. Exponentially growing cells were treated with tunicamycin (Tm) (1 µg/mL) for 3 h. Only the BFP and mNeonGreen channels are shown. Two examples are shown for the cells with tagged Snf7, one with a Bro1p punctum and one without. The same display range is shown for the mNeonGreen channel to appreciate the relative signal intensities between genotypes. The scale bar indicates 2 µm. The strains were generated by Oliver Pajonk and me.
D: Western Blot of Bro1p-sfGFP and Snf7 from cell lysates (input) and eluates of co-immunoprecipitation of Bro1p-sfGFP. Cells were stably expressing Bro1p-sfGFP in the *VPS27* deletion background, to avoid stress-dependent degradation of Bro1p, either with or without Snf7-mScarlet-i expressed from the *VPS24* promoter. Exponentially growing cells were treated with tunicamycin (Tm) (1 µg/mL) for 3 h. Bro1p-sfGFP was pulled down from cell lysates using GFP-binder beads. Membranes were probed against GFP and Snf7. Bro1p-sfGFP remained under the detection limit in input samples. The asterisk (*) indicates a faint band for endogenous Snf7p in the eluate of treated cells without tagged Snf7.
E: Quantification of Bro1p-mNeonGreen puncta at ER clusters per cell in strains with and without Snf7-mScarlet-i expressed from the *VPS24* promoter after treatment with tunicamycin (1 µg/mL) for 3 h from C. Puncta and cells were counted manually by blind analysis. Over 450 cells per genotype were quantified in independent biological replicates (n=3). The error bar indicates the standard error of the mean. The strains were generated by Oliver Pajonk and me.

I quantified Bro1p-mNeonGreen puncta at ER clusters after 3 h of tunicamycin-induced ER stress in cells with and without expression of Snf7-mScarlet-i. I confirmed that whereas more than 0.9 Bro1p-mNeonGreen puncta per cell form in presence of tagged Snf7, only a minor fraction of puncta (0.005 puncta per cell) were observed at ER clusters in cells without tagged Snf7 (Fig. 4C and E). Moreover, the remaining puncta were less bright than the Bro1p-mNeonGreen puncta in presence of tagged Snf7. Thus, additional expression of tagged Snf7 is not neutral in stress-induced ESCRT recruitment to ER clusters but rather seems to promote or stabilize accumulation of Bro1p-mNeonGreen at ER clusters. ER clusters were still present in strains without tagged Snf7, implying that endogenous Snf7p is sufficient for their formation and that they are not an artifact created by expression of tagged Snf7. Moreover, Oliver Pajonk could show that deletion of *SNF7* in cells expressing tagged Snf7 abolished the

recruitment of tagged Snf7 to ER clusters, underlining that tagged Snf7 is non-functional in ESCRT recruitment to the ER and that endogenous Snf7p is essential for puncta formation (Pajonk, PhD dissertation, 2025).

Bro1p and Snf7p interact in ESCRT-mediated processes like MVB sorting (Wemmer et al., 2011). To find out whether Bro1p interacts with both endogenous and tagged Snf7 upon ER stress, I performed a co-immunoprecipitation of Bro1p-sfGFP using GFP-binder beads and probed against Snf7. Lysates from cells with and without Snf7-mScarlet-i treated for 3 h with tunicamycin were used to determine whether expression of tagged Snf7 affects the interaction between Bro1p and endogenous Snf7p. In stressed cells without tagged Snf7 a small amount of endogenous Snf7p was pulled down with Bro1p-sfGFP (Fig. 4D). In stressed cells expressing tagged Snf7, both tagged and endogenous Snf7 interacted with Bro1p-sfGFP. Remarkably, more endogenous Snf7p interacted with Bro1p-sfGFP upon ER stress in cells that also expressed Snf7-mScarlet-i. The presence of tagged Snf7 promoted Bro1p interaction with endogenous Snf7p. Since Snf7 puncta at ER clusters are very prominent upon ER stress, it is likely that this finding reported on an interaction of Bro1p with both versions of Snf7 at ER clusters. However, it cannot be excluded that interaction also takes place at other ESCRT processes upon ER stress. Still, I showed that Bro1p was able to interact with both endogenous Snf7p and Snf7-mScarlet-i upon ER stress.

Thus, I could further confirm that even though the expression of tagged Snf7 from the *VPS24* promoter is not neutral in stress-induced ESCRT recruitment to ER clusters, its stabilizing effect makes it a valuable tool for studying this process.

3.1.2. Features of Bro1p required for Snf7 recruitment to ER clusters

After determining the effect of non-functional tagged Snf7 on its interplay with Bro1p and on ESCRT recruitment to the ER, I set out to characterize the features of Bro1p that are essential for ESCRT recruitment. Previously, Carlos Martin de Hijas had shown during his lab rotation that the Bro1 domain of Bro1 expressed ectopically from the *LYP1* locus in a *BRO1* deletion background was sufficient for Snf7 recruitment to the ER upon stress. Moreover, K246A and Y320D mutations in Bro1 strongly decreased Snf7 puncta formation in this background. Since the difference in the chromosomal context by ectopic expression of Bro1 might result in altered regulation and expression levels of the protein, I set out to verify these findings by mutating endogenous Bro1p and assessing the effect on Snf7 recruitment to ER clusters. I generated strains with the Bro1 domain only, $bro1^{1\text{-}387}$, as well as strains with chromosomal point mutations in the TPR-like domain, $bro1^{K246A}$, and the second hydrophobic patch, $bro1^{Y320D}$, both within the Bro1 domain.

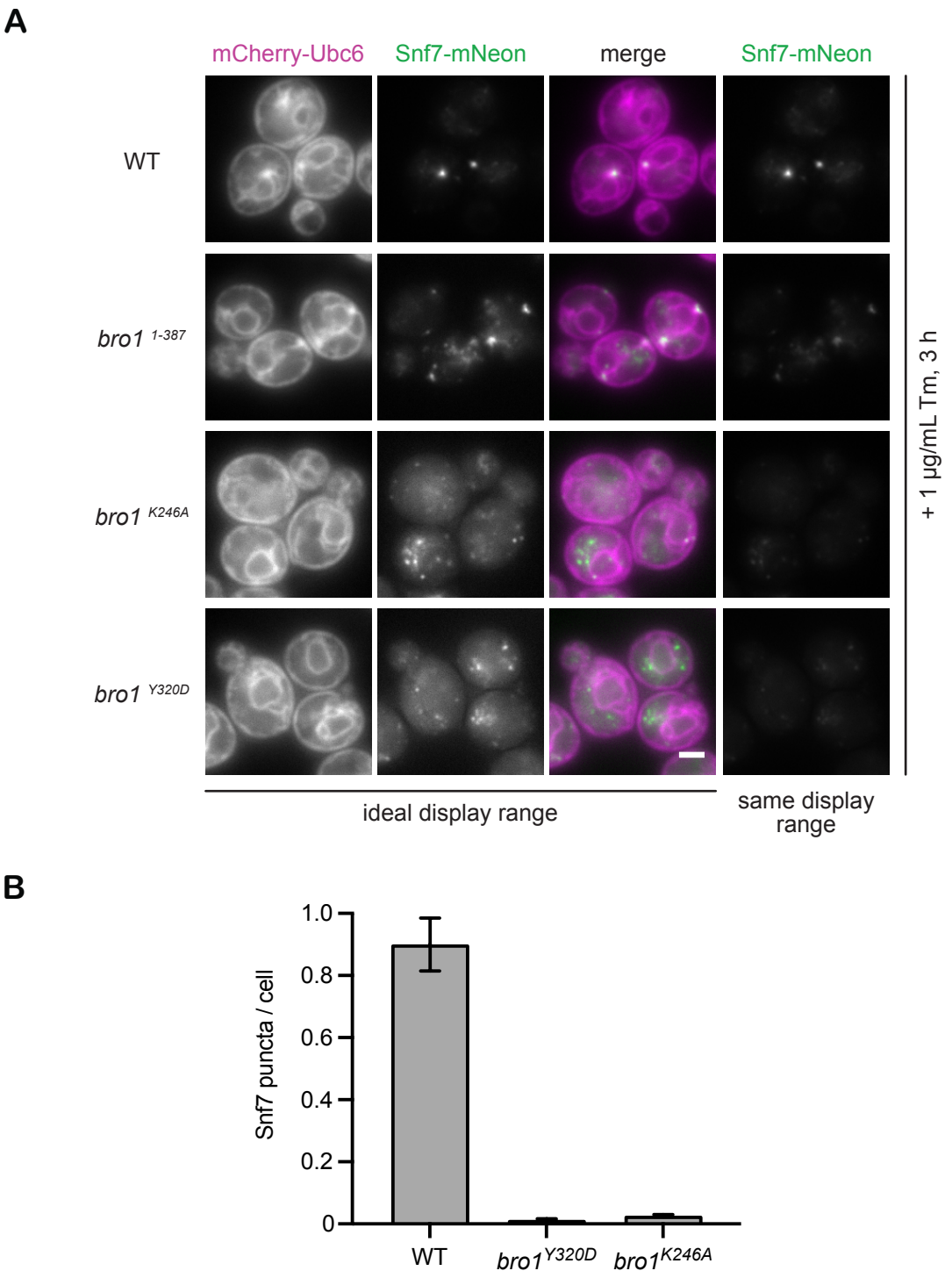

Figure 5: Bro1 point mutants bro1^{K246A} and bro1^{Y320D} decrease Snf7 recruitment efficiency to ER clusters upon ER stress.

A: Fluorescence microscopy images of cells stably expressing the general ER marker mCherry-Ubc6, Snf7-mNeonGreen from the *VPS24* promoter and different Bro1 variants. Exponentially growing cells were treated with tunicamycin (Tm) (1 µg/mL) for 3 h. The Snf7-mNeonGreen signal is shown in two different display ranges to portray both the signal distribution in each genotype (ideal display range) and the relative intensities of the signal between genotypes (same display range, comparable between genotypes). The scale bar indicates 2 µm. The strains were generated by Jasmin Schäfer, Oliver Pajonk and me.

B: Quantification of Snf7-mNeonGreen puncta at ER clusters per cell in strains with different Bro1 variants after treatment with tunicamycin (1 µg/mL) for 3 h. Puncta and cells were counted manually in a blind analysis. Over

200 cells per genotype were quantified in independent biological replicates (n=3). The error bars indicate the standard error of the mean. The strains were generated by Jasmin Schäfer, Oliver Pajonk and me.

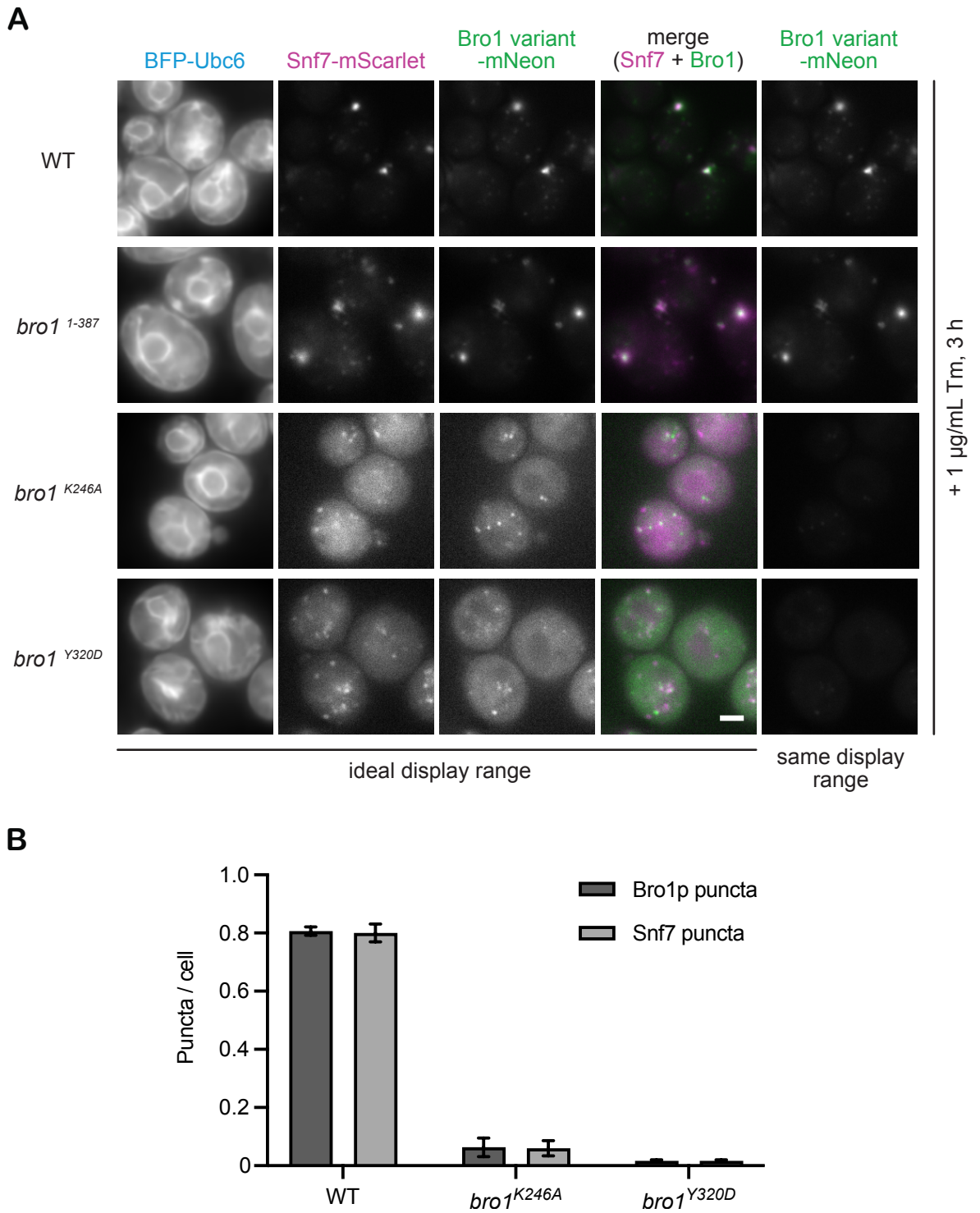

Figure 6: Bro1 point mutants bro1^{K246A} and bro1^{Y320D} show decreased recruitment efficiency to ER clusters upon ER stress.

A: Fluorescence microscopy images of cells stably expressing the general ER marker BFP-Ubc6, Snf7-mScarlet-i from the *VPS24* promoter and different Bro1 variants tagged with mNeonGreen. Exponentially growing cells were treated with tunicamycin (Tm) (1 µg/mL) for 3 h. The mNeonGreen signal is shown in two different display ranges to portray both the signal distribution of the different Bro1 variants (ideal display range) and the relative intensities of the signal between variants (same display range, comparable between variants). The scale bar

indicates 2 µm. The strains were generated by Oliver Pajonk and me.
B: Quantification of Snf7-mScarlet-i puncta and puncta of mNeonGreen-tagged Bro1 variants at ER clusters per cell in strains with different Bro1 variants after treatment with tunicamycin (1 µg/mL) for 3 h. Puncta and cells were counted manually in a blind analysis. Over 200 cells per genotype were quantified in independent biological replicates (n=3). The error bars indicate the standard error of the mean. The strains were generated by Oliver Pajonk and me.

I then studied the effect of the different Bro1 variants on Snf7 puncta formation in cells that also stably expressed an ER marker and Snf7-mNeonGreen from the *VPS24* promoter. After 3 h of tunicamycin treatment, stressed cells with full-length wildtype Bro1p showed prominent Snf7-mNeonGreen puncta at ER clusters with a ratio of around 0.9 puncta per cell (Fig. 5B). Cells with bro1$^{1\text{-}387}$ still had Snf7 puncta at ER clusters. However, they appeared weaker in many cases and were much more disperse, preventing a proper quantification (Fig. 5A). The respective ER clusters were more variable in size and more dispersed all over the ER. Thus, in presence of the Bro1 domain, Snf7 was still recruited to ER clusters, but the defined morphology of the clusters and puncta seemed to require the remaining parts of Bro1p. The K246A and Y320D point mutations almost completely abolished Snf7 recruitment to ER clusters, with less than 0.05 puncta per cell remaining (Fig. 5B). ER clusters were still observed in these cells, but they appeared less defined and were rarely associated with Snf7-mNeonGreen puncta.

To determine whether these mutations only interfered with Snf7 recruitment to ER clusters, or whether they affected the localization of Bro1 itself, I repeated the same experiment using cells stably expressing the Bro1 variants tagged with mNeonGreen, an ER marker and Snf7-mScarlet-i from the *VPS24* promoter. Snf7 and wildtype Bro1p colocalized at ER clusters upon ER stress, as Oliver Pajonk had shown previously (Fig. 6A; Pajonk, PhD dissertation, 2025). I observed that bro1$^{1\text{-}387}$-mNeonGreen also colocalized with Snf7 at ER clusters in the same disperse manner as observed above. However, both Bro1 point mutants, bro1^{K246A}-mNeonGreen and bro1^{Y320D}-mNeonGreen, remained mostly cytosolic with some endosomal puncta and only in a few rare cases colocalized with Snf7-mScarlet-i at ER clusters. The ratio of Bro1 variant puncta per cell mimicked the ratio of Snf7 puncta per cell, showing that the K246A and Y320D point mutations in Bro1 impaired both Bro1 and Snf7 recruitment to ER clusters during ER stress (Fig. 6B).

The fact that bro1^{K246A}-mNeonGreen and bro1^{Y320D}-mNeonGreen still associated with endosomal puncta during ER stress suggested that their role in multivesicular body formation is not affected by the mutations. Moreover, wildtype Bro1p, as well as the two point mutants showed a similar distribution in the cytosol and on endosomes in untreated cells (Fig. 7A).

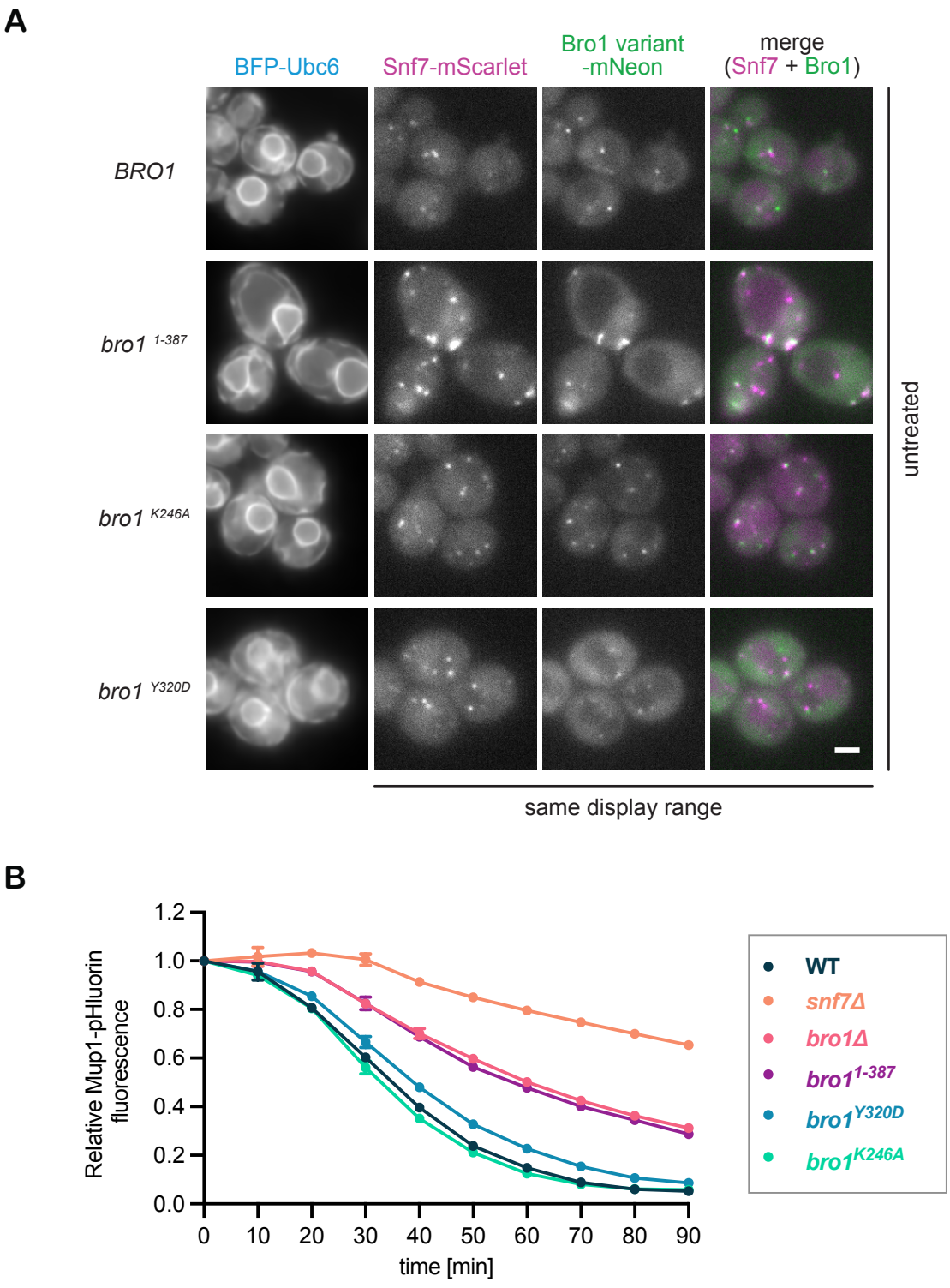

Figure 7: Bro1 variants in multivesicular body formation.

A: Fluorescence microscopy images of exponentially growing cells stably expressing the general ER marker BFP-Ubc6, Snf7-mScarlet-i from the *VPS24* promoter and different Bro1 variants tagged with mNeonGreen. All channels are shown in the same display range to appreciate the relative intensities of the signal between variants. To allow for better comparison of the signal between variants, both the mScarlet-i and mNeonGreen channels of the *bro1*$^{1-387}$ cells contain saturated pixels (less than 0.5% of pixels). The scale bar indicates 2 µm. The strains were generated by Oliver Pajonk and me.

B: Mup1-pHluorin assay of cells stably expressing Mup1-pHluorin and cytosolic BFP in presence of different Bro1 variants. Cells were grown to exponential growth phase in absence of methionine. At t=0 min, one set of cultures was supplemented with methionine inducing endocytosis of Mup1-pHluorin and its vacuolar degradation via

MVBs. The graph shows the relative Mup1-pHluorin fluorescence intensity of cells supplemented with methionine compared to cells growing in absence of methionine for the entire timeframe of the experiment. GFP autofluorescence was subtracted and Mup1-pHluorin intensities were normalized to the cytosolic BFP signal to adjust for cell size and translational capacity. Results from independent biological replicates are shown (n=3). The error bars indicate the standard error of the mean. The strains were generated by Petra Hubbe, Oliver Pajonk, Sebastian Schuck and me.

To assess the impact of the different Bro1 variants on MVB sorting more directly, I used the Mup1-pHluorin assay with cells stably expressing cytosolic BFP and Mup1-pHluorin in different Bro1 variant backgrounds. Deletion of *BRO1* partially impaired MVB sorting, although to a lesser extent than a *SNF7* deletion (Fig. 7B). Cells that only contained the Bro1 domain, bro1$^{1\text{-}387}$, showed similarly impaired MVB sorting. Fluorescence microscopy also showed that these cells appeared larger and that bro1$^{1\text{-}387}$ forms very bright and partially clustered puncta, hinting at a possible defect in MVB sorting as well (Fig. 7A). As for the Bro1 point mutants, the MVB sorting efficiency in the Mup1-pHluorin assay was similar to wildtype cells, indicating that ESCRT function at MVBs was indeed still intact, despite the point mutations (Fig. 7B). This is consistent with data from CPS sorting assays performed by (Kim et al., 2005).

Thus, the TPR-like domain and the second hydrophobic patch of Bro1p play a role in stress-induced ESCRT recruitment to ER clusters, but not in MVB sorting. The K246A mutation was proposed to have a destabilizing effect on the whole TPR-like domain, whereas the Y320D mutation might abolish an interaction interface with a yet unknown interaction factor of Bro1p (Kim et al., 2005).
Therefore, the point mutants bro1^{K246A} and bro1^{Y320D} can serve as tools to uncouple the ESCRT function at the ER during stress from one of the major other ESCRT-mediated processes in MVB formation.

3.2. Proximity-dependent biotinylation using Bro1p-TurboID to identify proteins involved in ESCRT recruitment and function

3.2.1. Establishing the method and proof-of-principle

Bro1p is essential for Snf7 recruitment and colocalizes with Snf7 at ER clusters during stress. However, both Bro1p and Snf7p are soluble proteins and need to be targeted to the ER membrane, a step which likely involves additional factors. Furthermore, it remained unclear what the function of the ESCRT machinery at ER clusters could be.
Thus, the next step was to systematically identify other factors involved in ESCRT recruitment and their function at ER clusters. Whereas genetic screens prior to this study determined genes that are important for Snf7 recruitment (Pajonk, PhD dissertation, 2025), I used a proximity-dependent biotinylation approach coupled to mass spectrometry (PDB-MS) to identify proteins enriched at ER clusters during ER stress. For this purpose, I made use of the fact that Bro1p, which can be endogenously tagged without impacting its function, is also present at ER clusters. More specifically, I

tagged Bro1p endogenously with a TurboID tag (Fig. 8A). This tag is a version of the promiscuous biotin ligase BirA* and had been engineered from the initial BioID tagfor a more efficient biotinylation of proximity partners (Choi-Rhee et al., 2004; Roux et al., 2012; Branon et al., 2018). Due to its enhanced labelling efficiency on a timescale of minutes and its high activity at 30°C, it is ideal for use in *S. cerevisiae*. PDB-MS using the TurboID tag has been shown to be an efficient tool for identification of proximity partners in fission yeast (Larochelle et al., 2019). Activated biotin is attached to proteins coming into proximity of Bro1p-TurboID (Fig. 5A).

During my Master thesis, I set up this method and performed a pilot run as a proof-of-principle. I generated a strain expressing endogenously tagged Bro1p-TurboID-3xmyc (hereafter: Bro1p-TurboID) in a background with Snf7-mNeonGreen expressed from the *VPS24* promoter to stabilize Snf7 puncta at ER clusters during ER stress and thus increase the probability of biotinylating proximity partners. I showed that tagging Bro1p with the TurboID tag did not interfere with Snf7 recruitment efficiency to the ER. Also, I was able to detect self-biotinylation of Bro1p-TurboID by Western Blot, as proposed before (Roux et al., 2012; Branon et al., 2018), confirming its enzymatic activity. Since ER stress induced by tunicamycin led to a Vps27p-dependent degradation of Bro1p, presumably via microautophagy (Hatakeyama 2019, Hatakeyama and Virgilio 2019), I included a *VPS27* deletion in the PDB-MS strain. Lastly, I deleted the vacuolar proteases Pep4p and Prb1p to reduce ongoing post-lysis degradation of proximity partners over the duration of the pull-down (Lis Albert, Master Thesis, 2020).

I then established the pull-down of biotinylated proteins with streptavidin-coupled beads, adapting protocols from Schopp and Béthune, 2018, and scaled up the procedure to achieve an appropriate yield in the eluate fractions to be analyzed by mass spectrometry. In collaboration with the ZMBH Mass Spectrometry Facility, I performed a PDB-MS pilot run with one biological replicate of untreated and tunicamycin-treated cells of the PDB strain and was able to detect proteins enriched in proximity of Bro1p during ER stress, confirming that this approach was suitable to identify proximity partners of Bro1p (Lis Albert, Master Thesis, 2020).

3.2.2. PDB-MS in triplicates

In order to gain a comprehensive understanding of proteins that come into proximity of Bro1p upon ER stress at ER clusters, I further optimized the PDB-MS procedure during my PhD and repeated it in biological triplicates. To ensure for identification of proximity partners specific to ESCRT recruitment to and function at ER clusters during stress, I added a *CHM7* deletion to the PDB strain to prevent known ESCRT functions at the nuclear envelope (Webster et al., 2016). Thus, the final PDB-MS strain background included endogenously tagged Bro1p-TurboID, Snf7-mNeonGreen expressed from the *VPS24* promoter and deletions of *VPS27*, *PEP4*, *PRB1* and *CHM7*.

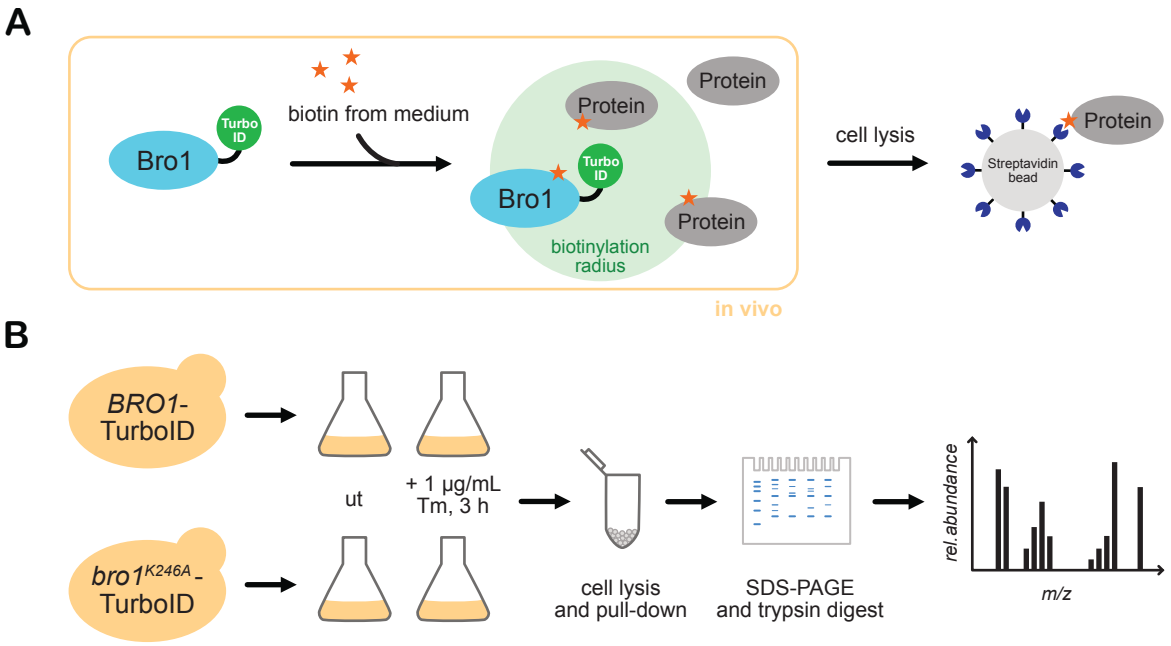
A
Bro1
Turbo ID
biotin from medium
Protein
Protein
Bro1
Turbo ID
Protein
biotinylation radius
in vivo
cell lysis
Streptavidin bead
Protein
B
BRO1-TurboID
bro1K246A-TurboID
ut
+ 1 µg/mL Tm, 3 h
cell lysis and pull-down
SDS-PAGE and trypsin digest
rel.abundance
m/z
C
BRO1-TurboID
bro1K246A-TurboID
1 µg/mL Tm, 3 h
-
+
-
+
Inp Elu Inp Elu Inp Elu Inp Elu
Snf7-mNeon
D
WT Bro1
Tm vs. ut
bro1K246A
Tm vs. ut
-log10(p-value)
log2 fold change
log2 fold change
E
Overlap of candidates
WT Bro1 total (148)
bro1K246A total (24)
128
20
4
WT Bro1 only
bro1K246A only
F
WT Bro1
ESCRT
ER proteins
Rim proteins
COPI
COPII
Ret2
Rim101
Ero1
Rim20
Sec63
Vta1
Sec21
Kar2
Sec24
Sec27
Heh1
Snf7
Sec16
Rtn1
Vps60
Sec28
Did2
Vps4
-log10(p-value)
log2 fold change

Figure 8: Proximity-dependent biotinylation by Bro1p-TurboID coupled to mass spectrometry to identify proteins involved in ESCRT recruitment to and function at ER clusters.
A: Schematic representation of the biotinylation of proximity partners by Bro1p-TurboID inside yeast cells. The TurboID tag, an engineered version of the promiscuous biotin ligase BirA*, converts biotin from the medium into biotinoyl-5'-AMP, which reacts with proteins coming into proximity of Bro1p-TurboID during the duration of the experiment (Branon et al., 2018). The biotinylation radius extends around 10 nm around the tag. Proteins entering this radius can be biotinylated, if not sterically obstructed, whereas proteins located further away will not be biotinylated. After cell lysis, biotinylated proteins can be pulled down by streptavidin beads.
B: Workflow of the proximity-dependent biotinylation experiment linked to mass spectrometry (PDB-MS). Cells stably expressing wildtype Bro1p-TurboID or bro1^{K246A}-TurboID, as well as Snf7-mNeonGreen from the *VPS24* promoter in a *VPS27*, *PEP4*, *PRB1* and *CHM7* deletion background were used. Exponentially growing cells were treated with tunicamycin (Tm) (1 µg/mL) for 3 h or left untreated. Cells were harvested and lysed. The cell lysates were used as input for a pull-down with streptavidin-coated beads. The eluates from the pull-down containing biotinylated proteins were loaded on SDS-PAGE gels. In-gel trypsin digestion and LC-MS/MS were performed by Thomas Ruppert, Sabine Merker and Marcin Luzarowski of the ZMBH Mass Spectrometry Facility.
C: Western Blot of Snf7-mNeonGreen from a biotinylation assay with cells stably expressing wildtype Bro1p-TurboID or bro1^{K246A}-TurboID, as well as Snf7-mNeonGreen from the *VPS24* promoter in a *VPS27*, *PEP4* and *PRB1* deletion background. Exponentially growing cells were treated with tunicamycin (Tm) (1 µg/mL) for 3 h or left untreated. Biotinylated proteins were pulled down from cell lysates using streptavidin-coupled beads. Input and eluate samples were loaded. Membranes were probed against mNeonGreen. The strains were generated by Oliver Pajonk and me.
D: Volcano plots of two-sided non-paired two-sample t-tests (FDR=0.05, 500 randomizations, S0=0.2) between tunicamycin-treated vs. untreated wildtype (WT) Bro1p strain (right) and tunicamycin-treated vs. untreated bro1^{K246A} point mutant strain (left). The data is from the PDB-MS experiment with cells stably expressing wildtype Bro1p-TurboID or bro1^{K246A}-TurboID, as well as Snf7-mNeonGreen from the *VPS24* promoter in a *VPS27*, *PEP4*, *PRB1* and *CHM7* deletion background explained in B. The output from the MaxQuant MS analysis by Georg Borner was used for further analysis using the Perseus software by me. Only proteins with a logFC>0 shown, since those were considered hits, being significantly enriched in tunicamycin-treated cells versus untreated cells in proximity of Bro1 WT or K246, respectively. The volcano lines indicate the cut-off as determined by the t-test with an FDR=0.05 and an S0=0.2. Data points above the volcano line (marked in grey) are considered hits. Samples were prepared in biological triplicates (n=3).
E: Venn diagram showing the overlap of hits from wildtype Bro1p and bro1^{K246A}. The hitlist of wildtype Bro1p included 148 proteins enriched in proximity of Bro1p upon tunicamycin treatment, 20 of which overlapped with hits from bro1^{K246A}, which in total included 24 proteins enriched in its proximity upon ER stress. The final hitlist of this experiment comprised all 128 hits that were only identified for wildtype Bro1p.
F: Volcano plot of two-sided non-paired two-sample t-test (FDR=0.05, 500 randomizations, S0=0.2) between tunicamycin-treated vs. untreated wildtype Bro1p strain illustrating the final hit list (dark grey and colored data points). Some datapoints were colored according to category: ESCRT machinery, ER-associated proteins, Rim pathway proteins, COPI components and COPII components. The remaining hits are colored in dark grey.

Since I established that ESCRT function at the ER can be uncoupled from MVB sorting by using point mutants of Bro1p, I used bro1^{K246A} tagged with the TurboID tag in the PDB-MS strain background as a control strain to account for proteins that are enriched in proximity of Bro1p upon ER stress at MVBs or other locations, and are thus not specific to ER clusters. A biotinylation assay approach using these two TurboID tagged Bro1 variants revealed that ER stress induced an increase in the biotinylation of Snf7 by Bro1p but not by bro1^{K246A}, thus justifying the use of the K246A mutant as specificity control (Fig. 8C).

For the PDB-MS experiment, cells of the wildtype Bro1p-TurboID and control bro1^{K246A} -TurboID strains were grown exponentially (Fig. 8B). One set of cultures was treated with 1 µg/mL tunicamycin for 3 h, whereas the other was left untreated. During this time, the TurboID tag was able to biotinylate proximity partners of Bro1p or bro1^{K246A} using the biotin present in the medium (2 µg/L) (Fig. 5A). After harvesting and lysing the cells, I performed a pull-down with streptavidin-coupled beads to isolate biotinylated proteins from the lysates (Fig. 8B). Triplicate mass spectrometry measurements were performed in collaboration with Thomas Ruppert, Sabine Merker and Marcin Luzarowski of the ZMBH Mass Spectrometry Facility (Fig. 8B). The initial data analysis by MaxQuant was performed by our collaborator Georg Borner. I performed the subsequent data analysis using the Perseus software. The data was filtered to remove contaminants and proteins only identified with post-translational modifications. Only proteins identified in all three replicates in at least one strain and condition were retained. I grouped the data according to strain (WT Bro1 or control) and condition (untreated or Tm-treated) and imputed missing values using the imputation procedure of the Perseus software. I performed two-sided non-paired two-sample t-tests with the data from tunicamycin-treated versus untreated WT Bro1p strain and from tunicamycin-treated versus untreated mutant bro1^{K246A} strain. Proteins enriched in proximity of Bro1p were defined by a positive log fold change and by an FDR below 0.05 with a S0 value of 0.2. This resulted in hitlists of proteins enriched in proximity of WT (148 proteins) or mutant Bro1 (24 proteins) during ER stress (Fig. 8D, dark grey data points, Supplementary Tables S1-S3). By removing the proteins that are shared between the two hitlists from the hitlist of WT Bro1, I determined the final hitlist of 128 proteins specifically enriched in proximity of WT Bro1p at ER clusters upon ER stress (Fig. 8E and F, Supplementary Table S1).

The hits were assigned to the following categories: ESCRT machinery, ER-associated, Rim pathway, ER-Golgi trafficking and Golgi internal trafficking (including COPI and COPII components), calcium signaling, the ubiquitin-proteasome system, chaperones and others (Fig. 8F and Table 1). Several categories of hits overlapped with categories from the genetic screens, especially hits involved in ER-Golgi trafficking, such as components of the COPI and COPII machineries (Pajonk, PhD dissertation, 2025). This suggests that these factors are not only enriched in proximity of ER clusters upon stress, but that their deletion also functionally impacts Snf7 recruitment.

The ESCRT machinery hits of the PDB-MS included Snf7p, which was expected to be enriched in proximity of Bro1p (Fig. 8C), as well as other ESCRT-III components, ESCRT-associated proteins and the AAA+ - ATPase Vps4p. ESCRT-0, -I and -II components were not found, consistent with the fact that upstream ESCRTs are not required for Snf7 recruitment to ER clusters.

The fact that several ER-associated proteins were among the hits served as a validation for the ER localization of the process. Oliver Pajonk had shown that Rtn1p-mCherry and Sec63p-mScarlet-i colocalized with Snf7-mNeonGreen at ER clusters upon ER stress.

Table 1. Summary of hits from the PDB-MS experiment categorized according to their location or function.

Category	Hits from PDB-MS
ESCRT machinery (6)	Snf7, Vps4, Vps60, Vta1, Did2, Src1
ER-associated (5)	Rtn1, Sec63, Kar2, Sec53, Ero1
Rim pathway (2)	Rim20, Rim101
ER-Golgi and Golgi internal trafficking (11) > incl. COPI components (5) > incl. COPII components (2)	Gyp1, Sgm1, Gyp5, Gga1 Ret2, Sec21, Sec27, Sec28, Arf1 Sec16, Sec24
Calcium signaling (2)	Cmk1, Rcn1
Ubiquitin-proteasome system (11)	Uba1, Cue3, Rpn1, Rpn5, Add66, Rup1, Ubp1, Ubp2, Doa1, Bre1, Rpt1
Redox signaling (3)	Grx1, Trx2, Mxr1
Chaperones (5)	Cct4, Ssa1, Cdc37, Hsp78, Vtc2
Others (92)	(complete list in Supplementary Table S1)

3.3. Validation of the PDB-MS hits

I set out to validate some of the hits by determining whether they colocalize with Snf7 at ER clusters, as well as assessing their effect on Snf7 recruitment to the ER. Whereas some proteins, like the UPS components or calcium signaling hits, could not be verified, others were validated and provided insights into ESCRT recruitment mechanism and ESCRT function at ER clusters. Specifically, the role of Rim proteins and of proteins of the ER-Golgi interface, in particular COPI components, were studied in the following.

3.3.1. Rim20p is required for Snf7 recruitment to ER clusters and shows partial redundancy to Bro1p

The PDB-MS experiment showed that some proteins of the Rim pathway, namely Rim20p and Rim101p, were enriched in proximity of Bro1p upon ER stress. The canonical Rim pathway senses changes in external pH at the plasma membrane in different fungi (Peñalva et al., 2014). A signaling platform is formed by the ESCRT machinery and Rim20p, which eventually mediates cleavage of Rim101p. The

generated cleavage product of Rim101p acts as a transcription factor and induces a transcriptional response to the pH change (Li & Mitchell, 1997).

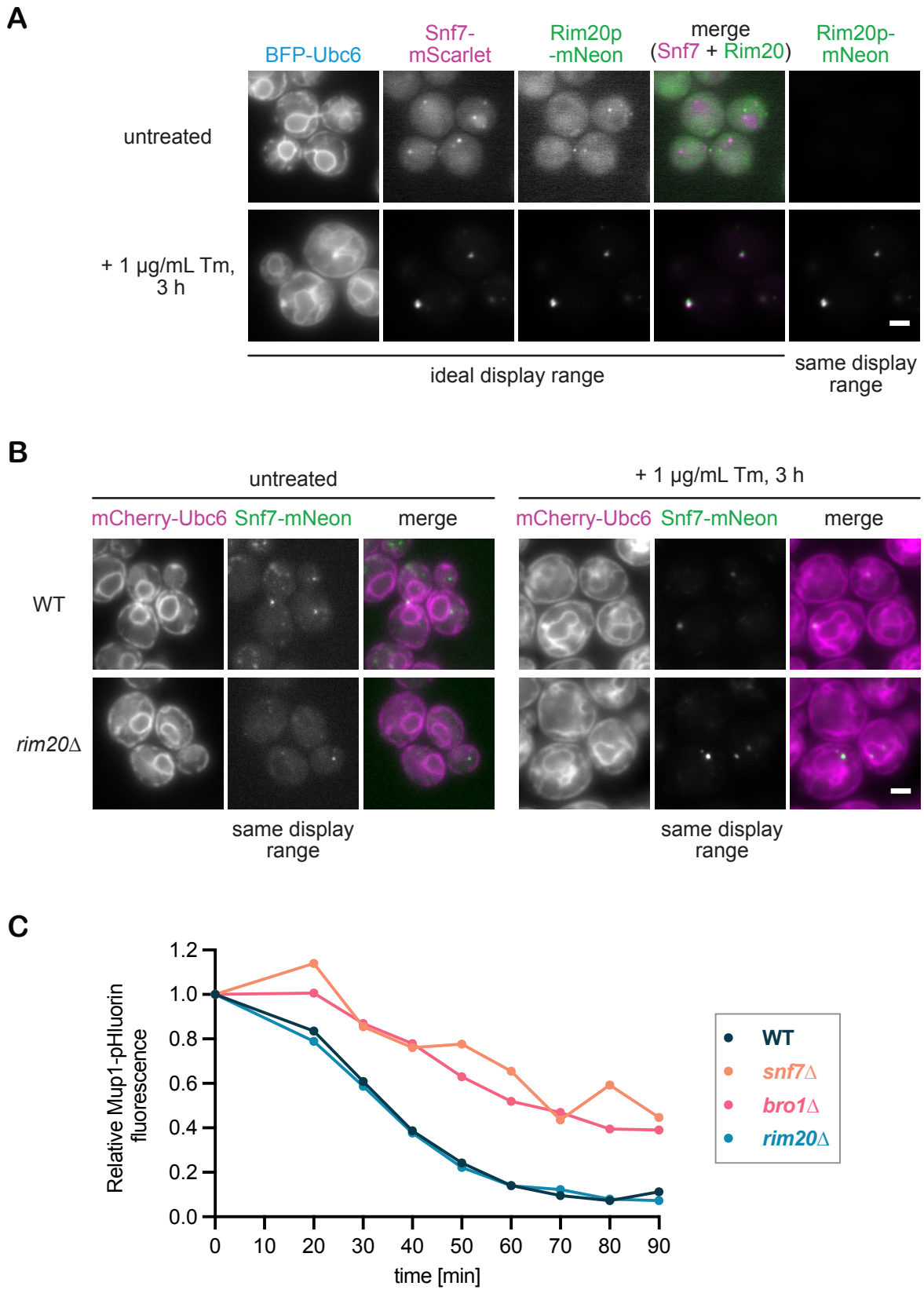

Figure 9: Rim20p colocalizes with Snf7 at ER clusters and is required for Snf7 recruitment to ER clusters but not MVB sorting.

A: Fluorescence microscopy images of cells stably expressing the general ER marker BFP-Ubc6 and Rim20p-mNeonGreen, as well as Snf7-mScarlet-i expressed from the *VPS24* promoter. Exponentially growing cells were treated with tunicamycin (Tm) (1 µg/mL) for 3 h or left untreated. The Rim20p-mNeonGreen signal is shown in two different display ranges to portray both the signal distribution in each condition (ideal display range) and the relative intensities of the signal between conditions (same display range, comparable between untreated and treated). The scale bar indicates 2 µm. This observation was originally made by Oliver Pajonk. The strain was generated by Oliver Pajonk .
B: Fluorescence microscopy images of cells stably expressing the general ER marker mCherry-Ubc6 and Snf7-mNeonGreen from the *VPS24* promoter in a wildtype or *RIM20* deletion background. Exponentially growing cells were treated with tunicamycin (Tm) (1 µg/mL) for 3 h or left untreated. The same display range is shown for the Snf7-mNeonGreen channel to appreciate the relative signal intensities between genotypes (comparable within untreated samples and treated samples). To allow for better comparison of the signal between variants, the image of *rim20Δ* cells after tunicamycin treatment contains saturated pixels (less than 0.05% of pixels). The scale bar indicates 2 µm. This observation was originally made by Oliver Pajonk. The strains were generated by Jasmin Schäfer and Sebastian Schuck.
C: Mup1-pHluorin assay of cells stably expressing Mup1-pHluorin and cytosolic BFP in wildtype cells and *SNF7*, *BRO1* or *RIM20* deletion strains. Cells were grown to exponential growth phase in absence of methionine. At t=0 min, one set of cultures was supplemented with methionine inducing endocytosis of Mup1-pHluorin and its vacuolar degradation via MVBs. The graph shows the relative Mup1-pHluorin fluorescence intensity of cells supplemented with methionine compared to cells growing in absence of methionine for the entire timeframe of the experiment. GFP autofluorescence was subtracted and Mup1p-pHluorin intensities were normalized to the cytosolic BFP signal to adjust for cell size and translational capacity. Results from one biological replicate are shown. Data from the 10 min timepoint was left out due to technical issues of the measurement. The measurement for the *snf7Δ* strain showed atypical variations, presumably also due to an issue during sample preparation or technical issues of the measurement. The strains were generated by Petra Hubbe, Oliver Pajonk, Sebastian Schuck and me.

I could show that deletion of *RIM101* did not affect Snf7 recruitment to the ER (data not shown). Since Rim101p was highly enriched in proximity of Bro1p in the PDB-MS and Oliver Pajonk showed that Rim101p-mNeonGreen colocalized with Snf7-mScarlet-i at ER clusters, we asked whether ER stress induces a transcriptional response via Rim101p from ER clusters. However, an RNA sequencing analysis, performed by Carlos Martin de Hijas during his Master Thesis, did not reveal any gene induction or repression mediated by Bro1-dependent Rim101p signaling during stress.

In the canonical Rim pathway, the ESCRT machinery adopts a scaffolding role for the Rim proteins instead of fulfilling its usual membrane remodeling role (Peñalva et al., 2014). Within the so-formed signaling platform, Rim20p interacts with Snf7p and Rim101p (Xu & Mitchell, 2001). Interestingly, Rim20p is a homologue of Bro1p with an N-terminal Bro1 domain, but a different C-terminus.

Oliver Pajonk showed that Rim20p-mNeonGreen colocalized with Snf7-mScarlet-i at ER clusters during ER stress (Fig. 9A). Additionally, he found that deletion of *RIM20* impaired the recruitment of Snf7 to the ER during stress (Fig. 9B). The cells showed some very bright Snf7 puncta, but rarely at ER clusters. I later quantified that Snf7 puncta at ER clusters were reduced to around 0.2 puncta per cell in absence of Rim20p (Fig. 10B). Thus, Rim20p promotes Snf7 recruitment to ER clusters.

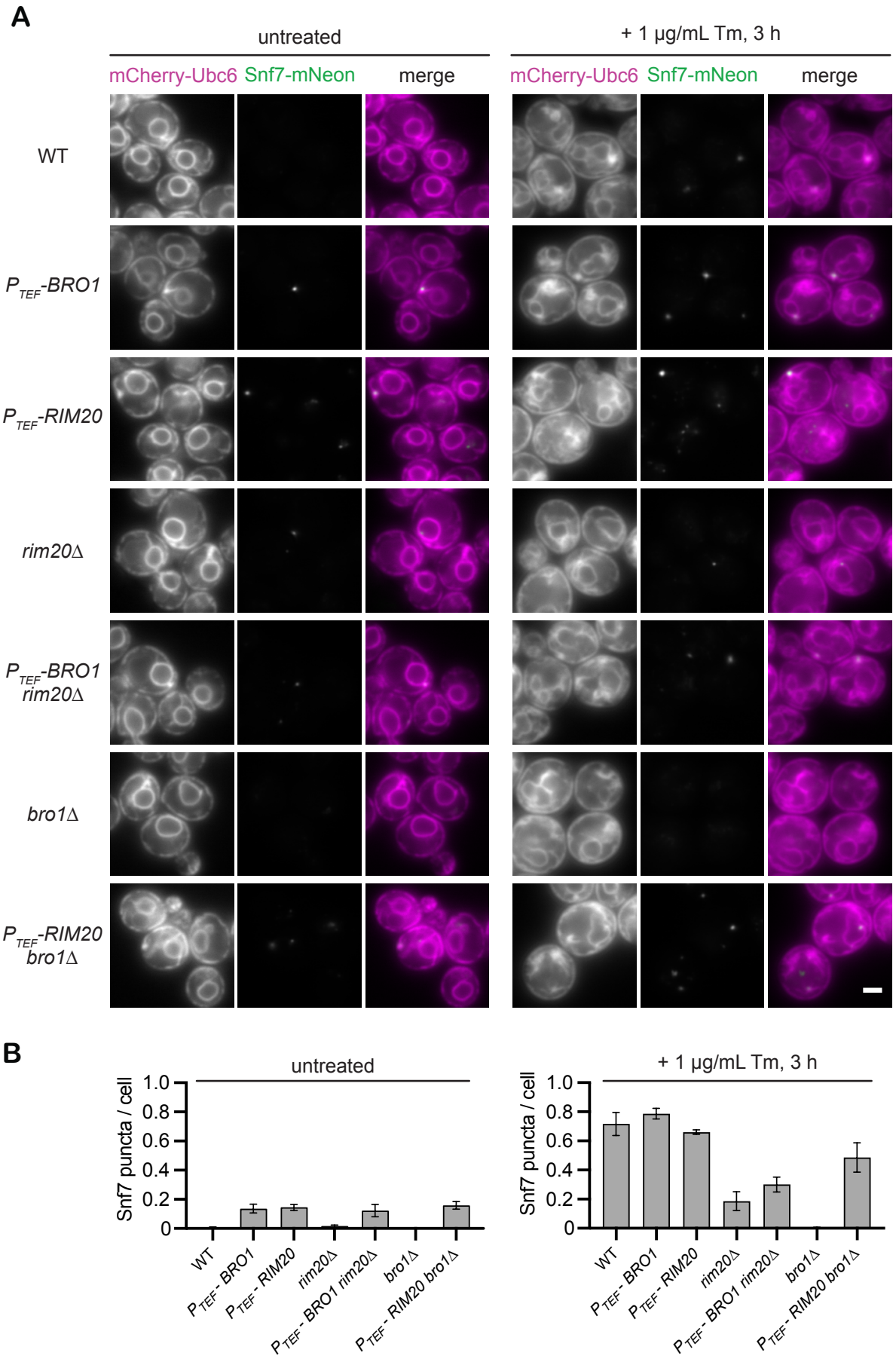

Figure 10: Rim20p and Bro1p are partially redundant in Snf7 recruitment to ER clusters.

A: Fluorescence microscopy images of cells stably expressing the general ER marker mCherry-Ubc6 and Snf7-mNeonGreen from the *VPS24* promoter in different *BRO1* and *RIM20* overexpression and deletion backgrounds of *RIM20* and *BRO1*. Exponentially growing cells were treated with tunicamycin (Tm) (1 µg/mL) for 3 h or left untreated. The same display range is shown for the Snf7-mNeonGreen channel for both untreated and tunicamycin-treated cells to appreciate the relative signal intensities between genotypes across conditions. The ideal display range for each genotype is shown for the ER marker. The scale bar indicates 2 µm. The strains were generated by Jasmin Schäfer, Sebastian Schuck and me.
B: Quantification of Snf7-mNeonGreen puncta at ER clusters per cell in strains with *BRO1* and *RIM20* overexpression and deletion backgrounds in untreated cells or after treatment with tunicamycin (1 µg/mL) for 3 h. Puncta and cells were counted manually in a blind analysis. Over 200 cells per genotype were quantified in independent biological replicates (n=3). The error bars indicate the standard error of the mean. The strains were generated by Jasmin Schäfer, Sebastian Schuck and me.

The remaining puncta that were observed localized to the nuclear envelope, to regions devoid of ER clusters. These possibly arise due to a bigger pool of tagged Snf7 available for ESCRT-mediated processes at the nucleus, once *RIM20* deletion releases it from ER clusters. However, this effect was not seen when *BRO1* was deleted.

Even though Rim20p is a homologue of Bro1p and works together with the ESCRT machinery in the context of the Rim pathway, it has not been studied in other ESCRT-mediated processes. Since it participates in Snf7 recruitment to ER clusters, I wondered whether it might also be involved in MVB sorting. Thus, I performed the Mup1-pHluorin assay with cells expressing Mup1-pHluorin and cytosolic BFP in the wildtype background, as well as *SNF7*, *BRO1* or *RIM20* deletion backgrounds to compare effects of these deletions. While the *SNF7* and *BRO1* deletions both impaired MVB sorting, as shown previously, *RIM20* deletion did not affect sorting (Fig. 9C). Thus, Rim20p is not required for MVB sorting but is required for proper Snf7 recruitment to the ER.

Bro1p and Rim20p both have an important role in Snf7 recruitment to ER clusters. Oliver Pajonk showed that Rim20p colocalized with Bro1p at ER clusters. He found that Rim20p recruitment requires Bro1p and endogenous Snf7p, but not upstream ESCRTs. Both Rim20p and Bro1p have a Bro1 domain with the two hydrophobic patches. In case of Bro1p, the first hydrophobic patch mediates interaction with Snf7p (Kim et al., 2005). It is conceivable that the same holds true for Rim20p, as its interaction with Snf7p also involves its Bro1 domain (Xu et al., 2004). This brought up the question whether Rim20p and Bro1p act redundantly in Snf7 recruitment to ER clusters, perhaps because the total amount of Bro1 domain protein determines Snf7 recruitment efficiency. To test this idea, I investigated whether overexpression of one Bro1 domain protein could rescue the loss of the other. I created strains that overexpressed either *RIM20* or *BRO1* by exchanging their endogenous promoter with the exceptionally strong *TEF* promoter. The cells were also expressing an ER marker and Snf7-mNeonGreen from the *VPS24* promoter either in a wildtype background, to check for the effect of the overexpression itself, or in a *RIM20* or *BRO1* deletion background, to check for a possible rescue of Snf7 recruitment. I studied the effect of the different combinations of overexpressions and deletions in untreated cells and cells

treated for 3 h with tunicamycin (1 µg/mL) and quantified Snf7 puncta at ER clusters.
In stressed cells, the overexpression of either Bro1p or Rim20p led to a similar number of Snf7 puncta per cell as in the wildtype (Fig. 10B). However, Snf7 puncta and ER clusters often appeared brighter and more defined (Fig. 10A). Rim20 overexpression resulted in some additional bright Snf7 puncta in the cytosol, not associated with ER clusters (Fig. 10A). Deletion of *RIM20* led to the aforementioned brighter puncta at the nuclear envelope, whereas Snf7 recruitment to ER clusters was strongly reduced to around 0.2 puncta per cell (Fig. 10). Also, the number of ER clusters was reduced. Overexpression of *BRO1* in the *RIM20* deletion cells led to a slight increase of the number of ER clusters and Snf7 puncta (around 0.3 puncta per cell), but did not show a full rescue. Intriguingly, overexpression of *RIM20* in a *BRO1* deletion strain increased the amount of Snf7 puncta from almost none in a *BRO1* deletion to around 0.5 puncta per cell. Although Snf7 recruitment did not reach the same efficiency as in wildtype cells, it was a notable increase, showing that *RIM20* was able to partially rescue the *BRO1* deletion phenotype. *RIM20* overexpression again led to formation of additional bright Snf7 puncta in the cytosol, whereas this was not the case for *BRO1*, suggesting that Rim20p has other non-redundant functions related to Snf7.
All in all, Bro1p and Rim20p are both required for proper Snf7 recruitment to ER clusters upon ER stress and have at least partially redundant functions in this recruitment.

Interestingly, this experiment also revealed that overexpression of *BRO1* and *RIM20* induced the formation of ER clusters and Snf7 puncta in untreated cells, both in a wildtype and the deletion backgrounds (Fig. 10). Even though Snf7 puncta formed at a lower rate than in stressed cells, with around 0.15 puncta per cell, and puncta often appeared slightly weaker than the ones observed in stressed cells, I could show that ER cluster formation and ESCRT recruitment can be induced in absence of ER stress by overexpression of Bro1 domain proteins. This finding underlines the essential role that Rim20p and Bro1p play at ER clusters and for Snf7 recruitment.

Since endogenously expressed Rim20p and Bro1p both colocalize with Snf7 at ER clusters, I next investigated whether the localization of the individual proteins is affected by overexpression of the respective other Bro1 domain protein. Therefore, I imaged cells stably expressing an ER marker, either Bro1p or Rim20p endogenously tagged with mNeonGreen, as well as Snf7 expressed from the *VPS24* promoter, in a wildtype background or with overexpression of either *BRO1* or *RIM20*. In untreated cells, Rim20p was present in Snf7 puncta induced by *BRO1* overexpression and vice versa (Fig. 11), suggesting that Snf7 puncta induced by overexpression of one Bro1 domain protein also involved the second one. In stressed cells, Rim20p still colocalized with Snf7 at ER clusters when Bro1p was overexpressed, but Rim20p puncta appeared much weaker than in the wildtype (Fig. 11A). A similar effect was observed for Bro1p puncta with *RIM20* overexpression (Fig. 11B). Thus, overexpression of one Bro1 domain protein partially displaced the respective other Bro1 domain protein from ER clusters.

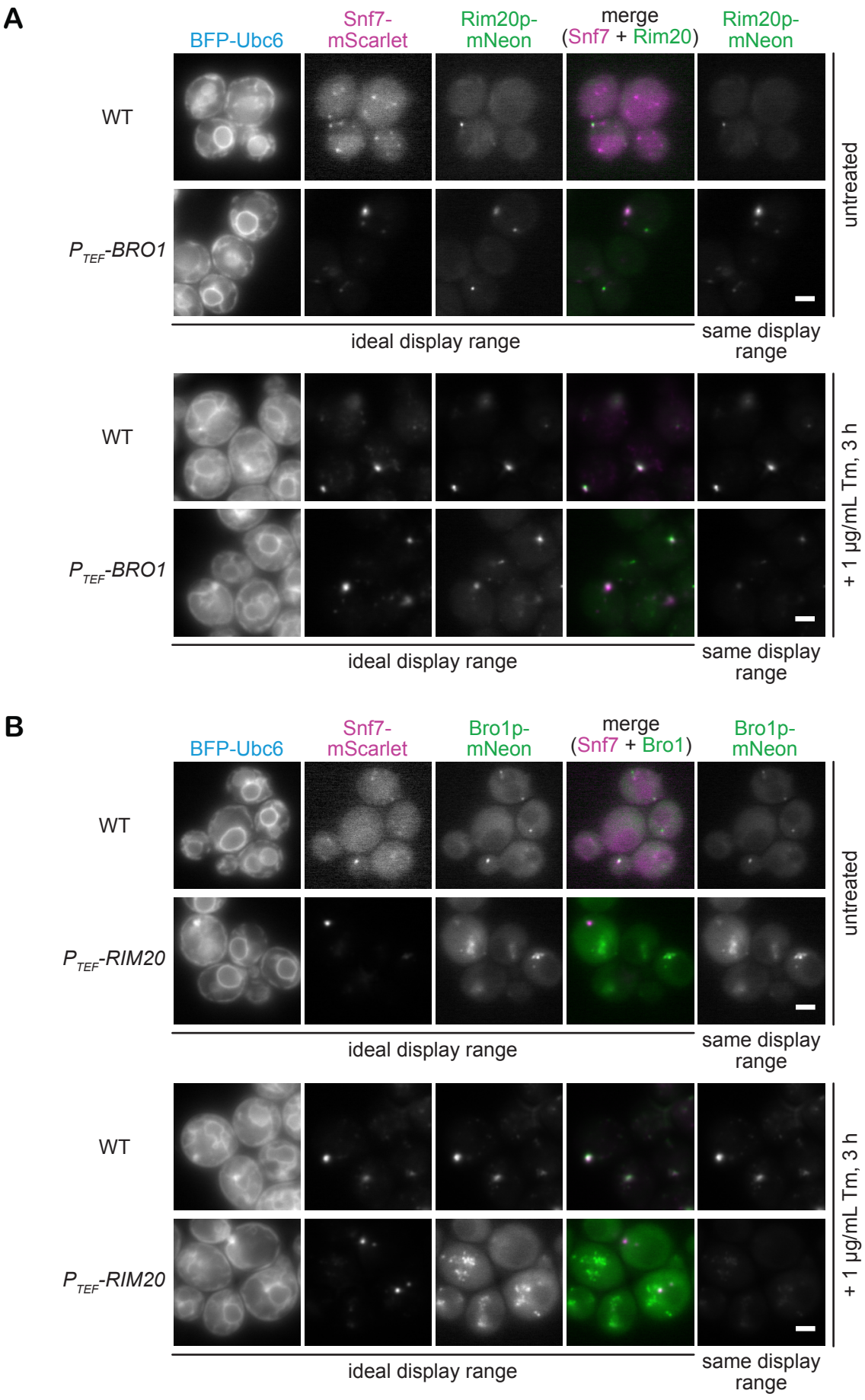

Figure 11: Overexpression of one Bro1 domain protein displaces the other from ER clusters.

A: Fluorescence microscopy images of cells stably expressing the general ER marker BFP-Ubc6 and Rim20p-mNeonGreen, as well as Snf7-mScarlet-i expressed from the *VPS24* promoter, in a wildtype or *BRO1* overexpression background. Exponentially growing cells were treated with tunicamycin (Tm) (1 µg/mL) for 3 h or left untreated. The Rim20p-mNeonGreen signal is shown in two different display ranges to portray both the signal distribution for each genotype (ideal display range) and the relative intensities of the signal between genotypes (same display range, comparable within untreated and within treated). The scale bar indicates 2 µm. The strains were generated by Oliver Pajonk and me.
B: Fluorescence microscopy images of cells stably expressing the general ER marker BFP-Ubc6 and Bro1p-mNeonGreen, as well as Snf7-mScarlet-i expressed from the *VPS24* promoter, in a wildtype or *RIM20* overexpression background. Exponentially growing cells were treated with tunicamycin (Tm) (1 µg/mL) for 3 h or left untreated. The Bro1p-mNeonGreen signal is shown in two different display ranges to portray both the signal distribution for each genotype (ideal display range) and the relative intensities of the signal between genotypes (same display range, comparable within untreated and within treated). The scale bar indicates 2 µm. The strains were generated by Oliver Pajonk and me.

Notably, apart from displacing Bro1p from ER clusters, Rim20p overexpression also resulted in a class E compartment-like distribution of Bro1p (Fig. 11B). Possibly, Rim20p has a dominant-negative effect in MVB sorting, as it can bind to Snf7p, but cannot replace Bro1p functionally at MVBs, which then turn into aberrant class E compartments. This effect was not seen for Rim20p distribution when Bro1p was overexpressed (Fig. 11A). This again implies that although there is some redundancy between Rim20p and Bro1p, their overexpression entails individual effects as well.
Taken together, Rim20p, besides Bro1p, is needed for full Snf7 recruitment to ER clusters, but not for MVB formation. Bro1p and Rim20p show partial redundancy and possibly coordinate Snf7 recruitment to ER clusters together.

3.3.2. COPI components colocalize with Snf7 at ER clusters

Another prominent category of hits from the PDB-MS experiment were COPI components. COPI proteins are involved in the retrograde transport of protein from the Golgi to the ER, as well as internal trafficking pathways between Golgi cisternae (Letourneur et al., 1994; Papanikou et al., 2015; C. K. Barlowe & Miller, 2013). Four out of seven COPI coat proteins (Ret2p, Sec21p, Sec27p, Sec28p), as well as the small GTPase Arf1p needed for COPI coat formation, were enriched in proximity of Bro1p upon ER stress (Fig. 8F, Table 1). Moreover, *COP1* was a hit in the genetic screen with the temperature-sensitive allele collection done by Oliver Pajonk complementary to the PDB-MS experiment. He could further show that Cop1p-mNeonGreen colocalized with Snf7-mScarlet-i puncta at ER clusters upon ER stress (Pajonk, PhD dissertation, 2025).
To validate the COPI hits from the PDB-MS experiment, I tagged the different coat proteins C-terminally with mNeonGreen in cells stably expressing an ER marker and Snf7-mScarlet-i from the *VPS24* promoter and investigated their localization after 3 h of tunicamycin treatment. Each COPI component showed a punctate distribution throughout the cells and often overlapped with Snf7-mScarlet-i puncta at ER clusters (Fig. 12A). Upon quantification of Snf7 puncta colocalizing with COPI components, I found

that around 60% of Snf7-mScarlet-I puncta colocalized with each of the COPI coat components, confirming the findings from the PDB-MS experiment (Fig. 12B). Paralell experiments by Oliver Pajonk demonstrated that COPI components are required for efficient Snf7 recruitment.

Thus, COPI components are present at the majority of ER clusters, implied in Snf7 recruitment and might be involved in downstream functions as well.

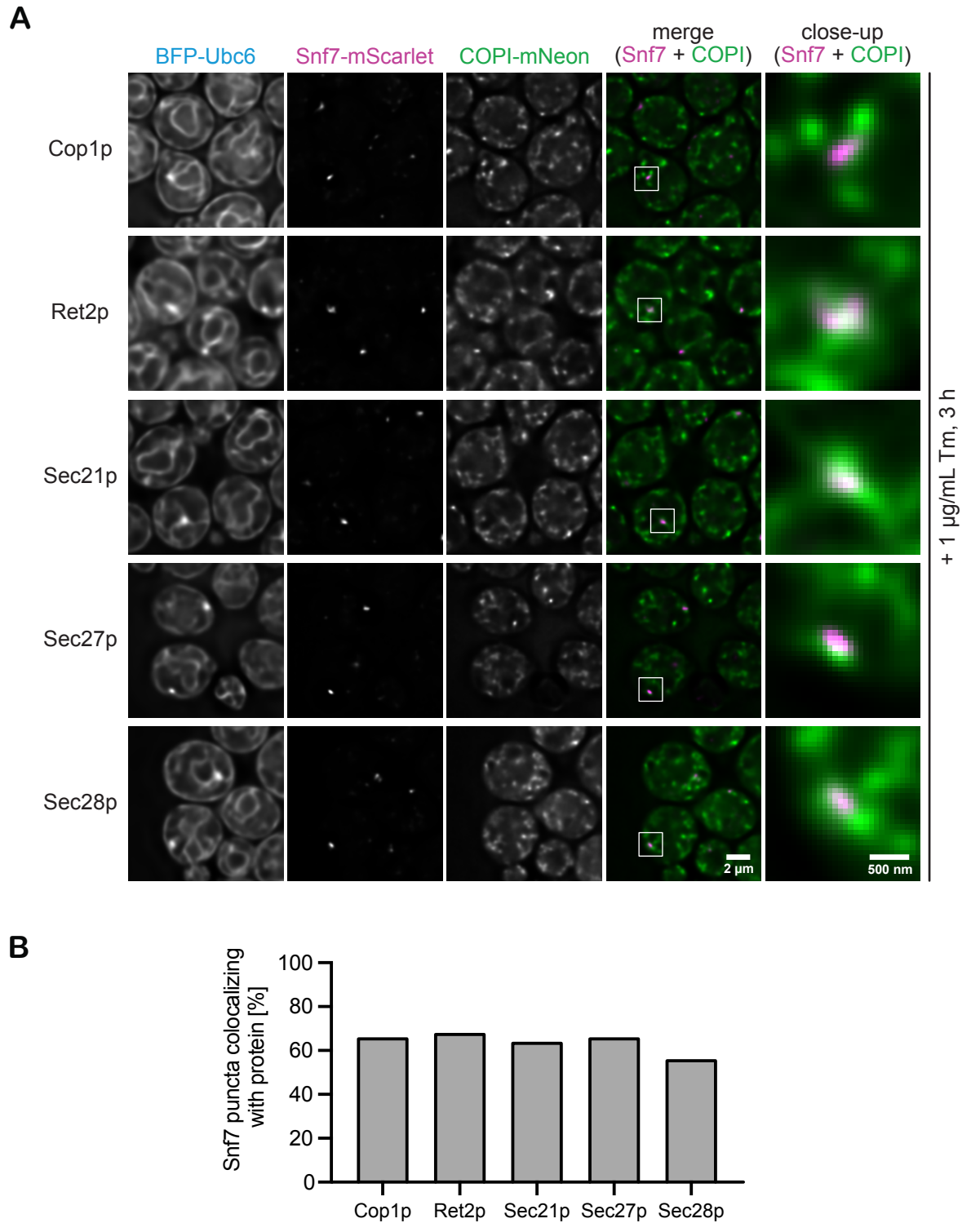

Figure 12: COPI components colocalize with Snf7 at ER clusters during ER stress.

A: Fluorescence microscopy images of cells stably expressing the general ER marker BFP-Ubc6 and different COPI components tagged with mNeonGreen, as well as Snf7-mScarlet-i from the *VPS24* promoter. Exponentially growing cells were treated with tunicamycin (Tm) (1 µg/mL) for 3 h. Images were deconvolved with the Richardson-Lucy algorithm (30 iterations with automatically determined noise level). Deconvolution leads to the appearance of some saturated pixels on the images and prevents quantitative comparison between genotypes. A close-up of a Snf7 punctum is shown as an example for each genotype. The strains were generated by Oliver Pajonk and me.
B: Quantification of colocalization between Snf7-mScarlet-i puncta at ER clusters and mNeonGreen tagged COPI components after treatment with tunicamycin (1 µg/mL) for 3 h. Colocalization was assessed manually in a blind analysis. 50 Snf7 puncta per genotype were considered. The strains were generated by Oliver Pajonk and me.

3.4. Spatial arrangement of COPI and COPII components at ER clusters

Taking together the categories of hits from the PDB-MS experiment and the genetic screens, the number of factors of the ER-Golgi interface was striking. Apart from the COPI components mentioned above, members of the Dsl1-tethering complex, which is involved in receiving COPI vesicles at the ER, were found in the genetic screens. Moreover, many components of the COPII machinery, responsible for vesicular transport from the ER to the Golgi, were part of the hitlists. Apart from the general ER export machinery, the genetic screens revealed genes related to the specific ER export of GPI-anchored proteins (GPI-AP), namely GPI-anchor remodeling enzymes and the p24 export receptor for GPI-APs. Upon validation of these hits, Oliver Pajonk could show that the export machinery for GPI-anchored proteins, COPII components and the Dsl1-tethering complex play a role in ER cluster formation and/or Snf7 recruitment to the ER upon ER stress (Pajonk, PhD dissertation, 2025).

We then set out to gain a better understanding of the spatial arrangement of the different factors at ER clusters. Oliver Pajonk found that Dsl1p, the p24 complex and Gas1, a model GPI-anchored protein, colocalized with Snf7 puncta at ER clusters (Pajonk, PhD dissertation, 2025). To further understand the relation between COPI and COPII components in the context of Snf7 puncta at ER clusters, I generated a strain stably expressing Sec24p-mNeonGreen and Ret2p-Halo, one COPII and one COPI component hit from the PDB-MS experiment, in a background with an ER marker and Snf7-mScarlet-i expressed from the *VPS24* promoter. Addition of the SiR-HaloTagLigand (HTL) allowed the observation of Ret2p in the far-red channel. Ret2p and Sec24p showed distinct punctate distributions at steady-state and after 3 h of tunicamycin treatment (Fig. 13A). The COPI component Ret2p often colocalized with Snf7 puncta upon ER stress, as observed previously, whereas the COPII component Sec24p arranged in smaller puncta around a central Snf7 punctum, creating a flower-like arrangement. Chrysafenia Papavissarion, a former rotation student, observed similar arrangements in cells expressing a different combination of COPII and COPI components, namely Sec24p-mNeonGreen and Cop1p-Halo (Fig. 13B).

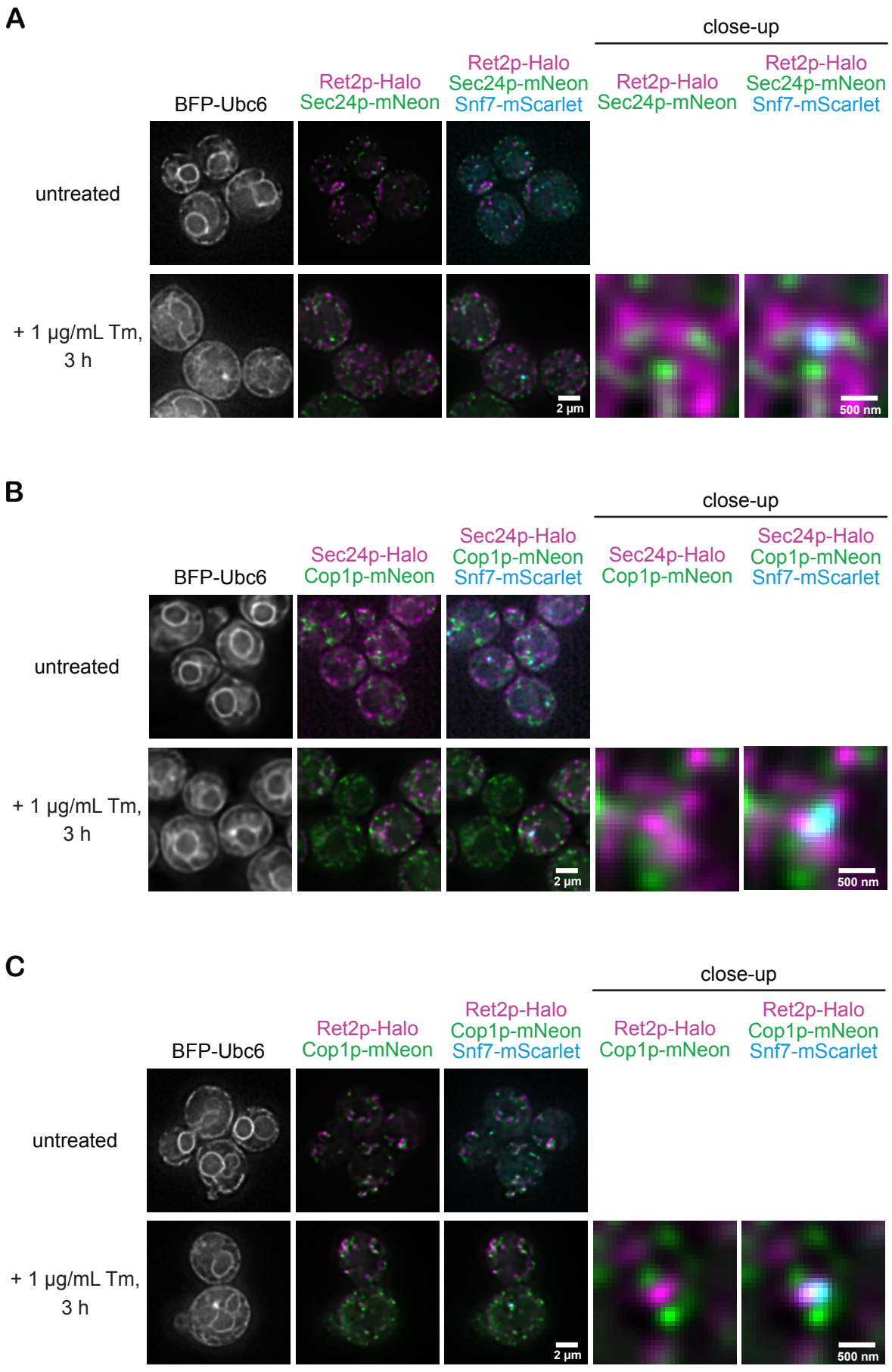

Figure 13: Spatial arrangement of COPI components, COPII components and Snf7 at ER clusters during ER stress.

A: Fluorescence microscopy images of cells stably expressing the general ER marker BFP-Ubc6, Sec24p-mNeonGreen, Ret2p-Halo and Snf7-scarlet-i from the *VPS24* promoter. Exponentially growing cells were treated with tunicamycin (Tm) (1 µg/mL) for 3 h or left untreated. They were imaged after adding the SiR-HaloTagLigand. Images were deconvolved with the Richardson-Lucy algorithm (30 iterations with automatically determined noise level). Deconvolution leads to the appearance of some saturated pixels on the images and prevents quantitative comparison between genotypes. A close-up of a Snf7 punctum is shown as an example for the treated cells.
B: Fluorescence microscopy images of cells stably expressing the general ER marker BFP-Ubc6, Cop1p-mNeonGreen, Sec24p-Halo and Snf7-scarlet-i from the *VPS24* promoter. Exponentially growing cells were treated with tunicamycin (Tm) (1 µg/mL) for 3 h or left untreated. They were imaged after adding the SiR-HaloTagLigand. Images were deconvolved with the Richardson-Lucy algorithm (30 iterations with automatically determined noise level). Deconvolution leads to the appearance of some saturated pixels on the images and prevents quantitative comparison between genotypes. A close-up of a Snf7 punctum is shown as an example for the treated cells. This observation was originally made by Chrysafenia Papavissarion and Oliver Pajonk. The strain was generated by Chrysafenia Papavissarion.
C: Fluorescence microscopy images of cells stably expressing the general ER marker BFP-Ubc6, Cop1p-mNeonGreen, Ret2p-Halo and Snf7-scarlet-i from the *VPS24* promoter. Exponentially growing cells were treated with tunicamycin (Tm) (1 µg/mL) for 3 h or left untreated. They were imaged after adding the SiR-HaloTagLigand. Images were deconvolved with the Richardson-Lucy algorithm (30 iterations with automatically determined noise level). Deconvolution leads to the appearance of some saturated pixels on the images and prevents quantitative comparison between genotypes. A close-up of a Snf7 punctum is shown as an example for the treated cells.

Since this spatial arrangement has been observed for two different COPI components, I wanted to determine whether those two components colocalized at ER clusters. Therefore, I tagged Ret2p with a HaloTag and Cop1p with mNeonGreen in cells expressing a general ER marker and Snf7 from the *VPS24* promoter. Surprisingly, Cop1p-mNeonGreen and Ret2p-Halo were only partially overlapping in both untreated and stressed cells (Fig. 13C). As for colocalization with Snf7 puncta, sometimes Cop1p-mNeonGreen colocalized and sometimes Ret2p-Halo colocalized. A more extensive overlap of the different COPI components would have been expected, since the COPI coat has been proposed to be recruited to membranes en bloc (Hara-Kuge, 1994). However, it cannot be excluded that tagging of two different COPI components might interfere with their localization and interaction.
These findings reveal a complex spatial arrangement of different factors at ER clusters in which Snf7 coincides with Dsl1p, a GPI-anchored protein, the p24 complex and COPI components and is surrounded by COPII components.

3.5. ER-tethers colocalize with Snf7 upon ER stress

After having gained more insight into the requirements for ER cluster and Snf7 puncta formation, as well as the spatial arrangement of the involved factors, we proceeded to investigate the possible functional output of the ESCRTs at ER clusters. Even though presence of general and specialized ER export machineries implied a role for the ESCRT machinery in protein export from the ER, no conclusive evidence supporting this hypothesis was found.
However, the occurrence of several Golgi-associated factors at ER-clusters suggested that ER clusters are Golgi-proximal regions of the ER, which raised the question whether ER clusters mediate contacts

to the Golgi during ER stress. Indeed, stress-induced ER-Golgi contacts have been described before in *S. cerevisiae*, entailing the re-localization of ER-tethering proteins Nvj2p and Tcb3p to these sites, which presumably facilitate non-vesicular ceramide transfer during ER stress (L.-K. Liu et al., 2017; Ikeda et al., 2020).

Oliver Pajonk observed that Nvj2p-mNeonGreen and Tcb3p-mNeonGreen colocalized with Snf7-mScarlet-i upon ER stress, suggesting that ER clusters indeed form stress-induced contact sites with the Golgi. He could further show that deletion of *NVJ2* and/or the tricalbin proteins *TCB1*, *TCB2* and *TCB3* did not substantially reduce Snf7 recruitment to ER clusters (Pajonk, PhD dissertation, 2025). They are not essential for Snf7 recruitment and might thus have a downstream role at ER clusters.

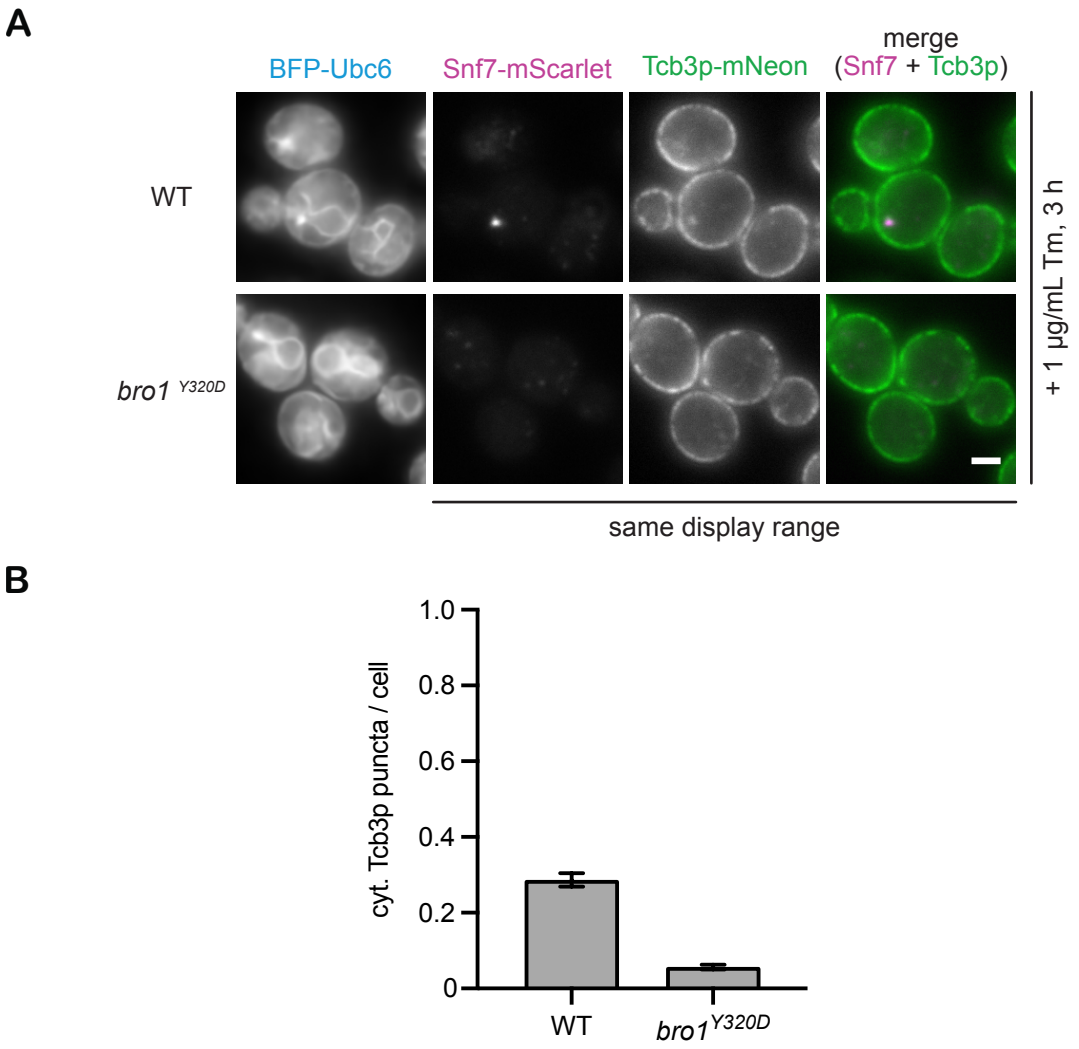

Figure 14: ER-tethering protein Tcb3p colocalizes with Snf7 at ER clusters during ER stress in a Bro1p-dependent manner.

A: Fluorescence microscopy images of cells stably expressing the general ER marker BFP-Ubc6 and Tcb3p-mNeonGreen, as well as Snf7-mScarlet-i expressed from the *VPS24* promoter, in a wildtype or *bro1*^{K246A} background. Exponentially growing cells were treated with tunicamycin (Tm) (1 µg/mL) for 3 h. The same display range is shown for the mScarlet-i and mNeonGreen channels to portray the relative intensities of the signal between genotypes. The scale bar indicates 2 µm. The strains were generated by Oliver Pajonk.

B: Quantification of cytosolic Tcb3p-mNeonGreen puncta in the wildtype and *bro1*^{K246A} background after

treatment with tunicamycin (1 µg/mL) for 3 h. Puncta and cells were counted manually in a blind analysis. Over 200 cells per genotype were quantified in independent biological replicates (n=3). The error bars indicate the standard error of the mean. Oliver Pajonk generated the strains, acquired images for two of the three replicates and quantified all replicates.

Since deletion of these tethering proteins did not affect Snf7 recruitment to the ER, we investigated whether ESCRT recruitment might affect their localization. Oliver Pajonk found that the number of cytosolic Tcb3p puncta was reduced in cells lacking *BRO1* (Pajonk, PhD dissertation, 2025). To understand whether this effect was dependent on ESCRT recruitment to the ER upon stress, Oliver and I imaged WT Bro1p and bro1^{Y320D} cells expressing a general ER maker, Tcb3p-mNeonGreen and Snf7 from the *VPS24* promoter upon 3 h of tunicamycin treatment. Quantification of cytosolic Tcb3p puncta revealed that the formation of these cytosolic puncta was indeed reduced in cells with a defect in stress-dependent ESCRT recruitment to ER clusters (Fig. 14).

Taken together, we could show that ESCRT recruitment to ER clusters is required for localization of the stress-induced ER-Golgi tethering protein Tcb3p to ER clusters. The ESCRT machinery might play a role in the formation or stabilization of these putative ER-Golgi contact sites.

3.6. Interplay between Snf7, ER-tethers and Cop1p as a Golgi marker

3.6.1. Spatial arrangement of Snf7 and typical *cis*-, *medial*- and *trans*-Golgi proteins

In order to further study the role of the ESCRT machinery at prospective ER-Golgi contact sites, I set out to determine a suitable Golgi marker for these structures. Additionally, I wanted to investigate whether there are any differences in the extent of association of Snf7 with different parts of the Golgi, as it has been proposed that Nvj2p and Tcb3p primarily mediate contacts between the ER and the *medial*-Golgi (L.-K. Liu et al., 2017; Ikeda et al., 2020).

In *S. cerevisiae*, *cis*-, *medial*- and *trans*-Golgi cisternae are distributed throughout the cell and are not arranged as stacks (Preuss et al., 1992). Thus, I tagged proteins assigned to the different parts of the Golgi (according to (Tojima et al., 2024)) either at the C-terminus with mNeonGreen or at the N-terminus with yeGFP in cells expressing an ER marker and Snf7-mScarlet-i from the *VPS24* promoter. All imaged Golgi proteins showed a punctate distribution throughout the cell at steady state (Fig. 15A). After 3 h of tunicamycin treatment, their distribution became more diffuse with a higher number of smaller puncta (Fig. 15B), suggesting that ER stress affected Golgi morphology as well. The Golgi proteins showed different degrees of overlap with Snf7 puncta at ER clusters. Whereas 30% of Snf7 puncta colocalized with *cis*-Golgi components Grh1p and Mnn9p, even fewer showed an overlap with *medial*-Golgi component Gos1p or *trans*-Golgi components Gga2p and Apl6p (Fig. 15C).

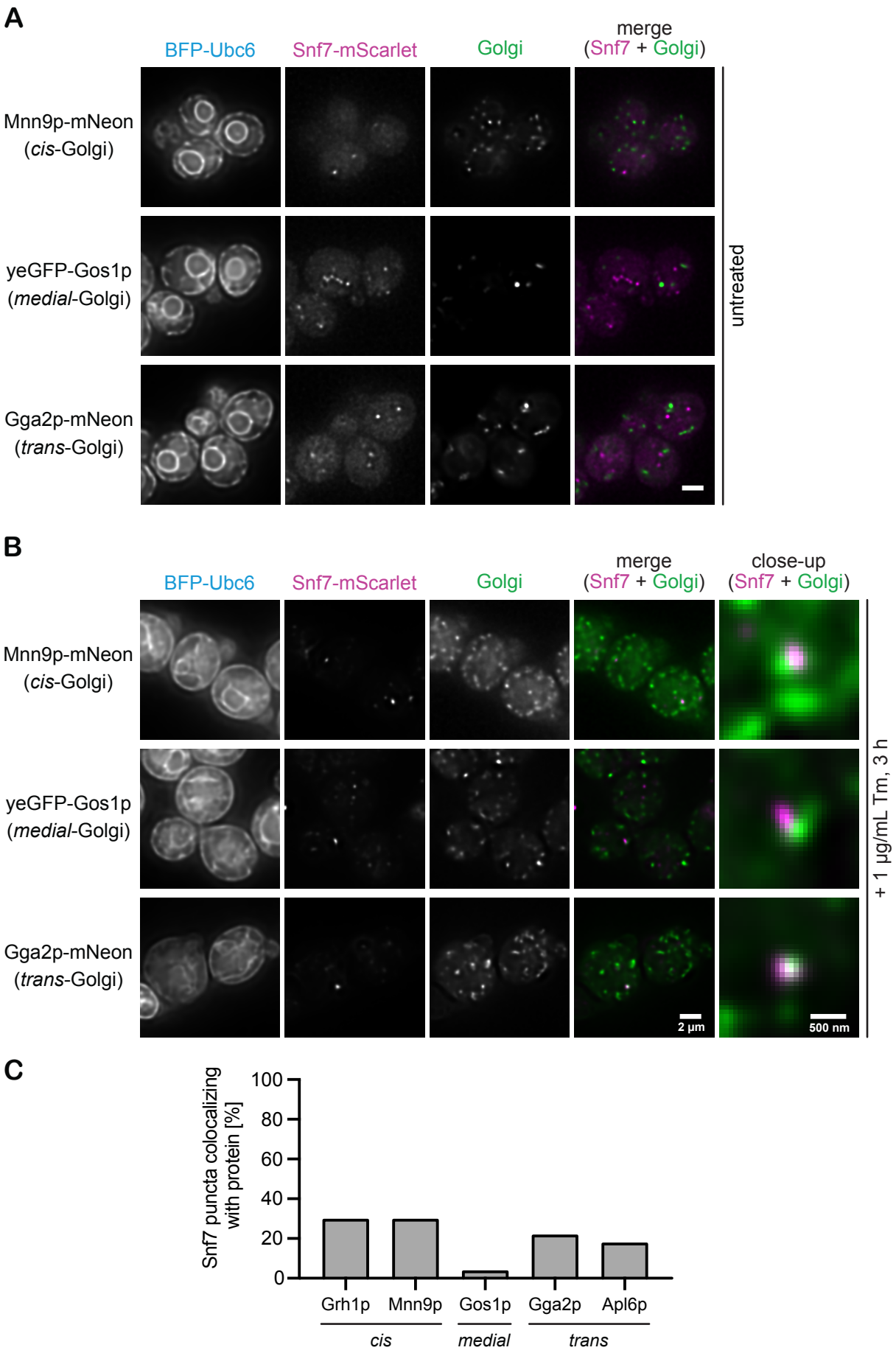

Figure 15: Snf7 puncta do not extensively colocalize with Golgi markers.

A: Fluorescence microscopy images of cells stably expressing the general ER marker BFP-Ubc6 and different Golgi proteins tagged with mNeonGreen, as well as Snf7-mScarlet-i expressed from the *VPS24* promoter. Exponentially growing cells were imaged. Images were deconvolved with the Richardson-Lucy algorithm (30 iterations with automatically determined noise level). Deconvolution leads to the appearance of some saturated pixels on the images and prevents quantitative comparison between genotypes. The scale bar indicates 2 µm.
B: Fluorescence microscopy images of cells stably expressing the general ER marker BFP-Ubc6 and different Golgi proteins tagged with mNeonGreen, as well as Snf7-mScarlet-i expressed from the *VPS24* promoter. Exponentially growing cells were treated with tunicamycin (Tm) (1 µg/mL) for 3 h. Images were deconvolved with the Richardson-Lucy algorithm (30 iterations with automatically determined noise level). Deconvolution leads to the appearance of some saturated pixels on the images and prevents quantitative comparison between genotypes. A close-up of a Snf7 punctum with the respective Golgi protein is shown as an example for each genotype.
C: Quantification of colocalization between Snf7-mScarlet-i puncta at ER clusters and mNeonGreen tagged Golgi proteins after treatment with tunicamycin (1 µg/mL) for 3 h. Colocalization was assessed manually in a blind analysis. 50 Snf7 puncta per genotype were considered.

In general, I could not observe an extensive overlap between Snf7 puncta at stress-induced ER clusters and any of the Golgi proteins I tested. Also, these findings did not support the idea that ER clusters preferentially associate with *medial*-Golgi due to the presence of Nvj2p and Tcb3p. However, it is possible that the few Golgi proteins that I selected are not part of the Golgi structures that are associated with ER clusters and thus I could not determine a greater degree of overlap.
Thus, none of the Golgi proteins tested here were suitable markers for Golgi structures at ER clusters. Interestingly, however, COPI components and Snf7 puncta showed a higher degree of colocalization, as described above, making them more informative Golgi markers to study ESCRTs at ER clusters.

3.6.2. COPI component Cop1p strongly colocalizes with Snf7 but only partially with other Golgi proteins

Apart from their role in retrograde transport from the Golgi to the ER, COPI components are also implied in internal recycling pathways within the Golgi. They appear to be present at many maturation stages of early Golgi cisternae (*cis*- and *medial*-Golgi) in *S. cerevisiae*, suggesting that they could serve as more general early Golgi markers (Papanikou & Glick, 2014; Papanikou et al., 2015).
To further explore the possibility of using COPI components, specifically Cop1p, as a marker for the Golgi at ER clusters, I investigated how Cop1p relates to different early Golgi proteins. Therefore, I imaged cells expressing Cop1p-Halo, an ER marker, Snf7-mScarlet-i from the *VPS24* promoter, and mNeonGreen-tagged Golgi proteins. I used the *cis*-Golgi proteins Mnn9p and Grh1p, that showed the most overlap with Snf7, as well as another *medial*-Golgi protein Aur1p, with mNeonGreen.
Cop1p-Halo and the Golgi proteins showed a punctate distribution at steady state with a more disperse distribution upon ER stress (Fig. 16). Cop1p only showed partial overlap with the other Golgi proteins in both untreated and stressed cells. Aur1p exhibited the most overlap with Cop1p, although still to a low degree (Fig. 16B). Instances where Snf7 overlapped with both Cop1 and another Golgi protein were

rare, suggesting that the Snf7 puncta colocalizing with early Golgi proteins were not a subset of the Snf7 puncta colocalizing with Cop1p. However, it cannot be excluded that tagging different proteins present at ER-Golgi contacts interferes with their location and/or their assembly at the contacts.

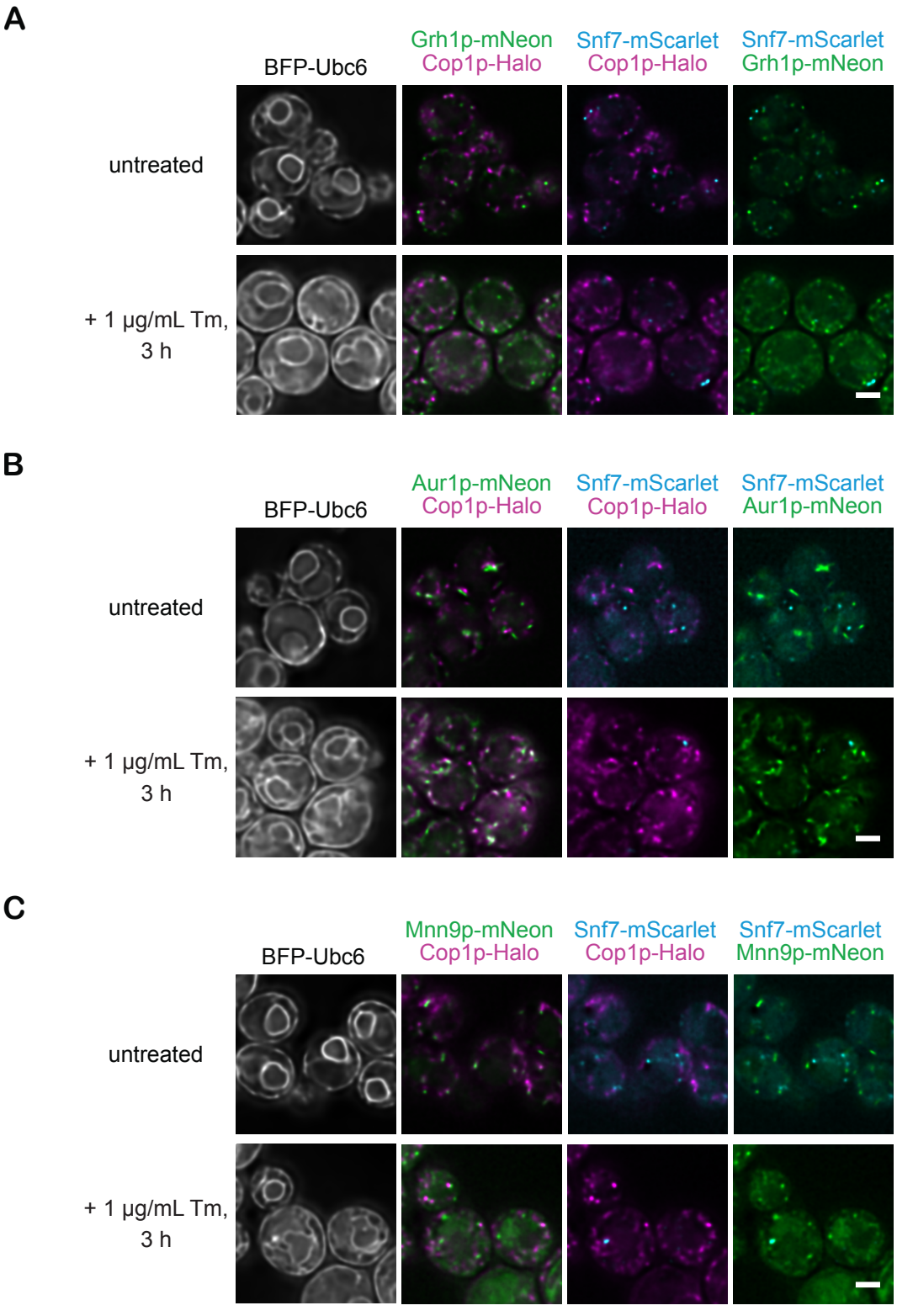

Figure 16: Spatial arrangement of Cop1p in relation to other Golgi proteins.

A: Fluorescence microscopy images of cells stably expressing the general ER marker BFP-Ubc6, Grh1p-mNeonGreen, Cop1p-Halo and Snf7-scarlet-i from the *VPS24* promoter. Exponentially growing cells were treated with tunicamycin (Tm) (1 µg/mL) for 3 h or left untreated. Cells were imaged after adding the SiR-HaloTagLigand. Images were deconvolved with the Richardson-Lucy algorithm (30 iterations with automatically determined noise level). Deconvolution leads to the appearance of some saturated pixels on the images and prevents quantitative comparison between genotypes. The scale bar indicates 2 µm.
B: Fluorescence microscopy images of cells stably expressing the general ER marker BFP-Ubc6, Aur1p-mNeonGreen, Cop1p-Halo and Snf7-scarlet-i from the *VPS24* promoter. Exponentially growing cells were treated with tunicamycin (Tm) (1 µg/mL) for 3 h or left untreated. Cells were imaged after adding the SiR-HaloTagLigand. Images were deconvolved with the Richardson-Lucy algorithm (30 iterations with automatically determined noise level). Deconvolution leads to the appearance of some saturated pixels on the images and prevents quantitative comparison between genotypes. The scale bar indicates 2 µm.
C: Fluorescence microscopy images of cells stably expressing the general ER marker BFP-Ubc6, Mnn9p-mNeonGreen, Cop1p-Halo and Snf7-scarlet-i from the *VPS24* promoter. Exponentially growing cells were treated with tunicamycin (Tm) (1 µg/mL) for 3 h or left untreated. Cells were imaged after adding the SiR-HaloTagLigand. Images were deconvolved with the Richardson-Lucy algorithm (30 iterations with automatically determined noise level). Deconvolution leads to the appearance of some saturated pixels on the images and prevents quantitative comparison between genotypes. The scale bar indicates 2 µm.

In summary, after exploring the relation between early Golgi proteins and Cop1p at ER clusters, I confirmed that Cop1p indeed serves as the best marker for the Golgi at ER clusters. Consequently, it was used as Golgi marker to further study ESCRT function at ER-Golgi contacts.

3.6.3. Tcb3p and Nvj2p colocalize with Golgi marker Cop1p but do not affect its colocalization with Snf7

To eventually combine our findings into a comprehensive view of ER-Golgi contacts at ER clusters, we imaged cells stably expressing an ER marker, Cop1p-Halo as a Golgi marker, Snf7-mScarlet-i from the *VPS24* promoter, and the ER-tethers Nvj2p or Tcb3p respectively tagged with mNeonGreen.
I observed that Nvj2p-mNeonGreen, Cop1p-Halo and Snf7-mScarlet-i often colocalized at ER clusters after 3 h of tunicamycin treatment, underlining the fact that all of these components come together at these sites upon ER stress (Fig. 17A). Similarly, Oliver Pajonk showed that 60% of Snf7 puncta at stress-induced ER clusters colocalize with both Tcb3p and Cop1p and the remaining puncta still colocalized either with Tcb3p or Cop1p (Pajonk, PhD dissertation, 2025).

Now that I established Cop1p as a marker for the Golgi at ER clusters, I wanted to determine whether the proximity between Snf7 and Cop1p is mediated by the stress-induced ER-Golgi tethers Nvj2p and Tcb3p. For this purpose, I deleted *NVJ2* and/or the tricalbins *TCB1*, *TCB2* and *TCB3* in cells stably expressing an ER marker, Cop1p-mNeonGreen and Snf7-mScarlet-i from the *VPS24* promoter (images not shown) and assessed the frequency of colocalization between Snf7 puncta at ER clusters and Cop1p after 3 h of tunicamycin treatment. Neither the individual deletions of *NVJ2* and *TCB1/2/3* nor the combined deletion led to a strong reduction of Snf7-Cop1p colocalization at ER clusters, showing that these ER tethers were dispensable for proximity between ER cluster localized Snf7 and Golgi-associated

Cop1p (Fig. 17B). Possibly, Nvj2p and Tcb3p cooperate with other tethers to stabilize these contacts, or they play another downstream role, possibly in transfer of ceramides as was proposed before (L.-K. Liu et al., 2017; Ikeda et al., 2020).

Taken together, these findings suggest that Snf7 is recruited to contacts between ER clusters and Cop1p-positive Golgi structures upon ER stress and that its recruitment mediates the efficient localization of stress-induced ER-Golgi tethers to these sites.

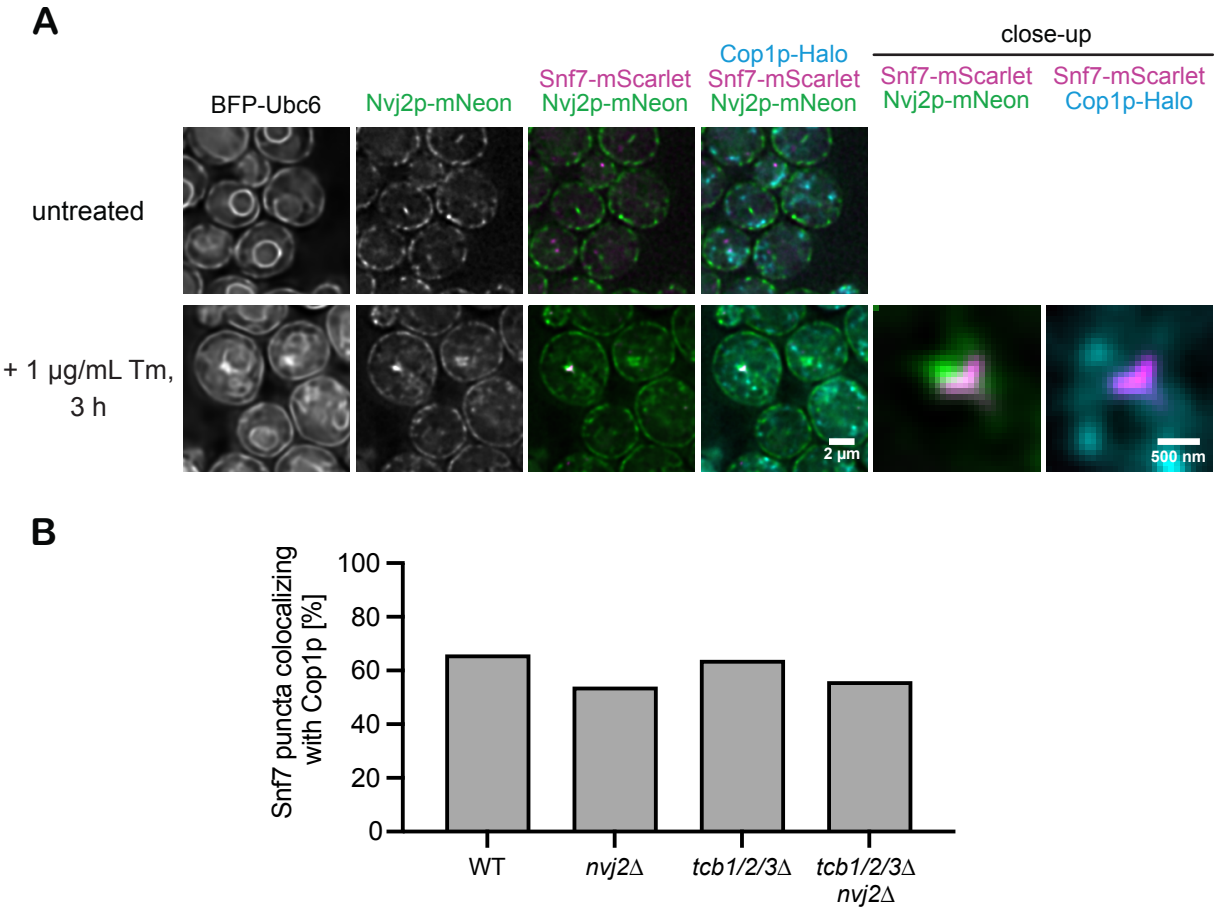

Figure 17: ER tethers, Cop1p and Snf7 colocalize at ER clusters upon ER stress.
A: Fluorescence microscopy images of cells stably expressing the general ER marker BFP-Ubc6, Nvj2p-mNeonGreen, Cop1p-Halo and Snf7-scarlet-i from the *VPS24* promoter. Exponentially growing cells were treated with tunicamycin (Tm) (1 µg/mL) for 3 h or left untreated. Cells were imaged after adding the SiR-HaloTagLigand. Images were deconvolved with the Richardson-Lucy algorithm (30 iterations with automatically determined noise level). Deconvolution leads to the appearance of some saturated pixels on the images and prevents quantitative comparison between genotypes. A close-up of a Snf7 punctum is shown as an example for the treated cells. **B:** Quantification of colocalization between Snf7-mScarlet-i puncta at ER clusters and Cop1p-mNeonGreen. Cells were stably expressing the general ER marker BFP-Ubc6, Cop1p-mNeonGreen and Snf7-scarlet-i from the *VPS24* promoter in a wildtype background as well as *NVJ2* and/or tricalbin (*TCB1, TCB2, TCB3*) deletion backgrounds. Exponentially growing cells were treated with tunicamycin (Tm) (1 µg/mL) for 3 h. Colocalization was assessed manually in a blind analysis. 50 Snf7 puncta per genotype were considered. The strains were generated by Oliver Pajonk and me.

4. DISCUSSION

4.1. A novel role of the ESCRT machinery at potential ER-Golgi contacts during ER stress

The recruitment of the ESCRT machinery to ER clusters during ER stress is a novel pathway. In this study, I identified important determinants for this recruitment and further provided insight into the possible function of the ESCRT machinery at putative contact sites between ER clusters and the Golgi.

My findings show that although expressing tagged Snf7 alongside endogenous Snf7p is not neutral regarding ESCRT recruitment to the ER, it is a valuable tool for studying this process. I found that the Bro1 domain of Bro1p was sufficient for ESCRT recruitment to the ER and that mutations of the second hydrophobic patch or the TPR-like domain within this domain almost completely abolished recruitment of Bro1p and Snf7 to the ER. These mutants do not affect ESCRT function in MVB sorting, highlighting a specific role of these sites for stress-induced recruitment to the ER and providing a way to uncouple these ESCRT-mediated processes. Using a proximity-dependent biotinylation approach coupled to mass spectrometry, I uncovered factors involved in the recruitment of ESCRTs to ER clusters. In particular, I established that Rim20p, a homologue of Bro1p, was required for proper Snf7 recruitment and is partially redundant with Bro1p in this process. I further found that Rim20p was not needed for MVB sorting, identifying it as another specific factor in Snf7 recruitment for this ESCRT process. The hits of my PDB-MS experiment, together with the hits from the genetic screens, provided evidence for an ER-Golgi contact site established at ER clusters during ER stress. I showed that COPI components colocalize with ER clusters and established Cop1p as a suitable Golgi marker at these sites. I further contributed to defining the spatial arrangement of different factors at ER clusters, where Snf7, Bro1p, Rim20p, COPI components, the Dsl1 complex, the p24 complex and Gas1 colocalized with ER clusters, whereas COPII components were surrounding them. Moreover, together with Oliver Pajonk, I found that ESCRT recruitment to ER clusters was essential for the proper localization of the ER-tether Tcb3p to stress-induced ER-Golgi contacts. Eventually, I investigated the role of the ER-tethers Nvj2p and Tcb3p, and thus indirectly of the ESCRT machinery, at ER clusters during stress. My findings suggest that Tcb3p and Nvj2p are not essential for the establishment of ER-Golgi contacts and thus might cooperate with other tethering proteins and/or play a downstream role, e.g. in ceramide transfer at these sites.

These findings, together with insights gained by Oliver Pajonk during his PhD, defined our current model of the ESCRT machinery at stress-induced ER-Golgi contact sites (Fig. 18). Upon ER stress, complex and highly curved clusters form at the ER. ER cluster formation requires factors involved in GPI-anchored protein export, suggesting that cluster formation is driven by accumulation of GPI-anchored proteins at these sites, potentially due to their compromised ER export (Pajonk, PhD dissertation, 2025). Consequently, ER clusters would also contain elevated ceramide levels, as these lipid species typically co-cluster with GPI-APs before their coordinated vesicular export (Lopez et al.,

2019). Elevated ceramide levels might serve as a trigger for Snf7 recruitment, since the amount of ceramide at the ER seems to correlate with the number of Snf7 (discussed below; Pajonk, PhD dissertation, 2025).

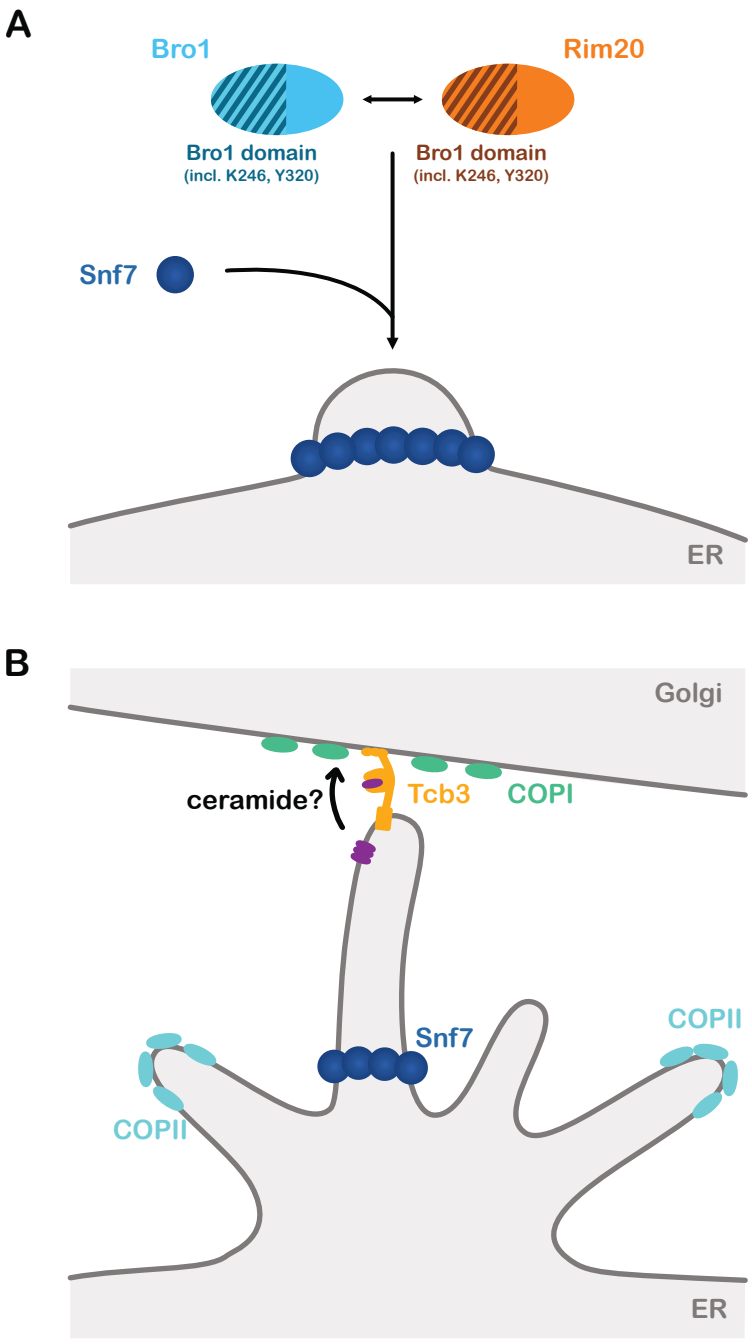

Figure 18: Model of ESCRT recruitment and possible function at ER-Golgi contact sites upon ER stress.
A: Schematic representation of the recruitment mechanism of Snf7 to ER clusters. Upon ER stress, initial ER cluster formation occurs and presumably first leads to recruitment of Bro1p and Rim20p. Subsequent Snf7 recruitment depends on Bro1p and Rim20p. They both contain a homologous Bro1 domain (indicated by the dashed area). Point mutations in the TPR-like domain (K246A) or the second hydrophobic patch (Y320D) of Bro1p almost completely abolish Bro1p and Snf7 recruitment to ER clusters.
B: Schematic representation of putative ESCRT function at ER-Golgi contact sites. Upon ER stress, complex

structures with a high degree of curvature form at the ER upon ER stress. A speculative representation of ER cluster morphology is shown here. Snf7 is recruited to a yet unknown part of those structures. COPII components localize more distally from Snf7 in these structures, possibly bound to GPI-AP cargo via GPI-AP export receptors. ER clusters contain the stress-induced ER-Golgi tethers Tcb3p and Nvj2p (not shown here) and colocalize with COPI-positive Golgi cisternae. Tcb3p localization to ER clusters depends on ESCRT recruitment. Furthermore, Tcb3p might mediate non-vesicular transport of ceramide from the ER to the Golgi at ER clusters.

The Bro1 domain proteins Bro1p and Rim20p coordinate Snf7 recruitment to ER clusters via their Bro1 domain. The TPR-like domain and the second hydrophobic patch of Bro1p are required for this recruitment (Fig. 18A). ER clusters also contain stress-induced ER-Golgi tethering proteins Nvj2p and Tcb3p, and they coincide with COPI-positive parts of the Golgi, suggesting that ER clusters form contacts with the Golgi. Moreover, these sites are surrounded by COPII components, possibly bound to GPI-AP receptors and cargo unable to leave the ER. Tcb3p localization to the potential ER-Golgi contacts depends on ESCRT recruitment. Thus, the ESCRT machinery seems to play a role at ER-Golgi contact sites, possibly in the formation of the contacts or by stabilizing pre-existing contacts. They might further be involved in non-vesicular transfer of ceramide at these sites via Tcb3p (Fig. 18B) (Ikeda et al., 2020). Since vesicular transport of GPI-APs and thus ceramides are possibly impaired, as suggested by spatial proteomics data from our lab (discussed below; (Platzek et al., 2025)), this ESCRT-mediated process would provide a way to avoid the toxic accumulation of ceramide within the ER upon ER stress.

4.2. Identification of upstream and downstream factors of ESCRT recruitment by proximity-dependent biotinylation

The proximity-dependent biotinylation approach coupled to MS used in this study enabled to identify Rim20p as recruitment factor for Snf7 to ER clusters, as well as suggesting proximity of ER clusters to the Golgi given that many hits were part of the ER-Golgi interface.

Upon validation by fluorescence microscopy, some proteins from the hitlist, like the UPS components, did not accumulate at ER clusters. These false-positive hits possibly arose due to the continuous biotinylation by Bro1p-TurboID throughout the experiment. An exogenous biotin pulse could have been employed to limit the temporal range for biotinylation and thus reducing the extent to which cytosolic proteins just passing by ER clusters become biotinylated. Another caveat of this approach is that steric obstruction can prevent the detection of proximity partners of Bro1p.

The microscopy-based genetic screens performed as a complementary approach enabled us to address the same question from a different angle (Pajonk, PhD dissertation, 2025). Overlaps between the two approaches included hits involved in ER-Golgi trafficking like COPI and COPII components. Other categories were only found by the genetic screens: GPI-anchor remodelers, the GPI-AP export receptor, the GET machinery, ER structural genes, lipid metabolism genes, ribosome or proteasome-related genes. Some of these hits could not be validated in our strain background or were indirect hits, as they

affected ER morphology in general. Genes related to ER export of GPI-APs were shown to play a role at ER clusters (Pajonk, PhD dissertation, 2025). Yet other categories of hits could only have been identified by PDB-MS, like the ESCRT proteins, since they were not part of the strain collections in the screen.

Thus, the combination of the two approaches indeed provided a more complete overview of the factors involved in ESCRT recruitment to and function at ER clusters during stress. The PDB-MS approach reports on proximity and thus identifies proteins more closely associated with ER clusters, or even interacting with Bro1p. The genetic screens brought up genes that play a role further upstream of ER cluster formation and ESCRT recruitment, as well as factors that could potentially sterically not be reached by Bro1p-TurboID.

4.3. Recruitment of the ESCRT machinery to ER clusters upon ER stress

4.3.1. Relevant features of Bro1p for recruitment to ER clusters

The ESCRT-III subcomplex can be recruited to target membranes in various ways. Recruitment of Snf7 to ER clusters upon ER stress requires Bro1p but not the upstream ESCRT-0, -I and -II complexes. Different roles have previously been ascribed to Bro1p regarding ESCRT activity, namely roles in activation of Snf7, de-ubiquitination of cargo and regulation of ESCRT-III disassembly by Vps4p (Tang et al., 2015; Luhtala & Odorizzi, 2004; Tseng et al., 2021). Which role Bro1p plays at ER clusters, apart from enabling Snf7 recruitment, remains unclear. So far, there is no evidence for the need of ubiquitin-binding domains of Bro1p in this process. An interaction between Bro1p and Vps4p at ER clusters is possible, as Vps4p was enriched in proximity of Bro1p-TurboID upon ER stress.

Data from this study and previous work by Carlos Martin de Hijas showed that the Bro1 domain of Bro1p is sufficient for proper recruitment of Bro1p and Snf7 to ER clusters. The ER clusters, as well as Bro1p and Snf7 puncta, are more disperse than in presence of full-length Bro1p, suggesting a role of the Bro1p C-terminus in the organization of ER clusters, possibly by mediating interactions with other proteins relevant for this process. Mutations of the TPR-like domain or the second hydrophobic patch within the Bro1 domain disrupted recruitment of Bro1p and Snf7 to ER clusters. The K246A mutation in the TPR-like domain did not cause a problem with MVB sorting but interfered with recruitment to ER clusters possibly due to the disruption of the structural properties of this domain or a potential interaction site. Similarly, the Y320D mutation within the second hydrophobic patch of the Bro1 domain abolished Snf7 recruitment. The highly conserved tyrosine at position 320 prominently sticks out of the Bro1 domain structure, making it a potential interaction site for a yet unknown factor that could be essential for its recruitment to the ER (Kim et al., 2005).

4.3.2. A novel recruitment mechanism of ESCRT-III by Bro1p and Rim20p

By showing that both Bro1p and Rim20p are needed for Snf7 recruitment to ER clusters, I defined a novel recruitment mechanism for ESCRT-III that implies two Bro1 domain proteins. Rim20p has not been described to play a role in ESCRT-mediated processes beyond the fungal Rim pathway for pH sensing (Boysen & Mitchell, 2006). Rim20p and Bro1p show partial redundancy in Snf7 recruitment to ER clusters, as Rim20p was able to rescue loss of *BRO1* to some extent. A full rescue was not observed, even though overexpression by the *TEF* promoter should lead to an amount of protein surpassing the combined amount of Bro1p and Rim20p in wildtype cells. Determining the levels of Bro1p and Rim20p in the overexpression strains used within this study would clarify whether the amount of Bro1 domain protein would have been sufficient. If so, Bro1p and Rim20p seem to play unique roles for Snf7 recruitment, likely involving the C-terminal domains of the proteins which could mediate interactions with other factors relevant for the ESCRT machinery at ER clusters. Alternatively, the overexpression of Bro1 domain proteins to levels considerably exceeding their natural level might have an inhibitory effect on Snf7 recruitment. In that case, the use of a weaker promoter might have led to a more pronounced rescue.

The fact that Rim20p does not play a role in MVB sorting, as shown in this study with the Mup1-pHluorin assay and previous studies for CPY and CPS sorting (Odorizzi et al., 2003), indicates that it cannot take over the role of its homologue in any Bro1-mediated process. This is further supported by the fact that Rim20p seems to have a dominant-negative effect on MVB sorting, as its overexpression leads to localization of Bro1p to class E compartments. Thus, Rim20p is specifically involved in some ESCRT-mediated processes, whereas it is not needed for others.

Prior to this study, Bro1p and Rim20p had not been described to jointly coordinate ESCRT-III recruitment, even though they are both known interactors of Snf7 (Bowers et al., 2004; Ito et al., 2001). Like for Bro1p, interaction of Rim20p with Snf7 also involves its Bro1 domain (Xu et al., 2004). Since Bro1p and Rim20p are both needed for recruitment of Snf7, and their own recruitment is dependent on each other with Rim20p needing Bro1p for recruitment to the ER and vice versa, it is conceivable that they act in concert and not subsequently. Interaction with Snf7 could rely on mixed dimers of Rim20p and Bro1p coordinating its recruitment to ER clusters. Dimerization could possibly even be driven by their second hydrophobic patches. Dimer formation had been described for ALIX, the mammalian homologue of Bro1, but has not been established for yeast Bro1p (Pires et al., 2009). However, dimerization of ALIX was described to involve its V-domain rather than parts of the Bro1 domain (Pires et al., 2009). Co-immunoprecipitation experiments performed in the context of this study did not provide evidence for an interaction between Rim20p and Bro1p so far (data not shown). A possible interaction could further be studied using the biotinylation assay with TurboID-tagged Bro1p or Rim20p variants in stressed cells and probing for the respective other Bro1 domain protein.

Alternatively, Bro1p and Rim20p might just individually interact with Snf7. In this case, they might be bridged by other factors or recognize similar features at the ER.

Intriguingly, overexpression of Bro1p or Rim20p induced the formation of ER clusters with Snf7 puncta to a small degree in the absence of ER stress. The need for a specific stress-induced trigger might be overruled by sufficient levels of Bro1p and Rim20p, or smaller preexisting ER clusters in untreated cells expand and become visible. During ER stress, Rim20p levels slightly increase as suggested by proteomics data from our lab (Platzek et al., 2025), hinting at a possible way to regulate ER cluster formation. Since ER clusters caused by overexpression show a spatial arrangement of COPI and COPII proteins reminiscent of stress-induced clusters (data not shown) and thus possibly mediate similar downstream functions, these clusters are not just overexpression artefacts.

All in all, Rim20p and Bro1p seem to play an organizational role for Snf7 at ER clusters. Furthermore, they may recognize a specific stress-induced recruitment factor or other stress-induced signal at ER, initiating ESCRT recruitment.

4.3.3. Recognition of the target membrane at ER clusters via Bro1p and Rim20p

In our current model, we propose that the accumulation of ceramides at ER clusters could serve as a trigger for Snf7 recruitment. In cells with deletions of *DGA1* and *LRO1* Snf7 puncta formed to a low extent at ER clusters in absence of ER stress (Pajonk, PhD dissertation, 2025). Dga1p and Lro1p convert ceramide into acyl-ceramide, enabling its subsequent storage into lipid droplets (LDs) (Voynova et al., 2012). Their deletion presumably results in a locally increased level of ceramide at the ER. Furthermore, deletion of *TSC3*, an activator of the serine palmitoyl transferase (SPT) complex mediating the first rate-limiting step of ceramide synthesis (Gable et al., 2000), decreased the number of Snf7 puncta upon tunicamycin treatment (Pajonk, unpublished). These findings suggested that the amount of ceramide at the ER correlate with the number of Snf7 puncta. Direct sensing of ceramides by Bro1 domain proteins has not been described so far, but it is conceivable that changes in membrane properties induced by high levels of ceramides lead to ESCRT recruitment, be it by direct association with the membrane or via interaction with another membrane-associated protein.

The PDB-MS approach could have identified potential recruitment factors bridging Bro1p and/or Rim20p and the ER. Although the hitlist included some ER-associated proteins, they were not specifically localized to ER clusters. Interaction with these proteins might still be possible, but additional factors would be needed for specific targeting to ER clusters. Possibly, not all proteins enriched in proximity of Bro1-TurboID were biotinylated due to steric effects, thus a potential recruitment factor might not have been captured by the PDB-MS approach. Assuming that the second hydrophobic patch of Bro1p and/or Rim20p is involved in recognition of the recruitment signal, a protein-protein interaction would be probable due to the prevalence of hydrophobic patches as mediators of protein-protein interactions (Rego et al., 2021). However, hydrophobic patches can also mediate interactions

between proteins and lipid bilayers, by inserting into the hydrophobic core of the bilayer, as is the case for phospholipase A_2 (PLA_2) enzymes (Lomize et al., 2007; Mouchlis et al., 2015). It is conceivable that Bro1p and/or Rim20p themselves associate with the membrane. In fact, ALIX, the mammalian homologue of Bro1, was shown to interact with the lipid LBPA (Matsuo et al., 2004). This interaction, however, was proposed to be mediated by a lipid-binding loop specific to the Bro1 domain of ALIX, which is not present in *S. cerevisiae* Bro1p (Bissig et al., 2013). Another way of Bro1p and/or Rim20p to associate with membranes independently of the second hydrophobic patch would be via the concave boomerang-shaped structure of the Bro1 domain, reminiscent of how BAR domain proteins associate with curved membranes (Kim et al., 2005; Peter et al., 2004).

Lipid composition and membrane shape could also determine ESCRT recruitment. GPI-anchored protein Gas1, as well as its export receptor, accumulates at ER clusters (Pajonk, unpublished). In *S. cerevisiae*, GPI-APs specifically cluster with ceramides with C26 acyl chains before their coordinated export, which drives the lateral segregation of GPI-APs and leads to local thickening of the ER membrane (Rodriguez-Gallardo et al., 2020; Lopez et al., 2019). Moreover, the C26 ceramides and the GPI-anchor exhibit a high degree of saturation, as opposed to the usually unsaturated nature of ER membrane (Lopez et al., 2019). Even though these changes in lipid composition take place in the exoplasmic leaflet of the ER membrane, they might affect overall ER membrane properties and possibly act as a recruitment signal for Snf7 recruitment to ER clusters, which could be directly or indirectly sensed by Bro1 domain proteins.

4.4. Contacts between ER clusters and the Golgi

4.4.1. Golgi proteins at ER clusters

After studying the localization of different Golgi proteins within this study, I determined Cop1p as the most reliable marker for Golgi at ER clusters. COPI components have been shown to localize throughout the early Golgi and colocalize with early Golgi markers, like Vrg4p (Papanikou et al., 2015). For the early Golgi markers in this study, I could not confirm a major overlap with Cop1p, neither at steady-state nor upon stress. However, it is possible that COPI components only overlap with early Golgi markers that were not tested in this study. Moreover, depending on the protein and fluorescent tag used, tagging several components that come into proximity at ER clusters might interfere with their localization. Additionally, during ER stress, the localization of various Golgi proteins might differ from what is described in literature at steady state. Changes in the distribution of the Golgi proteins observed in this study are consistent with findings stating that ER stress also induces molecular and structural changes within the Golgi. The UPR can for instance modulate the activity of proteins involved in Golgi organization and trafficking, such as the Arf-GTPase Arl1p (Hsu et al., 2016). Moreover, increased ER-Golgi contact formation can lead to spatial reorganization of the Golgi (L.-K. Liu et al., 2017).

COPI coat proteins mediate internal recycling pathways within the early Golgi and retrograde transport from the Golgi to the ER (Letourneur et al., 1994; Papanikou et al., 2015). Whether the Cop1p-positive Golgi membranes associated with ER clusters represent retrograde COPI vesicles or membranes involved in internal Golgi trafficking remains unclear. On the one hand, the presence of the Dsl1-tethering complex at ER clusters could hint at a mechanism for receiving retrograde COPI-coated vesicles at ER clusters. Coincidence between ERES and ER-arrival sites (ERAS) had been described in *P. pastoris* and *S. cerevisiae* (Roy Chowdhury et al., 2020; Schröter et al., 2016). On the other hand, the presence of several stress-induced ER-Golgi tethers suggests contact with early Golgi cisternae (L.-K. Liu et al., 2017; Ikeda et al., 2020). Another option would be that COPI is present on tubular ERES, reminiscent of those that have been observed in mammalian cells for export of large protein assemblies such as procollagen (Weigel et al., 2021). In that case, COPI components were proposed to localize near the rims of this ER based structure (Weigel et al., 2021). However, such ER-Golgi carriers have not been observed in *S. cerevisiae* so far.

Studying the dynamics of Cop1p at ER clusters might shed some light on the stability of the association between Cop1p-positive membranes and the ER and thus help to discriminate between these different options.

4.4.2. Role of ER-Golgi contact sites during ER stress

Our current hypothesis suggests that ER clusters form contacts with the Golgi. Cells can adapt the frequency and function of membrane contact sites to changing conditions. Since they integrate signals from different compartments, MCSs play important roles in stress mechanisms, including ER stress (Prinz et al., 2020). Stress-induced ER-Golgi contact sites that form in *S. cerevisiae* involve ER-tethers Nvj2p and Tcb3p (L.-K. Liu et al., 2017; Ikeda et al., 2020). We found that those tethers coincide with Snf7 at ER clusters upon ER stress and thus we assume that ER clusters represent stress-induced contacts with the Golgi.

At steady-state, Nvj2p is enriched at NVJs, membrane contact sites tethered by Nvj1p at the ER and Vac8p at the vacuole (Pan et al., 2000). Tcb3p mediates tethering at PM-ER contact sites with five other tethering proteins, namely the tricalbins Tcb1p and Tcb2p, the VAP homologues Scs2p and Scs22p, and Ist2p (Manford et al., 2012). Tcb3p is involved in curvature generation at the ER facing the plasma membrane together with the other tricalbins (Collado et al., 2019). Both Nvj2p and Tcb3p are anchored to the ER by a single transmembrane domain and comprise a synaptotagmin-like mitochondrial lipid-binding protein (SMP) domain. SMP domains have been implicated in lipid transfer (Schauder et al., 2014; Toulmay & Prinz, 2012). Tcb3p is involved in the regulation of phosphatidylserine homeostasis at the PM in response to heat stress (Thomas et al., 2022). At ER-Golgi contact sites, Nvj2p and Tcb3p were proposed to impact ceramide transfer (L.-K. Liu et al., 2017; Ikeda et al., 2020). Whether Nvj2p and Tcb3p adopt similar roles in establishment of contacts, curvature induction and lipid transfer at

stress-induced ER clusters remains to be elucidated.

The loss of the tricalbins and/or Nvj2p did not lead to a decrease of Snf7-Cop1p colocalization within this study, implying that they are not essential for tethering the ER and the Golgi. It is possible that the effect of the deletions was masked by the presence of other ER-Golgi tethering proteins. I found that Scs2p also colocalized with a subset of Snf7 puncta (data not shown). It would be interesting to determine whether these same Snf7 puncta also colocalize with Cop1p. In general, determining which other tethers are present at ER clusters and studying the effect of their deletion on the frequency of Snf7 puncta would provide insight into which proteins play a role in tethering.

During ER stress, ceramide transfer from the ER to the Golgi is adapted. At steady-state, yeast cells rely mostly on vesicular transfer of ceramide to the Golgi, whereas non-vesicular transfer at MCSs mediated by Svf1p and tricalbin proteins plays a minor role (Funato & Riezman, 2001; Limar et al., 2023; Ikeda et al., 2020). During ER stress, non-vesicular transfer of ceramides via stress-induced tethers like Nvj2p seems to become more relevant as suggested by elevated ceramide levels observed in *nvj2Δ* cells (L.-K. Liu et al., 2017). Vesicular transport of ceramides together with GPI-APs might be compromised during ER stress due to overload of misfolded proteins within ER (Lopez et al., 2019; L.-K. Liu et al., 2017). In general, there are opposing views on the state and the regulation of ER export mechanisms upon ER stress. ER-Golgi transport genes are upregulated upon ER stress, indicating the possibility that ER export might be promoted upon ER stress, possibly to alleviate protein load in the ER (Travers et al., 2000). However, whether proteins can leave the ER upon ER stress seems to depend on their folding state, the type of protein and the organism. In mammalian cells, the ATF6 branch of the UPR relies on the vesicular transport of ATF6 from the ER to the Golgi during ER stress (Chen et al., 2002; Schindler & Schekman, 2009). Also, the quantitative export of GPI-anchored proteins during stress via the so-called RESET pathway has been described in mammalian cells (Satpute-Krishnan et al., 2014; Cheatham et al., 2023). However, spatial proteomics data from our lab suggested that newly synthesized GPI-anchored proteins remain in the ER upon tunicamycin treatment in *S. cerevisiae*, likely because they cannot mature properly (Platzek et al., 2025). Together with the fact that GPI-anchored protein Gas1, GPI-AP export receptors and COPII components accumulate at and around ER clusters (Pajonk, PhD dissertation, 2025), this led us to believe that GPI-anchored proteins might be stuck in their specialized ERES at ER clusters. Consequently, ceramide transfer could be maintained by Tcb3p and Nvj2p via contacts between ER clusters and the Golgi.

4.5. Role of the ESCRT machinery at ER clusters

4.5.1. Membrane remodeling

Our current hypothesis suggests that the ER clusters comprise contacts to the Golgi. What role the ESCRT machinery plays at these sites will be subject to further studies. The ESCRT machinery mediates

membrane remodeling by sequential exchange of ESCRT-III subunits by Vps4p, which can be followed by scission, depending on the subset of ESCRT-III proteins involved (Pfitzner et al., 2020). As both Vps4p and its regulator Vta1p, as well as two other ESCRT-III proteins Did2p and Vps60p, were enriched in proximity of Bro1p-TurboID, it is possible that a dynamic exchange of subunits and membrane remodeling takes place at ER clusters. Did2p promotes constriction of narrower membrane necks compared to Snf7 and together with Ist1p leads to membrane scission (Pfitzner et al., 2020). The later was however not found as a hit in the PDB-MS. Vps60p was described to initiate alternative ESCRT-III filaments to the Snf7-based filaments, implying that different kinds of ESCRT assemblies might form at ER clusters (Pfitzner et al., 2023).

Electron microscopy (EM) approaches used prior or in parallel to this study gave some insight into the morphology of ER clusters. CLEM imaging by Jasmin Schäfer revealed tubular structures extending from the ER. Fluorescence microscopy guided cryo-electron tomography done by Leanne De Jager, a collaborator in the Förster Lab at Utrecht University, provided a 3D impression of ER clusters, revealing various structures ranging between 200-500 nm with a high degree of curvature (De Jager, PhD dissertation, 2025). The limited resolution of the fluorescence microscopy prevented us however from determining the localization of Snf7 within these structures.

Initial ER cluster formation seems to occur prior to Snf7 recruitment, since ER clusters were observed to some extent by fluorescence microscopy in the absence of Bro1p. Different factors present at ER clusters have curvature-inducing capacities. Deletion of GPI-anchor remodelers and the GPI-AP receptor reduced the amount of ER clusters (Pajonk, PhD dissertation, 2025). Accumulation of long chain ceramides together with GPI-APs at ER clusters might induce curvature (Zelnik et al., 2020; Lima et al., 2025). Furthermore, COPI and COPII machineries drive vesicle budding by assembling into cage-like structures (C. K. Barlowe & Miller, 2013). Since they colocalize or localize in proximity of Snf7, respectively, both machineries might be involved in shaping ER clusters prior to Snf7 recruitment or in concert with Snf7. Moreover, the ER-shaping protein Rtn1p was enriched in proximity of Bro1p upon ER stress.

After initial ER cluster formation, Snf7 and other ESCRT-III components seem to mediate further remodeling, since ER clusters appear more defined in fluorescence microscopy in presence of Snf7 recruitment. Also, the overexpression of Rim20p and Bro1p results in formation of Snf7-positive ER clusters without stress. Since Rim20p and Bro1p are not known to induce curvature by themselves, this finding reports on ability of Snf7 to remodel prospective ER clusters.

4.5.2. Stabilization of membrane structures

Apart from membrane remodeling, the ESCRT machinery might also play a role in stabilizing ER cluster structures and act as a scaffold, as it does in the Rim pathway providing a signaling platform or in the formation of viral replication compartments by stabilizing the neck of the bud (Peñalva et al., 2014;

Diaz et al., 2015). Since ER clusters appear to be complex membrane structures, it is conceivable that stabilizing factors are needed. Furthermore, during ER stress, the membrane at ER clusters might be destabilized due to the accumulation of ceramides and GPI-anchored proteins, possibly altering the membrane tension. In vitro studies have shown that ESCRT-III remodeling activity is higher when membrane tension is lower (Booth et al., 2019). The ESCRT machinery might stabilize these regions to prevent damage.

In the context of ER-Golgi contact sites, both remodeling and stabilizing functions might increase proximity of ER clusters to the Golgi, as shown for other contact sites like at ER-PM or ER and autophagosomes (Collado et al., 2019; Bieber et al., 2022). Parts of the membranous structures observed by cryo-EM were devoid of ribosomes (De Jager, PhD dissertation, 2025). These might represent Golgi structures, but due to limited amount of EM data on the Golgi in *S. cerevisiae*, it impossible to make a clear distinction at this point. Ribosome-free zones at the ER have also been described previously for ER-exit sites and membrane contact sites (G. Palade, 1975; Phillips & Voeltz, 2016). Higher order ESCRT assemblies on the cytosolic leaflet of the ER membrane might also play a role in restricting the localization of ribosomes at ER clusters.

4.5.3. Enabling ceramide transfer via Tcb3p and Nvj2p

Lastly, this study, together with data from Oliver Pajonk, showed that Tcb3p and Nvj2p colocalize with ESCRT proteins Snf7 and Bro1p and Golgi marker Cop1p at ER clusters during stress. Furthermore, we established that localization of Tcb3p to cytosolic puncta, representative of its contacts to the Golgi, was dependent on Bro1p, and more specifically on the ability of Bro1p to recruit Snf7 to ER clusters. The ESCRT machinery might thus indirectly play a role in ceramide transfer at ER clusters by efficiently recruiting Tcb3p to these sites. Additionally, its membrane remodeling function might facilitate lipid extraction from positively curved membranes, which seems to be more energetically favorable compared to extraction from flat membranes. This has been shown for instance for PA extraction by the yeast lipid transfer protein Ups1, mediating PA transfer within the mitochondrial intermembrane space (Sadeqi et al., 2025).

4.6. Implications of ESCRT function at ER clusters on the ER stress response

The fact that Snf7 recruitment to ER clusters upon ER stress is very prominent and that stress-induced Golgi tethers localize to ER clusters, implies that this process is specific for ER stress. However, we cannot exclude that the ESCRT machinery also plays a role at ER-Golgi contact sites in untreated cells, possibly promoting transfer of ceramide. Non-vesicular ceramide transfer only accounts for a minority of ceramide transfer at steady-state in *S. cerevisiae* (Funato & Riezman, 2001), thus these sites might not be visible by fluorescence microscopy. Nevertheless, the extent of ESCRT recruitment to ER clusters drastically increases upon tunicamycin treatment, implying that it might play a role in the cellular stress

response. Oliver Pajonk previously showed in *hac1Δ* cells that Snf7 recruitment to ER clusters is independent of the UPR (Pajonk, PhD dissertation, 2025). Still, the ESCRT function at ER clusters might help alleviate ER stress in cooperation with the UPR. To test whether Bro1 mutants show increased sensitivity to ER stress, I used a Hac1-splicing reporter assay to compare Hac1-splicing in wildtype Bro1p and Bro1 mutants after tunicamycin treatment, but the results were inconclusive (data not shown; (Pincus et al., 2010)). The setup would need further optimization to ensure that the maximal degree of UPR activation is not already reached for the wildtype.

A cooperation between the UPR and the ESCRT function at ER clusters is conceivable. Accumulation of ceramide within the ER membrane can trigger the UPR and eventually lead to cell death (Eisenberg & Büttner, 2014). Moreover, the ERAD system is impaired upon ceramide accumulation, as it prevents the extraction of ubiquitinated proteins from the membrane (Hwang et al., 2023). By promoting the transfer of ceramide to the Golgi, the ESCRT machinery might alleviate this burden.

4.7. Conservation of ESCRT recruitment and function at ER clusters

As the ESCRT machinery and many ESCRT-mediated processes are highly conserved, it is conceivable that the ESCRT recruitment to ER clusters is conserved as well. In mammalian cells, the homologues of Snf7p and Bro1p, CHMP4 and ALIX respectively, work together to remodel membranes e.g. in cytokinesis, plasma membrane wound repair, as well as HIV release from cells (Morita et al., 2007; Jimenez et al., 2014; Garrus et al., 2001; Strack et al., 2003). Mammalian cells have two other Bro1 domain proteins, HD-PTP and BROX. Collaboration between these Bro1 domain proteins for CHMP4 recruitment, as we found for Rim20p and Bro1p, has not yet been described but would be possible. As for ER-Golgi contact sites in mammalian cells, the architecture might vary due to the stacking of the Golgi compartments. These contacts contain VAPA/B proteins as tethers, as well as lipid transfer proteins such as OSBP and CERT (Venditti et al., 2019; Wyles et al., 2002; Hanada et al., 2003). Ceramide transfer from the ER to the trans-Golgi is predominantly mediated through the non-vesicular route via CERT (Hanada et al., 2003). So far, the homologues of Nvj2 and Tcb3, TEX2 and extended synaptotagmins (E-Syts) respectively, have not been implicated at ER-Golgi contacts. The human homologue of Nvj2, can compensate for the loss of NVJ2 in non-vesicular ceramide transfer in *S. cerevisiae* (L.-K. Liu et al., 2017). E-Syts are known tethers for ER-PM contacts (Giordano et al., 2013).

4.8. Challenges encountered within this study

The initial findings of this study underline that expression of tagged Snf7 alongside the endogenous Snf7p is not neutral in ESCRT recruitment to the ER, although it does not affect MVB sorting as shown in this and previous studies (Teis et al., 2008; Adell et al., 2017). Presumably, the integration of tagged Snf7 proteins into the hetero-oligomeric assemblies specifically formed at ER clusters stabilizes them and thus changes the dynamics of a usually faster process. While this stabilization served as a valuable

tool to identify proteins present at ER clusters and needed for Snf7 recruitment, it might interfere with the functional outcome usually mediated by the ESCRT machinery at ER clusters. To increase the chances of identifying the role of the ESCRT machinery at ER clusters, it would be ideal to use strains without tagged Snf7 for future functional studies.

Another issue for studying the role of ESCRTs at ER clusters is that identification of ER clusters becomes more difficult when ESCRT recruitment is prevented by Bro1 point mutants, as tagged Snf7 is not present at the clusters to mark them. So far, we did not find another marker that remains present at ER clusters when ESCRT recruitment is impaired.

Furthermore, this study lacks controls regarding the colocalization between Snf7 and different Golgi proteins. I quantified the frequency with which Golgi or COPI proteins overlap with Snf7 puncta, without considering how much overlap would randomly be expected between them due to their punctate distribution. The extent of overlap between Snf7 and different parts of the Golgi seems to correlate with the number of puncta observed for the specific Golgi protein, raising the question whether the effect might be random. However, the fact that Mnn9p and Cop1p both showed a similar number of puncta and yet did not show the same amount of overlap with Snf7 puncta speaks against a random effect. Future quantifications should include a step in which the amount of overlap between the original Snf7 channel and the Golgi protein channel reflected across the axis of each cell is assessed, allowing comparison between random overlap of signals and actual colocalization.

4.9. Future directions

This study presents a novel recruitment mechanism of ESCRT-III protein Snf7 by Bro1p and Rim20p. The interplay between the two Bro1 domain proteins could be further explored using co-IP experiments studying the interaction between each protein with Snf7 in presence and absence of the respective other. Alternatively, biotinylation assays with Rim20p and Bro1p tagged with TurboID and probing for Snf7 could be used. Moreover, timelapse imaging with minimal time intervals could provide information on the temporal sequence of recruitment to ER clusters.

It is possible that not all factors involved in ESCRT recruitment were identified by the PDB-MS approach or the genetic screens. To gain a more complete overview of the molecular environment of Bro1p and/or Rim20p during stress, co-IPs followed by MS could be performed as a third complementary method. Furthermore, the PDB-MS approach could be refined by using a split-TurboID approach (Cho et al., 2020). For this, Bro1p and Rim20p would be tagged with inactive fragments of TurboID respectively and proximity labelling could only occur in instances when Rim20p and Bro1p are in close proximity.

The contact sites between ER clusters and the Golgi could be further characterized by electron microscopy-based imaging. In this case, immunogold labelling of Snf7 could be included to gain better spatial resolution. The location of Snf7 within ER clusters might reveal where ESCRT-mediated

remodeling and/or ER-Golgi contacts occur. Contact sites could also be visualized and studied with the help of split fluorescent protein approaches. Moreover, live imaging could provide insight into the dynamics of Cop1p, which would be expected to be more static at ER clusters if these indeed form contacts with Cop1p positive Golgi.

Our current model suggests that the ESCRT machinery plays a role in ceramide transfer at ER clusters, together with Tcb3p and Nvj2p, and thus might be recruited by elevated ceramide levels at the ER. As there is no suitable ceramide sensor to probe for ceramide-rich regions, the effect of ceramide levels on Snf7 recruitment could be assessed only indirectly. Local thickening induced by accumulation of ceramide and GPI-APs could be detected by sensors with specific TMD length (Rodriguez-Gallardo et al., 2020; Prasad et al., 2020). Also, ceramide levels at the ER could be decreased by use of the drug fumonisin B, which inhibits the ceramide synthase Lag1p/Lac1p at the ER (Wang et al., 1991), to check whether the frequency of Snf7 puncta upon ER stress decreases, similarly to what was observed for the *tsc3Δ* strain (Pajonk, unpublished). Vice versa, the increase of ceramide levels at the ER, either by use of phosphomimetic and thus constitutively active mutants of Lag1p/Lac1p, or by deletion of ceramidases Ydc1p and Ypc1p at the ER, might lead to an increase in Snf7 puncta (Fresques et al., 2015; Mao, Xu, Bielawska, & Obeid, 2000; Mao, Xu, Bielawska, Szulc, et al., 2000). Whether the ESCRT machinery directly impacts non-vesicular ceramide transfer at ER clusters still needs to be determined. Lipidomics approaches could be used as a read-out for ceramide transfer. Ceramide is synthesized in the ER and converted into complex sphingolipids, such as inositol phosphorylceramide (IPC), after transport to the Golgi (Levine et al., 2000). The ratio between the levels of ceramides and complex sphingolipids in wildtype vs bro1^{Y320D} cells could thus report on the efficiency of ceramide transport from the ER to the Golgi in these strains. A similar approach was used by Limar et al to study ceramide transfer by Svf1p (Limar et al., 2023). Determinants of other ceramide transfer pathways, such as non-vesicular transfer to the Golgi mediated by Svf1p, or storage in lipid droplets after conversion into acylceramide by Lro1p and Dga1p, could be deleted to increase specificity. Using both untreated cells and cells treated with tunicamycin could reveal whether ESCRT recruitment to the ER generally impacts ceramide transfer or whether this process is specific for ER stress. A flux analysis using radioactively labelled serine and/or inositol and measuring incorporation into complex sphingolipids over time, as employed by Limar et al and Liu et al, could further detect differences between wildtype and bro1^{Y320D} cells (Limar et al., 2023; L.-K. Liu et al., 2017).

To understand whether the ESCRT machinery actively remodels ER clusters, the dynamics of the ESCRTs at the ER could be studied. Timelapse, multi-color imaging of different factors involved at ER clusters could provide insight into how stable these structures are. Studying the dynamics in absence of tagged Snf7 would prevent stabilization of the structures.

All in all, this study presents an ESCRT-mediated pathway initiated by a novel recruitment mechanism in *S. cerevisiae*, underlining the versatility of the ESCRT remodeling machinery. It further advances our understanding of ER-Golgi trafficking and membrane contact site formation at the ER, in particular during ER stress.

5. MATERIALS AND METHODS

5.1. Materials

5.1.1. Drugs and chemical compounds

Table 2. Drugs and chemical compounds used in this study.

Compound	Supplier
Acrylamide mix (30%; 37,5:1)	Roth
Tunicamycin (Tm)	Sigma-Aldrich
Dithiothreitol (DTT)	Roche
Phenylmethylsulfonyl fluoride (PMSF)	Applichem
cOmplete protease inhibitors	Roche
DNA stain G	Serva
G418	Biochrom
Hygromycin B	Invivogen
Nourseothricin (ClonNat)	Werner BioAgents
Biotin	Sigma-Aldrich
TEMED	Applichem
dATP	Thermo Fisher Scientific
dGTP	Thermo Fisher Scientific
dCTP	Thermo Fisher Scientific
dTTP	Thermo Fisher Scientific
Acetonitrile (for MS)	Biosolve
H_2O (for MS)	Biosolve
Formic Acid (for MS)	ProteoChem
Orange G	Merck

5.1.2. Buffers and solutions

Table 3. Buffers and solutions used in this study.

Buffer/Solution	Composition
Amino Acid mix	2% (w/v) in water, autoclaved
Ammonium persulfate (APS)	10% (w/v) in water
Betaine	5 M in water containing 0.5% orange G, sterile-filtered
Blotting buffer	25 mM Tris 192 mM glycine 20% (v/v) ethanol
Colony PCR buffer (10x)	200 mM Tris, pH 8.8 100 mM $(NH_4)_2SO_4$ 100 mM KCl 25 mM $MgCl_2$
cOmplete protease inhibitors (25x)	1 tablet in 2 mL water
Dithiothreitol (DTT)	1 M in water
dNTPs	10 mM of each in water
Elution buffer (Streptavidin IP)	1 x SDS-PAGE sample buffer 2 mM biotin
Glucose (10x)	20% (w/v) in water, autoclaved

Glycerol (2x)	30% (v/v) in water, autoclaved
Lithium acetate	1 M in water, sterile-filtered
Loading dye for agarose gels (5x)	50% (v/v) glycerol 10% (v/v) 10x TAE buffer 0.05% (w/v) orange G
Lysis Buffer (GBP co-IP)	50 mM HEPES, pH 7.5 150 mM NaCl 1% (v/v) Trition X-100 2 mM EDTA
Lysis Buffer (Streptavidin IP)	50 mM Tris, pH 7.5 150 mM NaCl 0.4% (w/v) SDS 2% (v/v) Trition X-100 5 mM EDTA
Methionine (stock for Mup1)	200 µg/mL in SCD-methionine
Na-deoxycholate	10% (w/v) in water
Phenylmethylsulfonyl fluoride (PMSF)	1 M in water
Polyethylene glycol (PEG) 3350	50% (w/v) in water, sterile-filtered
Salmon sperm DNA	10 mg/mL in water
SDS-PAGE running buffer	0.1% (w/v) SDS 25 mM Tris-HCl 192 mM Glycine
SDS-PAGE sample buffer (4x)	278 mM Tris-HCl, pH 6.8 44.4% (v/v) glycerol 4.4% (w/v) LDS 0.02% (w/v) bromophenol blue 0.1 volumes ß-mercaptoethanol, freshly added
Separating gel buffer	2 M Tris-HCl, pH 8.8
Sodium dodecyl sulfate (SDS)	15% (w/v) in water
Stacking gel buffer	0.5 Tris-HCl, pH 6.8
TAE buffer (50x)	2 M Tris 1 M acetic acid 50 mM EDTA
TBS	10 mM Tris, pH 7.4 150 mM NaCl
TBS/Tween (TBST)	10 mM Tris, pH 7.4 150 mM NaCl 0.1% (v/v) Tween-20
Transformation Mix	33% (w/v) PEG 3350 100 mM lithium acetate 0.28 µg/mL salmon sperm DNA, freshly boiled before use
Triton X-100	10% (v/v) in water
Tunicamycin (Tm)	1 mg/mL or 10 mg/mL in DMSO
Wash buffer (GBP co-IP)	150 mM HEPES, pH 7.5 150 mM NaCl 2 mM EDTA
Wash buffer 1 (Streptavidin IP)	50 mM Tris, pH 7.5 150 mM NaCl 0.4% (w/v) SDS 2% (v/v) Triton X-100 5 mM EDTA

	1x cOmplete protease inhibitors 1 mM DTT
Wash buffer 2 (Streptavidin IP)	2% (w/v) SDS in water
Wash buffer 3 (Streptavidin IP)	50 mM HEPES, pH 7.4 500 mM NaCl 1 mM EDTA 1% (v/v) Triton X-100 0.1% (w/v) Na-deoxycholate
Wash buffer 4 (Streptavidin IP)	50 mM Tris, pH 7.5 50 mM NaCl 0.1% (v/v) Triton X-100
Yeast nitrogen base (YNB)	6.9% (w/v) in water, autoclaved

5.1.3. Growth media and plates

Table 4. Synthetic complete amino acid mix.

Amino Acid	Amount
Adenine	0.5 g
Alanine	2 g
Arginine	2 g
Asparagine	2 g
Aspartic acid	2 g
Cysteine	2 g
Glutamine	2 g
Glutamic acid	2 g
Glycine	2 g
Histidine	2 g
Inositol	2 g
Isoleucine	2 g
Leucine	4 g
Lysine	2 g
Methionine	2 g
para-Aminobenzoic acid	0.2 g
Phenylalanine	2 g
Proline	2 g
Serine	2 g
Threonine	2 g
Tryptophan	2 g
Tyrosine	2 g
Uracil	2 g
Valine	2 g

Table 5. Media used in this study.

Medium	Composition
SCD	2% (w/v) glucose 0.69% (w/v) YNB 0.2% (w/v) amino acid mix
YPD	1% (w/v) yeast extract 2% (w/v) peptone 2% (w/v) glucose

Table 6. Plates used in this study.

Plates	Composition
SCD plates	0.69% (w/v) YNB 0.2% (w/v) amino acid mix 2% (w/v) glucose 2% (w/v) agar
YPD plates	1% (w/v) yeast extract 2% (w/v) peptone 2% (w/v) glucose 2% (w/v) agar
YPD G418 plates	1% (w/v) yeast extract 2% (w/v) peptone 2% (w/v) glucose 2% (w/v) agar 400 µg/mL Geneticin (G418)
YPD hph plates	1% (w/v) yeast extract 2% (w/v) peptone 2% (w/v) glucose 2% (w/v) agar 400 µg/mL hygromycin B
YPD nat plates	1% (w/v) yeast extract 2% (w/v) peptone 2% (w/v) glucose 2% (w/v) agar 100 µg/mL nourseothricin (ClonNat)
5-FOA plates	0.69% (w/v) YNB 0.2% (w/v) amino acid mix 2% (w/v) glucose 2% (w/v) agar 1 mg/mL 5-Fluorooratic Acid (5-FOA)

SCD dropout plates or media were prepared using amino acid mix omitting the respective amino acid.

5.1.4. Enzymes, Standards and Kits

Table 7. Enzymes used in this study.

Enzyme	Supplier
OptiTaq DNA polymerase	Roboklon
Taq DNA Polymerase	Sigma-Aldrich
Q5 High-fidelity DNA polymerase	New England Biolabs
Restriction Enzymes	New England Biolabs

Table 8. Standards used in this study.

Standard	Supplier
GeneRuler 1kb Plus DNA Ladder	Thermo Fisher Scientific
PageRuler Plus Prestained Protein Ladder	Thermo Fisher Scientific

Table 9. Kits used in this study.

Kit	Supplier
miniBio Column Plasmid MiniPrep	miniBio Life Science Products
miniBio Gel and PCR Cleanup	miniBio Life Science Products
Pierce Rapid Gold BCA Protein Assay Kit	Thermo Fisher Scientific
SuperSignal West Pico PLUS Chemiluminescent Substrate	Thermo Fisher Scientific

5.1.5. Beads and antibodies

Table 10. Beads used in this study.

Beads	Source
Pierce High Capacity Streptavidin Agarose Beads	Thermo Fisher Scientific
GFP-binder beads	Home-made according to (Galmozzi et al., 2019)

Table 11. Antibodies used in this study.

Antibodies		Dilution	Source
Primary	Mouse anti-mNeonGreen (32F6)	1:2000	Chromotek
	Mouse anti-GFP (7.1/13.1)	1:5000	Roche
	Rabbit anti-Snf7	1:5000	Ralf Kölling Lab
Secondary	Goat anti-mouse HRP (31452)	1:10000	Thermo Fisher Scientific
	Goat anti-mouse Alexa-680 (A21057)	1:10000	Thermo Fisher Scientific
	Donkey anti-rabbit IRDye-800CW (926-32213)	1:10000	LI-COR

5.2. Molecular biology methods

5.2.1. Plasmids

Table 12. Plasmids used in this study.

Plasmids	Source
p413-bro1(K246A)	This study (Carlos Martin De Hijas)
p413-bro1(Y320D)	This study (Carlos Martin De Hijas)

5.2.2. Oligonucleotides

Table 13. Oligonucleotides used in this study.

Primers	Sequences
Bro1+434-S1	CGAGGGAGAATATCAATGAGGACTACAAAAACTCAATCGCCGTACGCTGCAGGTCGAC
Bro1+963-S2	GCCTTAATGGAATCAACCTGCACAACGGCTGGAACGCTTTCATCGATGAATTCGAGCTCG
Bro1+415	CGAGGGAGAATATCAATGAGG
Bro1+983	GCCTTAATGGAATCAACCTGC
Bro1+180_fw	GCAAATGGAGAACTAGCACC
Bro1+1295_rev	GGTCCCTCATCAATTGTCCC
Bro1+1161-F2	GGAAAGTATTTACTCAGAAGAAAAAGCGACGCTGTTGAGACGGATCCCCGGGTTAATTAA
Bro1+1161-F2-like	GGAAAGTATTTACTCAGAAGAAAAAGCGACGCTGTTGAGATAAGGCGCGCCACTTCTAAA
F2-like-comp	TTTAGAAGTGGCGCGCCTTA

5.3. Yeast methods

5.3.1. Yeast strains

Table 14. Yeast strains used in this study.

Strain genotype	Alias	Source
leu2-3,112 trp1-1 can1-100 ura3-1 his3-11,15	SSY122	(Szoradi et al., 2018)
ura3::P_{VPS24}-Snf7-mScarlet-i-URA3 trp1::P_{GPD}-BFP-Ubc6-TRP1 BRO1-mNeonGreen::nat	SSY2834	This study (Oliver Pajonk)
trp1::P_{TEF}-BFP-Ubc6-TRP1 BRO1-mNeonGreen::nat	SSY4710	This study
BRO1-sfGFP::kan vps27Δ::nat	SSY3485	This study
BRO1-sfGFP::kan ura3:: P_{VPS24}-Snf7-mScarlet-i-URA3 vps27Δ::nat	SSY3510	This study
his3::P_{GPD} -BFP-hph	SSY795	(Schmidt et al., eLife 2019)
his3::P_{GPD} -BFP-hph ura3::Mup1-pHluorin-URA3	SSY3677	This study (Petra Hubbe)
his3::P_{GPD} -BFP-hph snf7Δ::nat ura3::Mup1-pHluorin-URA3	SSY3669	This study (Petra Hubbe)
his3::P_{GPD} -BFP-hph ura3::Mup1-pHluorin-URA3 leu2:: P_{VPS24}-Snf7-mScarlet-i-LEU2	SSY4375	This study
his3::P_{GPD} -BFP-hph ura3::Mup1-pHluorin-URA3 leu2:: P_{VPS24}-Snf7-mScarlet-i-LEU2 snf7Δ::nat	SSY4469	This study
ura3::P_{VPS24}-Snf7-mNeonGreen-URA3 trp1::P_{GPD}-cherry-Ubc6-TRP1	SSY2544	This study (Jasmin Schäfer)
bro1^{Y320D} ura3:: P_{VPS24}-Snf7-mNeonGreen-URA3 trp1::P_{GPD}-cherry-Ubc6-TRP1	SSY4323	This study (Oliver Pajonk)
bro1^{K246A} ura3::P_{VPS24}-Snf7-mNeonGreen-URA3 trp1::P_{GPD}-cherry-Ubc6-TRP1	SSY4324	This study (Oliver Pajonk)
ura3::P_{VPS24}-Snf7-mNeonGreen-URA3 trp1::P_{GPD}-cherry-Ubc6-TRP1 bro1$^{1-387}$::nat	SSY4470	This study
bro1^{K246A}-mNeonGreen-HA::HIS3 trp1::P_{TEF}-TagBFP-Ubc6-TRP1 ura3::P_{VPS24}-Snf7-mScarlet-i-URA3	SSY3378	This study

bro1^{Y320D}-mNeonGreen-HA::HIS3 trp1::P$_{TEF}$-BFP-Ubc6-TRP1 ura3::P$_{VPS24}$-Snf7-mScarlet-i-URA3	SSY3474	This study
ura3::P$_{VPS24}$-Snf7-mScarlet-i-URA3 trp1::P$_{GPD}$-BFP-Ubc6-TRP1 bro1$^{1-387}$-mNeonGreen-HA::HIS3	SSY4541	This study
his3::P$_{GPD}$-BFP-hph bro1Δ::nat ura3::Mup1-pHluorin-URA3	SSY3707	This study (Petra Hubbe)
his3::P$_{GPD}$-BFP-hph bro1Δ::nat ura3::Mup1-pHluorin-URA3 bro1$^{1-387}$::nat	SSY4315	This study (Oliver Pajonk)
bro1^{K246A} his3::P$_{GPD}$-BFP-hph ura3::Mup1-pHluorin-URA3	SSY3735	This study
bro1^{Y320D} his3::P$_{GPD}$-BFP-hph ura3::Mup1-pHluorin-URA3	SSY3733	This study
ura3::P$_{VPS24}$-Snf7-mNeonGreen-URA3 BRO1-TurboID-3xmyc::kan vps27Δ::nat pep4Δ::hph prb1Δ::klTRP1 chm7Δ::HIS3	SSY3290	This study
ura3::P$_{VPS24}$-Snf7-mNeonGreen-URA3 bro1^{K246A}-TurboID-3xmyc::kan vps27Δ::nat pep4Δ::hph prb1Δ::klTRP1 chm7Δ::HIS3	SSY3292	This study
ura3::P$_{VPS24}$-Snf7-mNeonGreen-URA3 BRO1-TurboID-3xmyc::kan vps27Δ::nat pep4Δ::hph prb1Δ::klTRP1	SSY3015	This study
ura3::P$_{VPS24}$-Snf7-mNeonGreen-URA3 bro1(K246A)-TurboID-3xmyc::kan vps27Δ::nat pep4Δ::hph prb1Δ::klTRP1	SSY3088	This study (Oliver Pajonk)
ura3::P$_{VPS24}$-Snf7-mScarlet-i-URA3 trp1::P$_{GPD}$-BFP-Ubc6-TRP1 RIM20-mNeonGreen-HA::HIS3	SSY3073	This study (Oliver Pajonk)
ura3::P$_{VPS24}$-Snf7-mNeonGreen-URA3 trp1::P$_{GPD}$-cherry-Ubc6-TRP1 rim20Δ::nat	SSY3040	This study (Sebastian Schuck)
his3::P$_{GPD}$-BFP-hph ura3::Mup1-pHluorin-URA3 rim20Δ::nat	SSY3796	This study
ura3::P$_{VPS24}$-Snf7-mNeonGreen-URA3 trp1::P$_{GPD}$-cherry-Ubc6-TRP1 bro1Δ::nat	SSY2555	This study (Jasmin Schäfer)
ura3::P$_{VPS24}$-Snf7-mNeonGreen-URA3 trp1::P$_{GPD}$-cherry-Ubc6-TRP1 hph-P$_{TEF}$-BRO1	SSY3556	This study
ura3::P$_{VPS24}$-Snf7-mNeonGreen-URA3 trp1::P$_{GPD}$-cherry-Ubc6-TRP1 hph-P$_{TEF}$-RIM20	SSY3557	This study
ura3::P$_{VPS24}$-Snf7-mNeonGreen-URA3 trp1::P$_{GPD}$-cherry-Ubc6-TRP1 hph-P$_{TEF}$-BRO1 rim20Δ::nat	SSY3558	This study

ura3::P_{VPS24}-Snf7-mNeonGreen-URA3 trp1::P_{GPD}-cherry-Ubc6-TRP1 hph-P_{TEF}-RIM20 bro1Δ::nat	SSY3559	This study
ura3::P_{VPS24}-Snf7-mScarlet-i-URA3 trp1::P_{GPD}-BFP-Ubc6-TRP1 BRO1-mNeonGreen::nat hph-P_{TEF}-RIM20	SSY3654	This study
ura3::P_{VPS24}-Snf7-mScarlet-i-URA3 trp1::P_{GPD}-BFP-Ubc6-TRP1 RIM20-mNeonGreen-HA::HIS3 P_{TEF}-BRO1::hph	SSY3643	This study
ura3::P_{VPS24}-Snf7-mScarlet-i-URA3 trp1::P_{GPD}-BFP-Ubc6-TRP1 COP1-mNeonGreen-HA::HIS3	SSY3493	This study (Oliver Pajonk)
ura3::P_{VPS24}-Snf7-mScarlet-i-URA3 trp1::P_{GPD}-BFP-Ubc6-TRP1 RET2-mNeonGreen-HA::HIS3	SSY3555	This study
ura3::P_{VPS24}-Snf7-mScarlet-i-URA3 trp1::P_{GPD}-BFP-Ubc6-TRP1 SEC21-mNeonGreen::HIS3	SSY4609	This study (Oliver Pajonk)
ura3::P_{VPS24}-Snf7-mScarlet-i-URA3 trp1::P_{GPD}-BFP-Ubc6-TRP1 SEC27-mNeonGreen::HIS3	SSY4610	This study (Oliver Pajonk)
ura3::P_{VPS24}-Snf7-mScarlet-i-URA3 trp1::P_{GPD}-BFP-Ubc6-TRP1 SEC28-mNeonGreen::HIS3	SSY4611	This study
ura3::P_{VPS24}-Snf7-mScarlet-i-URA3 trp1::P_{GPD}-BFP-Ubc6-TRP1 COP1-mNeonGreen-HA::HIS3 RET2-Halo::kan	SSY4040	This study
ura3::P_{VPS24}-Snf7-mScarlet-i-URA3 trp1::P_{GPD}-BFP-Ubc6-TRP1 SEC24-mNeonGreen-HA::HIS3 RET2-Halo::kan	SSY4041	This study
ura3::P_{VPS24}-Snf7-mScarlet-i-URA3 trp1::P_{GPD}-BFP-Ubc6-TRP1 COP1-mNeonGreen-HA::HIS3 SEC24-Halo::kan	SSY3897	This study (Chrysafenia Papavissarion)
ura3::P_{VPS24}-Snf7-mScarlet-i-URA3 trp1::P_{GPD}-BFP-Ubc6-TRP1 TCB3-mNeonGreen::HIS3	SSY4153	This study (Oliver Pajonk)
bro1^{Y320D} trp1::P_{TEF}-BFP-Ubc6-TRP1 ura3::P_{VPS24}-Snf7-mScarlet-i-URA3 TCB3-mNeonGreen::HIS3	SSY4190	This study (Oliver Pajonk)
ura3::P_{VPS24}-Snf7-mScarlet-i-URA3 trp1::P_{GPD}-BFP-Ubc6-TRP1 GRH1-mNeonGreen::HIS3	SSY4170	This study
ura3::P_{VPS24}-Snf7-mScarlet-i-URA3 trp1::P_{GPD}-BFP-Ubc6-TRP1 nat-P_{ADH}-yeGFP-GOS1	SSY4174	This study
ura3::P_{VPS24}-Snf7-mScarlet-i-URA3 trp1::P_{GPD}-BFP-Ubc6-TRP1 GGA2-mNeonGreen::HIS3	SSY4175	This study
ura3::P_{VPS24}-Snf7-mScarlet-i-URA3 trp1::P_{GPD}-BFP-Ubc6-TRP1 APL6-mNeonGreen::HIS3	SSY4176	This study

ura3::P_{VPS24}-Snf7-mScarlet-i-URA3 trp1::P_{GPD}-BFP-Ubc6-TRP1 MNN9-mNeonGreen::HIS3	SSY4213	This study
ura3::P_{VPS24}-Snf7-mScarlet-i-URA3 trp1::P_{GPD}-BFP-Ubc6-TRP1 MNN9-mNeonGreen::HIS3 COP1-Halo::kan	SSY4465	This study
ura3::P_{VPS24}-Snf7-mScarlet-i-URA3 trp1::P_{GPD}-BFP-Ubc6-TRP1 GRH1-mNeonGreen::HIS3 COP1-Halo::kan	SSY4466	This study
ura3::P_{VPS24}-Snf7-mScarlet-i-URA3 trp1::P_{GPD}-BFP-Ubc6-TRP1 AUR1-mNeonGreen::HIS3 COP1-Halo::kan	SSY4467	This study
ura3::P_{VPS24}-Snf7-mScarlet-i-URA3 trp1::P_{GPD}-BFP-Ubc6-TRP1 NVJ2-mNeonGreen::HIS3 COP1-Halo::kan	SSY4748	This study
ura3::P_{VPS24}-Snf7-mScarlet-i-URA3 trp1::P_{GPD}-BFP-Ubc6-TRP1 tcb3Δ::hph tcb2Δ::nat tcb1Δ::LEU2 COP1-mNeonGreen-HA::HIS3	SSY4708	This study
ura3::P_{VPS24}-Snf7-mScarlet-i-URA3 trp1::P_{GPD}-BFP-Ubc6-TRP1 tcb3Δ::hph tcb2Δ::nat tcb1Δ::LEU2 nvj2Δ::kan COP1-mNeonGreen-HA::HIS3	SSY4709	This study
ura3::P_{VPS24}-Snf7-mScarlet-i-URA3 trp1::P_{GPD}-BFP-Ubc6-TRP1 nvj2Δ::kan COP1-mNeonGreen-HA::HIS3	SSY4747	This study

5.3.2. Yeast strain generation

All yeast strains in this study are based on the *Saccharomyces cerevisiae* W303 background with mating type a. In the wildtype strain used as a basis for all further strains in our lab, the *ADE2* locus was repaired, thus rescuing the *ade2-1* mutation present in the original W303 wildtype strain.

Yeast strains with gene deletions, endogenous protein tags or exchanged promoters were generated using the PCR-based method established by (Longtine et al., 1998) and modified by (Janke et al., 2004). Primers for tagging and deletion and plasmids of the pFA6a series were used as described in these publications and are not included in Tables 12 and 14. PCRs were done using the OptiTaq DNA Polymerase (Roboklon) or the Q5 High-fidelity DNA polymerase (New England Biolabs) according to the suppliers' guidelines. Loading dye (Table 3) was added to the PCR products and they were checked on 1% agarose gels in 2x TAE containing Stain G.

For ectopic expression of proteins, genomic integration of expression constructs by homologous recombination was done as described by Sikorski and Hieter, 1989. Plasmids of the pRS series were used and either digested by restriction enzymes (New England Biolabs) according to the supplier's guidelines or amplified by knock-in PCR using the OptiTaq DNA Polymerase (Roboklon) into the specific locus prior to transformation.

To generate strains with the bro1 point mutants *bro1^{K246A}* and *bro1^{Y320D}*, a two-step procedure was used to first delete a part of the *BRO1* gene (between nucleotides 434 and 963) including the nucleotides

that should be mutated using the *URA3* cassette and then re-introducing that part of BRO1 containing the mutated nucleotides. For the first step, the standard procedure for deletions as described above was performed with the Bro1+434-S1 and Bro1+963-S2 primers, annealing up- and downstream of the respective part of *BRO1*, and the pFA6a-URA3MX6 plasmid as a template. The wildtype strain was transformed with the resulting PCR product. Cells were plated on SC-URA selective plates and clones were tested for integration by colony PCR with primers binding upstream of the *BRO1* locus and within the transformed cassette. The resulting strain was used as a parent strain for both point mutants. In the second step, PCR products were generated using the Bro1+415 and Bro1+983 primers and the p413-bro1(K246A) or p413-bro1(Y320D) plasmids (generated by Carlos Martin de Hijas) respectively using the OptiTaq DNA Polymerase (Roboklon) according to the supplier's indications. The resulting PCR products contained the part of *BRO1* that we previously deleted and overhangs on both sides that are homologous to the neighboring regions in the *BRO1* gene, as well as the K246A or Y320D mutations, respectively. The strain resulting from the first step was transformed with either of the two PCR products and cells were plated on YPD plates. Plates were incubated for 24 h at room temperature, then they were replica plated onto 5-FOA plates to counter select for the *URA3* cassette and grown at 30°C. Once colonies were visible, they were restreaked on YPD plates, on which they grow if they integrated the PCR product, and on SC-URA plates, on which they should not grow. Single colonies were then tested by colony PCR using the Bro1+415 and Bro1+983 primers. PCR products were sent to sequencing to check for successful introduction of the point mutations. Another round of sequencing with primers annealing further away from the point mutation, Bro1+180_fw and Bro1+1295_rev, was performed to make sure that the regions between the insert and genome were intact.

Strains with the Bro1 domain mutant, $bro1^{1-387}$, were generated by partial deletion of *BRO1*. The standard procedure for tagging was used as described above to either create tagged versions of $bro1^{1-387}$ using the pFA6a-neon-natNT2 or pFA6a-neon-HIS3MX6 plasmids as template with the Bro1+1161-F2 and Bro1-S2 primers, or to create $bro1^{1-387}$ without tag but including a stop codon using the same template plasmids and the Bro1+1161-F2-like and Bro1-S2 primers. The F2-like primer anneals to a region in the template plasmids that contains a stop codon and precedes the terminator of the tag, thus allowing to add these features to the end of the truncated *BRO1* gene. Microscopy or colony PCR with Bro1+415 and F2-like-comp primers were used to check for successful generation of the mutant strains.

5.3.3. Growth conditions

Yeast cells were grown in glass tubes (for imaging and harvesting) or 96-deep-well plates (for flow cytometry) at 30°C in a shaking incubator. For experiments, cells in logarithmic growth phase, namely

with an OD_{660nm} = 0.2-1, were used. Cells were generally grown in SCD medium or in SCD-methionine medium for the Mup1-pHluorin assays. For transformations, cells were grown in YPD medium.

ER stress was induced by treating cells with tunicamycin. For this, cultures with an OD_{660nm} = 0.3 were treated with a final concentration of 1 µg/mL tunicamycin for 3 h. For the Mup1-pHluorin assay, cells were grown to exponential growth phase in SCD-methionine medium and part of the cultures were then supplemented with methionine to a final concentration of 20 µg/mL to induce internalization of the Mup1 receptor.

For long-term storage, saturated yeast cell cultures were mixed in a 1:1 ratio with 30% (w/v) glycerol and stored at -80°C.

5.3.4. Yeast Transformation

For transformation, yeast strains were grown into saturation in YPD medium at 30°C overnight. Cells were diluted in 5 mL fresh YPD in order to reach an OD_{660nm}= 1 after four hours of growth. Cells were then harvested by centrifugation at 1,000 x g for 5 min, washed with 1 mL of water, and spun down again at 10,000 x g for 2 min. The supernatant was discarded. The transforming DNA was added to the pellet (1/10 of a PCR product for tagging or deletion of genes, 0.25 µg for linearized plasmids), which was then resuspended in 360 µL of transformation mix (Table 3). Cells were subjected to a heat shock at 42°C for 40 min. After that, cells were spun down at 10,000 x g for 2 min, the supernatant was discarded and cells were resuspended in 1 mL of YPD medium. 100 µL of the cell suspension were plated onto the respective selective plate using glass beads. In cases where the transforming DNA contained an antibiotic resistance gene, cells were grown for 3-6 h at 30°C before plating. Plates were incubated for 2-3 days at 30°C until colonies grew. Colonies were restreaked on a new selective plate and integration of the transforming DNA was verified by colony PCR, microscopy or flow cytometry.

5.3.5. Colony PCR

To confirm whether cells had acquired the desired genetic modification, colony PCRs were performed. Single colonies from the transformation plates were restreaked onto a new plate. A small amount of yeast from the different clones on those plates was transferred into a 0.5 mL PCR tube each. Cells were resuspended in 40 µL of colony PCR mix (Table 15). Primers that bind upstream of the gene locus in the genome and within the transformed cassette were used. PCR was performed using the Taq polymerase (Sigma-Aldrich) according to a standard PCR protocol by the manufacturer. 8 µL of each PCR reaction were then run on a 1% agarose gel in 2x TAE containing Stain G, to check for positive clones. GeneRuler 1kb Plus DNA ladder (ThermoFisher Scientific) was used as size marker.

Table 15. Recipe for colony PCR mix.

Colony PCR mix (per colony)	
10 x colony PCR buffer	4 µL
dNTPs (10 mM)	1.5 µL
Betaine (5 M)	4 µL
Forward primer (10 µM)	2 µL
Reverse primer (10 µM)	2 µL
Taq DNA Polymerase (Sigma)	0.5 µl
Water	26 µl

5.3.6. Fluorescence microscopy

Microscopy experiments were performed at two different widefield microscopes throughout this study. On the one hand, the Olympus IX81 CellSens microscope equipped with a PLAPO 100x/1.45 Oil DIC objective lens (Olympus), an Orca R2 camera (Hamamatsu) and a Spectra X illumination system (Lumencor) was used at the ZMBH imaging facility of Heidelberg University. This was the case for images acquired for Figures 3A, 9A, 10A and 11. On the other hand, the Nikon Ti2 microscope equipped with a PLAN APO 100x/1.45 objective lens (Nikon) and an Orca Fusion-BT camera (Hamamatsu) was used at our lab. This was the case for images acquired for Figures 3B, 4C, 5, 6, 7A, 9B, 10B, 12-17.

Cells were grown in SCD medium. Prior to imaging, 1 mL of yeast cultures in logarithmic growth phase were spun down at 10,000 x g for 2 min, the supernatant was removed leaving only about 20 µL remaining. Cells were resuspended in the remaining liquid and 3 µL were pipetted onto a glass cover slip. To keep cells in the same plane and facilitate imaging, cell suspensions on the cover slip were covered with a pad of 1% agarose in SCD medium.

For strains expressing a protein with a HaloTag, cells were treated with the SiR-HaloTagLigand (provided by the Johnsson lab at the MPI for Biomedical Research in Heidelberg), a far-red dye, prior to imaging. For this, 1 mL of yeast cultures in logarithmic growth phase were spun down at 10,000 x g for 2 min, the supernatant was removed completely, and cells were resuspended in 50 µL sterile PBS. SiR-HTL was added to the cell suspension (final concentration of 500 nM) which was then incubated for 10 min at room temperature, shaking at 800 rpm. Cells were then prepared for imaging as described above. Multichannel, z-stack images were acquired at the microscopes with a default step size of 1 µm and a step size of 0.2 µm for images that were subsequently deconvolved. When used for quantification, z-stacks were recorded such that the entirety of the cells was covered.

5.3.7. Image processing of light-microscopy images and quantification of puncta

The Fiji software was used to assemble hyperstacks and collages of images, to create maximum intensity projections and manually count puncta (Schindelin et al., 2012; Rueden et al., 2017).

For deconvolution of images acquired at the Olympus IX81 CellSens microscope, the in-built

deconvolution algorithm, “Wiener filter”, was used. This was done for Figure 3A. For deconvolution of images acquired at the Nikon Ti2 microscope, the NIS Elements Software (Nikon) was used. The “Richardsson-Lucy” algorithm with 30 iterations and automatic detection of noise level was applied. This was the case for Figures 12, 13, 15, 16, 17.

For manual quantification of Snf7 and Bro1 puncta, maximum intensity projections were created, and image names were randomized using the “Blind Analysis Tool” plugin in Fiji to allow for an unbiased assessment. Both the number of puncta at ER clusters and the total cell number were counted to determine the ratio of puncta/cell. At least 200 cells were considered per strain and replicate.

Quantification of colocalization of Snf7 with other proteins was manually done on deconvolved images. Image names were randomized using the “Blind Analysis Tool” plugin (Astha Jaiswal and Holger Lorenz) in Fiji. 50 Snf7 puncta per strain were chosen and checked for colocalization with the respective other protein in each z-stack.

5.3.8. Mup1-pHluorin assay for ESCRT function

Strains expressing Mup1-pHluorin and cytosolic BFP were used. For each strain background, a version without tagged Mup1 was included to serve as a control for autofluorescence. Yeast cells were first grown to saturation overnight at 30°C in SC-methionine medium in 96-deepwell plates. Different dilutions of overnight cultures were prepared for each strain by adding 1, 2, 4 and 8 µL of the saturated precultures to 1 mL fresh SCD-methionine in a 96-deepwell plate. Cultures were incubated in a programmable incubator, which first kept cells at 14°C, then shifted to 30°C and shaking at 750 rpm at midnight or 2 am, so that one of the dilutions of the cultures reached an OD_{660nm} = 0.5 before the start of the experiment. The cultures closest to OD_{660nm} = 0.5 were then chosen for each strain and two new cultures at OD_{660nm} = 0.05 were prepared per strain in 900 µL SCD-methionine. For each strain, 100 µL of SCD-methionine were added to one culture, serving as a control. 100 µL of 200 µg/mL methionine were added to the other culture (final concentration of 20 µg/mL) to induce internalization of the Mup1 receptor. Cultures were grown at 30°C and shaking at 750 rpm. For each timepoint, 100 µL of the control and test cultures were transferred into a regular 96-cell plate and GFP and BFP fluorescence were measured by flow cytometry.

For the analysis, the geometric mean of GFP and BFP fluorescence was first calculated. Then, the GFP autofluorescence of the treated and untreated cultures of the autofluorescence control strain was subtracted from the mean GFP values of the respective Mup1-pHluorin strains. Next, the GFP/BFP ratios were determined. Lastly, the GFP/BFP ratio from samples supplemented with methionine were divided by the GFP/BFP ratio in samples without methionine, to calculate the methionine induced quenching of Mup1-pHluorin.

5.3.9. Flow Cytometry

Flow Cytometry measurements for yeast strain generation and the Mup1-pHluorin assay were performed at a FACS Canto flow cytometer (BD Biosciences) using a high throughput sample (HTS) loader. Laser settings were 465 V for the 488 nm laser, 410 V for the 405 nm laser and 575 V for the 561 nm laser. Settings for sample collection were 10,000 recorded events and a flow rate of 1 µL/second. To check for successful integration of a fluorescent tag during strain generation, the respective wavelength was used. For the Mup1-pHluorin assay, the 488 nm and 405 nm lasers were used to measure fluorescence of Mup1-pHluorin and of the cytosolic BFP.

5.4. Biochemistry Methods

5.4.1. Cell lysis

Cells were lysed by glass bead lysis. First, cells in logarithmic growth phase were harvested by centrifugation at 3,000 x g for 5 min at 4°C, resuspended in one volume of cold water and spun down again at 10,000 x g for 2 min. Cell pellets were either immediately used for cell lysis (for GBP co-IP) or frozen in liquid nitrogen and stored at -80°C until use (for Streptavidin IP).

For co-immunoprecipitation with GFP-binder beads (GBP), 30 ODs were harvested. In this case, the pellets were resuspended on ice in 20 µL/OD cold lysis buffer (GBP co-IP) (Table 3) containing 1x cOmplete protease inhibitors (Roche, Table 3). The cell suspension was transferred into pre-cooled 2 mL screw-cap tubes with 0.7 g 1-mm glass beads and lysed by vortexing for 40 seconds at 6 m/s on the FastPrep 24 (MP Biomedical). Lysates were collected by piercing a hole at the bottom of the screw-cap tube, placing it atop a new microfuge tube and centrifugation at 1,000 x g for 10 seconds. The lysates were cleared by centrifugation at 13.000 x rpm for 2 min at 4°C and the supernatant was transferred into a new tube.

For streptavidin bead pull-downs, 50 ODs were harvested for the biotinylation assay experiment (Fig. 8C) and 500 ODs for the PDB-MS experiment (Fig. 8D-F). The pellets were resuspended on ice in 10 µL/OD cold Lysis Buffer (Streptavidin IP) (Table 3) containing 1x cOmplete protease inhibitors (Roche, Table 3) and 1 mM DTT. The cell suspension was transferred into pre-cooled 2 mL screw-cap tubes with 0.7 g 1-mm glass beads and lysed by vortexing for 40 seconds at 6 m/s on the FastPrep 24 (MP Biomedical). If more than 40 ODs of cells were used, the samples were split into multiple screw-cap tubes with glass beads to allow for efficient rupture. Lysates were collected by piercing a hole at the bottom of the screw-cap tube, placing it atop a new microfuge tube and centrifugation at 1,000 x g for 10 seconds. The collected lysate was incubated at 65°C for 5 minutes. The lysates were cleared by centrifugation at 13,000 x rpm for 2 min at 4°C and the supernatant was transferred into a new tube. For the PDB-MS experiment (Fig. 8D-F), cells were harvested with some modifications: Cells were first spun down by centrifugation at 3,000 x g for 15 min at 4°C in 1L centrifugation buckets, the pellet was

washed with 16 mL of cold water, transferred to a 50 mL falcon tube and cells were spun down again for 5 min at 1,000 x g.

5.4.2. Protein determination

Protein concentration of cell lysates was determined using the Pierce Rapid Gold Protein Assay Kit (Thermo Fisher Scientific) in 96-well plates. BSA stock solutions ranging from 0-20 mg/mL protein were used to prepare a reference series. 10 µL of the BSA standard solutions were pipetted in duplicates. 1 µL of cell lysate was diluted with 9 µL of water, also in duplicates. BCA reagents A and B were mixed in a 50:1 ratio, as indicated by the manufacturer, and 200 µL of the BCA solution were added to each sample and standard well. Samples were incubated for 10-30 minutes at room temperature, before measuring absorbance at 480 nm using a plate reader (Tecan infinite50). Protein concentrations of the cell lysates were calculated using the standard curve obtained by the BSA reference samples .
When normalization of protein concentration was required before proceeding with the following steps, lysates were diluted with the respective lysis buffer to the required concentration.

5.4.3. Co-immunoprecipitation with GFP-binder beads

Home-made Sepharose beads coupled to GFP-binder protein from our lab (prepared according to the protocol in (Galmozzi et al., 2019)) were used for co-immunoprecipitation (co-IP) experiments of Bro1p-sfGFP.

3 mg of protein in a volume of 900 µL were used for the pull-down. Pull-downs were performed in microfuge tubes. 150 µL of bead slurry were used per sample. They were first washed twice with 1 mL Lysis Buffer (GBP co-IP) (Table 3) and spun down at 450 x g for 1 min and the supernatant was completely removed. Then the cell lysate was added to the beads, and the suspension was incubated on a rotating wheel at 4°C for 45 min. Beads were then spun down at 450 x g for 1 min and the supernatant was discarded. Next, several washing steps were performed. For each wash step, 1 mL of the respective buffer was added, beads were resuspended, incubated for 5 min on a rotating wheel, spun down again at 450 x g for 1 min and the supernatant was discarded. Wash steps were as follows: three times with Lysis Buffer (GBP co-IP) at 4°C and once with Wash Buffer (GBP co-IP) at 4°C (Table 3). After the last wash step, the remaining supernatant was removed completely. 75 µL 2x SDS-PAGE sample buffer (Table 3) were added to each sample, beads were resuspended and then incubated for 10 min at 65°C. Beads were then spun down at 450 x g for 1 min and the supernatant was collected as the eluate fraction. The eluates were stored at -20°C until further use.

5.4.4. Proximity-dependent biotinylation and pull-downs with Streptavidin beads

The principle of proximity-dependent biotinylation using Bro1 variants tagged with a TurboID tag was used in this study for a biotinylation assay to check specifically for biotinylation of Snf7 by Bro1p (Fig.

8C), as well as for a whole cell approach using PDB coupled to mass spectrometry to identify proximity partners of Bro1p (Fig. 8D-F). Biotinylation was not triggered by an exogenous biotin pulse but was based solely on the biotin present in the SCD medium (2 µg/L). The pull-down protocol was adapted from (Schopp & Béthune, 2018).

For the biotinylation assay, 2 mg of protein in a volume of 500 µL were used for the pull-down. High Capacity Streptavidin Agarose Beads (ThermoFisher Scientific) were used. Pull-downs were performed in microfuge tubes. 15 µL of 50% bead slurry were used per sample. They were first washed twice with 200 µL Lysis Buffer (Streptavidin IP) (Table 3) and spun down at 2,000 x g for 2 min and the supernatant was completely removed. Then, the cell lysate was added to the beads, and the suspension was incubated on a rotating wheel at 4°C for 3 h. Beads were then spun down at 2,000 x g for 2 min and the supernatant was discarded. Next, several washing steps were performed. For each wash step, 500 µL of the respective buffer were added, beads were resuspended, incubated for 5 min on a rotating wheel, spun down again at 2,000 x g for 2 min and the supernatant was discarded. Wash steps were as follows: twice with Wash Buffer 1 (Streptavidin IP) at 4°C, twice with Wash Buffer 2 (Streptavidin IP) at room temperature, twice with Wash Buffer 3 (Streptavidin IP) at 4°C and twice with Wash Buffer 4 (Streptavidin IP) at 4°C (Table 3). After the last wash step, the remaining supernatant was removed completely. 25 µL Elution Buffer (Streptavidin IP) (Table 3) were added to each sample, beads were resuspended and then incubated for 10 min at 65°C. Beads were then spun down at 2,500 x g for 2 min and the supernatant was collected as the eluate fraction. The eluates were stored at -20°C until further use.

For the PDB-MS the procedure was similar, except for the following changes. 500 ODs of cells were harvested and lysed. Protein concentrations were normalized to 25 mg of total protein and sample volume adjusted to 4.8 – 5.0 mL. Pull-downs were performed in 15 mL falcon tubes. 60 µL of 50% bead slurry were used per sample. They were first washed twice with 1 mL Lysis Buffer (Streptavidin IP) (Table 3) and spun down at 2,000 x g for 2 min and the supernatant was completely removed. The pull-down and the washes were performed as described above, except that all washes were performed at room temperature. Proteins were eluted in 30 µL Elution Buffer (Streptavidin IP) (Table 3).

5.4.5. Mass spectrometry for proximity-dependent biotinylation samples

Samples for mass spectrometry were generated using in-gel tryptic digestion. Preparation of this step was done together with Sabine Merker from the ZMBH mass spectrometry facility of Heidelberg University. Eluate fractions from the streptavidin pull-down were first loaded on precast 10% Bis-Tris Plus Bolt SDS-PAGE gels (Invitrogen). The PageRuler Unstained Protein Ladder (ThermoFisher Scientific) was used as a marker. The gels were run in 1x MOPS running buffer (Thermo Fisher Scientific) at 80 V until the samples entered the gel, then at 120 V until the running front entered 1 cm of the gel. Coomassie staining was used to visualize protein bands. Some bands of endogenously biotinylated

proteins were very prominent. Since the high amount of Arc1 at 50 kDa might have distorted MS measurements, each gel lane was cut into 2 pieces at the 60 kDa marker band. Thus, per sample, 2 gel pieces were further processed individually, one with proteins above 60 kDa (gel piece A) and one with proteins running below 60 kDa (gel piece B).

Mass spectrometry was performed by Sabine Merker, Marcin Luzarowski and Thomas Ruppert from the ZMBH mass spectrometry facility. In-gel tryptic digestion and LC-MS/MS analysis were performed as described previously (Bärenz et al., 2013). In summary, all gel pieces were reduced, alkylated and digested with trypsin. After peptide extraction from the gel, they were concentrated in a vacuum centrifuge and dissolved in 15 µl 0.1% TFA. Nanoflow LC-MS2 analysis was performed with an Ultimate 3000 liquid chromatography system coupled to an Orbitrap QE HF (Thermo Fisher Scientific). For this, an in-house packed analytical column (75 µm x 200 mm, 1.9 µm ReprosilPur-AQ 120 C18 material (Dr. Maisch, Germany)) was used. Mobile phase solutions were prepared with solvent A containing 0.1% formic acid/1% acetonitrile and solvent B consisting of 0.1% formic acid and 89.9% acetonitrile. Peptides generated from the upper part of the gel (gel piece A) were separated in a 60 min linear gradient started from 3% B and increased to 23% B over 50 min and to 38% B over 10 min, followed by washout with 95% B. Peptides generated from the lower part of the gel (gel piece B) were separated in a 25 min linear gradient started from 3% B and increased to 23% B over 21 min and to 38% B over 4 min, followed by washout with 95% B. The mass spectrometer was operated in data-dependent acquisition mode, automatically switching between MS and MS2. MS spectra (m/z 400–1600) were acquired in the Orbitrap at 60,000 (m/z 400) resolution and MS2 spectra were generated with normalized collision energy of 27 and isolation width of 1.4 m/z for up to 15 precursors.

The raw data from the mass spectrometry was used by our collaborator Georg Borner as a basis for data analysis. The MaxQuant 2.0.1.0 software (J. Cox & Mann, 2008) was used and the MS/MS spectra were searched against the Uniprot *S. cerevisiae* protein database from March 2022. The reference strain was ATCC 204508. Statistical analyses were performed by me using the Perseus software (Tyanova et al., 2016). LFQ intensities were considered for the analysis. The data was first pre-filtered removing the 1% false hits introduced by MaxQuant software, proteins that were only identified by peptides with a modification and contaminants. LFQ intensities were log2 transformed. Normalization was not needed, as the data was normally distributed. Samples were grouped according to strain and condition into “Wildtype untreated”, “Wildtype Tunicamycin”, “Control untreated”, “Control Tunicamycin” (4 protein groups à 3 replicates). To ensure that the analysis is based on reliably identified proteins, the data was filtered to retain only proteins with 3 valid values in at least one of the groups. Missing values were imputed with the imputation procedure of Perseus from a normal distribution with a width of 0.3 and a 1.8 standard deviation down shift. Two-sided non-paired two-sample t-tests were performed for the following combinations of samples: tunicamycin-treated vs. untreated

wildtype strain and tunicamycin-treated vs. untreated bro1 mutant strain. Volcano plots served as an output with the following settings: 500 randomizations, a false discovery rate of 0.05 and an S0 value of 0.2. Hits were termed significant when the FDR-based q-value was below 0.05. To create a final candidate of proteins enriched in proximity of wildtype Bro1 during tunicamycin treatment, both hit lists of wildtype and mutant bro1 were first filtered for significant hits with a positive log fold change (resulting in lists with 150 and 24 proteins respectively). Proteins that only came up as hits for wildtype Bro1, but not mutant Bro1, were included in the final candidate list (128 proteins).

5.4.6. SDS-PAGE

Samples for SDS-PAGE were prepared by diluting cell lysates with water to equal volumes and to the preferred amount of total protein. Then, 4x SDS-PAGE sample buffer (Table 3) containing 0.1 volumes ß-mercaptoethanol were added to each sample to a final concentration of 1x. For eluate fractions from pull-downs that were already eluted using SDS-PAGE sample buffer, no further buffer was added. Samples were incubated at 65°C for 5 min and either immediately further used or stored at -20°C.

Samples were loaded onto an SDS-PAGE gel (7.5 – 10%) (Tables 16, 17 and 18). For input samples, 20 µg of total protein were loaded. In the case of streptavidin pull-down experiments, the whole eluate fractions were loaded. For the GBP co-immunoprecipitation, a third of the eluates was loaded. The PageRuler Prestained Protein Ladder (Thermo Fisher Scientific) was used as a marker. Gels were run in 1x SDS-PAGE running buffer (Table 3) at 200 V for 40-50 min.

Table 16. Recipe for 7.5% separating gel.

7.5% separating gel	
H_2O	3.2 mL
Separating gel buffer	1.2 mL
30% acrylamide mix	1.5 mL
15% SDS	40 µL
10% APS	60 µL
TEMED	6 µL

Table 17. Recipe for 10% separating gel.

10% separating gel	
H_2O	2.7 mL
Separating gel buffer	1.2 mL
30% acrylamide mix	2 mL
15% SDS	40 µL
10% APS	60 µL
TEMED	6 µL

Table 18. Recipe for 4% stacking gel.

4% stacking gel	
H_2O	1.2 mL
Separating gel buffer	0.5 mL
30% acrylamide mix	0.27 mL
15% SDS	13 µL
10% APS	20 µL
TEMED	2 µL

5.4.7. Western Blot

The wet blotting procedure was used. Western Blot sandwiches were assembled in the cassettes between sponges using one layer of Whatman paper, the SDS-PAGE gel, a nitrocellulose membrane (GE Healthcare) and another layer of Whatman paper. Proteins were blotted at 100 V for 1 h at 4°C in 1x blotting buffer (Table 3). After disassembly of the sandwich, the membrane was rinsed in TBST and incubated for 30 min in TBS (if developed with the Licor system) or TBST (if developed with chemiluminescence) with 5% (w/v) skimmed milk powder for blocking.

The membrane was then incubated with the primary antibody (Table 11) diluted in TBST containing 5% (w/v) skimmed milk at 4°C overnight. The membrane was washed 3 times for 5 min in TBST and was then incubated with a fluorophore-coupled or HRP-coupled secondary antibody (Table 11) diluted in TBST containing 5% (w/v) skimmed milk at room temperature for 1 h.

For fluorescent signal detection using fluorophore-coupled secondary antibodies, membranes were again washed 3 times for 5 min, twice with TBST and once with TBS. They were then scanned at the Odyssey CLx system (LI-COR Biotech) in the 680 or 790 channel, depending on the fluorophore. For detection of chemiluminescent signal using HRP-coupled secondary antibodies, membranes were washed 3 times for 5 min with TBST. For visualization, SuperSignal West Pico Plus Chemiluminescent substrate solutions A and B (Thermo Fisher Scientific) were mixed in a 1:1 ratio and added to the membrane for a 5 min incubation at room temperature. The membrane was scanned at an Amersham Imager 600.

6. SUPPLEMENT

Table S1. Final Hitlist (WT only hits) of the PDB-MS.

Protein IDs	Gene names	Protein names
Q03790	NUP53	Nucleoporin NUP53
P43621	RET2	Coatomer subunit delta
Q08484	GYP1	GTPase-activating protein GYP1
P33400	RIM101	pH-response transcription factor pacC/RIM101
Q03103	ERO1	Endoplasmic oxidoreductin-1
P39078	CCT4	T-complex protein 1 subunit delta
P40340	YTA7	Tat-binding homolog 7
Q12033	RIM20	pH-response regulator protein palA/RIM20
P14742	GFA1	Glutamine-fructose-6-phosphate aminotransferase [isomerizing]
P16474	KAR2	78 kDa glucose-regulated protein homolog
P14906	SEC63	Protein translocation protein SEC63
P39723	SPC72	Spindle pole component SPC72
Q04368	CSI1	Cop9 signalosome-interactor 1
P10591	SSA1	Heat shock protein SSA1
P14743	NMT1	Glycylpeptide N-tetradecanoyltransferase
Q00764	TPS1	Alpha,alpha-trehalose-phosphate synthase [UDP-forming] 56 kDa subunit
P27466	CMK1	Calcium/calmodulin-dependent protein kinase I
P25373	GRX1	Glutaredoxin-1
P39730	FUN12	Eukaryotic translation initiation factor 5B
P07276	RAD2	DNA repair protein RAD2
Q06505	SPN1	Transcription factor SPN1
P07246	ADH3	Alcohol dehydrogenase 3, mitochondrial
P04806	HXK1	Hexokinase-1
P41895	TFG1	Transcription initiation factor IIF subunit alpha
P40361	YJL070C	Inactive deaminase YJL070C
Q03761	TAF12	Transcription initiation factor TFIID subunit 12
P09959	SWI6	Regulatory protein SWI6
Q03707	SRC1	Inner nuclear membrane protein SRC1
Q08641	ABP140	tRNA(Thr) (cytosine(32)-N(3))-methyltransferase
P22515	UBA1	Ubiquitin-activating enzyme E1 1
P53137	CUE3	CUE domain-containing protein 3
P34110	VPS35	Vacuolar protein sorting-associated protein 35
P17106	CBF1	Centromere-binding protein 1
Q06344	ESF1	Pre-rRNA-processing protein ESF1
Q08971	YPL225W	Protein PBDC1 homolog
P38764	RPN1	26S proteasome regulatory subunit RPN1
P39926	SSO2	Protein SSO2
Q12343	MED4	Mediator of RNA polymerase II transcription subunit 4
P32528	DUR1,2	Urea amidolyase;Urea carboxylase;Allophanate hydrolase
Q12250	RPN5	26S proteasome regulatory subunit RPN5
P38845	CRP1	Cruciform DNA-recognizing protein 1
P40316	PDS1	Securin
P50111	ZDS1	Protein ZDS1
P36047	SDS22	Protein phosphatase 1 regulatory subunit SDS22
P36040	ADD66	Proteasome assembly chaperone 2
Q03533	TDA1	Serine/threonine-protein kinase TDA1
P47018	MTC1	Maintenance of telomere capping protein 1
Q12242	RUP1	UBA domain-containing protein RUP1
P25037	UBP1	Ubiquitin carboxyl-terminal hydrolase 1
P15019;P53228	TAL1	Transaldolase
P36037	DOA1	Protein DOA1

P53111	ARI1	NADPH-dependent aldehyde reductase ARI1
Q06677	SWA2	Auxilin-like clathrin uncoating factor SWA2
P40482	SEC24	Protein transport protein SEC24
P07264	LEU1	3-isopropylmalate dehydratase
P38822	BZZ1	Protein BZZ1
P53981	YNL010W	Uncharacterized phosphatase YNL010W
Q12265	PRS5	Ribose-phosphate pyrophosphokinase 5
Q06263	VTA1	Vacuolar protein sorting-associated protein VTA1
Q12044	RCN2	Regulator of calcineurin 2
P52553	YKE2	Prefoldin subunit 6
P32074	SEC21	Coatomer subunit gamma
P09938	RNR2	Ribonucleoside-diphosphate reductase small chain 1
Q06671	ATG23	Autophagy-related protein 23
P39929	SNF7	Vacuolar-sorting protein SNF7
P07283	SEC53	Phosphomannomutase
P35207	SKI2	Antiviral helicase SKI2
Q01476	UBP2	Ubiquitin carboxyl-terminal hydrolase 2
P06101	CDC37	Hsp90 co-chaperone Cdc37
Q08977	YPL260W	UPF0662 protein YPL260W
P14832	CPR1	Peptidyl-prolyl cis-trans isomerase
Q06523	YPR148C	Uncharacterized protein YPR148C
Q06685	VIP1	Inositol hexakisphosphate and diphosphoinositol-pentakisphosphate kinase
Q12514	NOT5	General negative regulator of transcription subunit 5
Q06385	VPS74	Vacuolar protein sorting-associated protein 74
P33416	HSP78	Heat shock protein 78, mitochondrial
P43585	VTC2	Vacuolar transporter chaperone 2
Q03558;P41816	OYE2	NADPH dehydrogenase 2
P48415	SEC16	COPII coat assembly protein SEC16
P43597	YFR016C	Uncharacterized protein YFR016C
Q08966	PCL8	PHO85 cyclin-8
P38749	YAP3	AP-1-like transcription factor YAP3
P47068	BBC1	Myosin tail region-interacting protein MTI1
Q07457	BRE1	E3 ubiquitin-protein ligase BRE1
P41811	SEC27	Coatomer subunit beta
P69771	DID2	Vacuolar protein-sorting-associated protein 46
P11154	PYC1	Pyruvate carboxylase 1
Q04947	RTN1	Reticulon-like protein 1
P39081	PCF11	Protein PCF11
P38255	RXT2	Transcriptional regulatory protein RXT2
P33328	SNC2	Synaptobrevin homolog 2
P14904	APE1	Vacuolar aminopeptidase 1
P32599	SAC6	Fimbrin
Q05027	TAF9	Transcription initiation factor TFIID subunit 9
P47166	SGM1	Protein SGM1
P25343	RVS161	Reduced viability upon starvation protein 161
P09032	GCD1	Translation initiation factor eIF-2B subunit gamma
P40219	OSW5	Outer spore wall protein 5
P17065	SEC2	Rab guanine nucleotide exchange factor SEC2
Q06336	GGA1	ADP-ribosylation factor-binding protein GGA1
P07806-2;P07806	VAS1	Valine--tRNA ligase, mitochondrial
Q12344	GYP5	GTPase-activating protein GYP5
P27351	APL1	AP-2 complex subunit beta
P04807	HXK2	Hexokinase-2
P43123	QRI1	UDP-N-acetylglucosamine pyrophosphorylase
Q04951	SCW10	Probable family 17 glucosidase SCW10
P22803	TRX2	Thioredoxin-2

P38903	RTS1	Serine/threonine-protein phosphatase 2A 56 kDa regulatory subunit delta isoform
P11076;P19146	ARF1;ARF2	ADP-ribosylation factor 1;ADP-ribosylation factor 2
P40029	MXR1	Peptide methionine sulfoxide reductase
P33299	RPT1	26S protease regulatory subunit 7 homolog
P40509	SEC28	Coatomer subunit epsilon
P32914	SPT4	Transcription elongation factor SPT4
Q12515	PAR32	Protein PAR32
P25558	BUD3	Bud site selection protein 3
Q12373	HIF1	HAT1-interacting factor 1
Q06449	PIN3	[PSI+] inducibility protein 3
Q03390	VPS60	Vacuolar protein-sorting-associated protein 60
Q08581	SLK19	Kinetochore protein SLK19
Q04533	YML082W	Putative cystathionine gamma-synthase YML082W
P38066	RIB1	GTP cyclohydrolase-2
P32419	MDH3	Malate dehydrogenase, peroxisomal
P16550	APA1	Protein APA1;5,5-P-1,P-4-tetraphosphate phosphorylase;ADP-sulfurylase
Q12494	KCS1	Inositol hexakisphosphate kinase 1
P32867	SSO1	Protein SSO1
P47044	YJL055W	LOG family protein YJL055W
P52917	VPS4	Vacuolar protein sorting-associated protein 4
P32776	TFB1	RNA polymerase II transcription factor B subunit 1

Table S2. Hits in both WT Bro1 and bro1^{K246A} of the PDB-MS.

Protein IDs	Gene names	Protein names
P15303	SEC23	Protein transport protein SEC23
Q00055	GPD1	Glycerol-3-phosphate dehydrogenase [NAD(+)] 1
P06780	RHO1	GTP-binding protein RHO1
P53250	TWF1	Twinfilin-1
P17709;Q04409	GLK1	Glucokinase-1
P18899	DDR48	Stress protein DDR48
P31539	HSP104	Heat shock protein 104
Q04792	GAD1	Glutamate decarboxylase
Q04279	SEG1	Eisosome protein SEG1
P00924	ENO1	Enolase 1
P38809	YHR097C	Uncharacterized protein YHR097C
P36139	PET10	Protein PET10
P22517	CMK2	Calcium/calmodulin-dependent protein kinase II
P34760;Q04120	TSA1	Peroxiredoxin TSA1
P38934	BFR1	Nuclear segregation protein BFR1
P53622	COP1	Coatomer subunit alpha
P17967	PDI1	Protein disulfide-isomerase
Q07551	YDL124W	NADPH-dependent alpha-keto amide reductase
P54838	DAK1	Dihydroxyacetone kinase 1
P11986	INO1	Inositol-3-phosphate synthase

Table S3. Hits in bro1^{K246A} only of the PDB-MS.

Protein IDs	Gene names	Protein names
P12385	SUP45	Eukaryotic peptide chain release factor subunit 1
P32527	ZUO1	Zuotin
P53912	YNL134C	Uncharacterized protein YNL134C
P06785	CDC21	Thymidylate synthase

7. REFERENCES

Adell, M. A. Y., Migliano, S. M., Upadhyayula, S., Bykov, Y. S., Sprenger, S., Pakdel, M., Vogel, G. F., Jih, G., Skillern, W., Behrouzi, R., Babst, M., Schmidt, O., Hess, M. W., Briggs, J. A., Kirchhausen, T., & Teis, D. (2017). Recruitment dynamics of ESCRT-III and Vps4 to endosomes and implications for reverse membrane budding. *eLife*, *6*, e31652. https://doi.org/10.7554/eLife.31652

Alam, S. L., Sun, J., Payne, M., Welch, B. D., Blake, B. K., Davis, D. R., Meyer, H. H., Emr, S. D., & Sundquist, W. I. (2004). Ubiquitin interactions of NZF zinc fingers. *The EMBO Journal*, *23*(7), 1411–1421. https://doi.org/10.1038/sj.emboj.7600114

Allison, R., Lumb, J. H., Fassier, C., Connell, J. W., Ten Martin, D., Seaman, M. N. J., Hazan, J., & Reid, E. (2013). An ESCRT–spastin interaction promotes fission of recycling tubules from the endosome. *Journal of Cell Biology*, *202*(3), 527–543. https://doi.org/10.1083/jcb.201211045

Babst, M. (1998). The Vps4p AAA ATPase regulates membrane association of a Vps protein complex required for normal endosome function. *The EMBO Journal*, *17*(11), 2982–2993. https://doi.org/10.1093/emboj/17.11.2982

Babst, M., Katzmann, D. J., Estepa-Sabal, E. J., Meerloo, T., & Emr, S. D. (2002). Escrt-III. *Developmental Cell*, *3*(2), 271–282. https://doi.org/10.1016/S1534-5807(02)00220-4

Babst, M., Katzmann, D. J., Snyder, W. B., Wendland, B., & Emr, S. D. (2002). Endosome-Associated Complex, ESCRT-II, Recruits Transport Machinery for Protein Sorting at the Multivesicular Body. *Developmental Cell*, *3*(2), 283–289. https://doi.org/10.1016/S1534-5807(02)00219-8

Bache, K. G., Brech, A., Mehlum, A., & Stenmark, H. (2003). Hrs regulates multivesicular body formation via ESCRT recruitment to endosomes. *The Journal of Cell Biology*, *162*(3), 435–442. https://doi.org/10.1083/jcb.200302131

Bärenz, F., Inoue, D., Yokoyama, H., Tegha-Dunghu, J., Freiss, S., Draeger, S., Mayilo, D., Cado, I., Merker, S., Klinger, M., Hoeckendorf, B., Pilz, S., Hupfeld, K., Steinbeisser, H., Lorenz, H., Ruppert, T., Wittbrodt, J., & Gruss, O. J. (2013). The centriolar satellite protein SSX2IP promotes centrosome maturation. *Journal of Cell Biology*, *202*(1), 81–95. https://doi.org/10.1083/jcb.201302122

Barlowe, C., & Helenius, A. (2016). Cargo Capture and Bulk Flow in the Early Secretory Pathway. *Annual Review of Cell and Developmental Biology*, *32*(1), 197–222. https://doi.org/10.1146/annurev-cellbio-111315-125016

Barlowe, C. K., & Miller, E. A. (2013). Secretory Protein Biogenesis and Traffic in the Early Secretory Pathway. *Genetics*, *193*(2), 383–410. https://doi.org/10.1534/genetics.112.142810

Bertolotti, A., Zhang, Y., Hendershot, L. M., Harding, H. P., & Ron, D. (2000). Dynamic interaction of BiP and ER stress transducers in the unfolded-protein response. *Nature Cell Biology*, *2*(6), 326–332. https://doi.org/10.1038/35014014

Bieber, A., Capitanio, C., Erdmann, P. S., Fiedler, F., Beck, F., Lee, C.-W., Li, D., Hummer, G., Schulman, B. A., Baumeister, W., & Wilfling, F. (2022). In situ structural analysis reveals membrane shape transitions during autophagosome formation. *Proceedings of the National Academy of Sciences*, *119*(39), e2209823119. https://doi.org/10.1073/pnas.2209823119

Bissig, C., Lenoir, M., Velluz, M.-C., Kufareva, I., Abagyan, R., Overduin, M., & Gruenberg, J. (2013). Viral Infection Controlled by a Calcium-Dependent Lipid-Binding Module in ALIX. *Developmental Cell*, *25*(4), 364–373. https://doi.org/10.1016/j.devcel.2013.04.003

Booth, A., Marklew, C. J., Ciani, B., & Beales, P. A. (2019). In Vitro Membrane Remodeling by ESCRT is Regulated by Negative Feedback from Membrane Tension. *iScience*, *15*, 173–184. https://doi.org/10.1016/j.isci.2019.04.021

Bowers, K., Lottridge, J., Helliwell, S. B., Goldthwaite, L. M., Luzio, J. P., & Stevens, T. H. (2004). Protein–Protein Interactions of ESCRT Complexes in the Yeast *Saccharomyces cerevisiae*. *Traffic*, *5*(3), 194–210. https://doi.org/10.1111/j.1600-0854.2004.00169.x

Boysen, J. H., & Mitchell, A. P. (2006). Control of Bro1-Domain Protein Rim20 Localization by External pH, ESCRT Machinery, and the *Saccharomyces cerevisiae* Rim101 Pathway. *Molecular Biology of the Cell*, *17*(3), 1344–1353. https://doi.org/10.1091/mbc.e05-10-0949

Braakman, I., Helenius, J., & Helenius, A. (1992). Manipulating disulfide bond formation and protein folding in the endoplasmic reticulum. *The EMBO Journal*, *11*(5), 1717–1722. https://doi.org/10.1002/j.1460-2075.1992.tb05223.x

Branon, T. C., Bosch, J. A., Sanchez, A. D., Udeshi, N. D., Svinkina, T., Carr, S. A., Feldman, J. L., Perrimon, N., & Ting, A. Y. (2018). Efficient proximity labeling in living cells and organisms with TurboID. *Nature Biotechnology*, *36*(9), 880–887. https://doi.org/10.1038/nbt.4201

Bravo, R., Vicencio, J. M., Parra, V., Troncoso, R., Munoz, J. P., Bui, M., Quiroga, C., Rodriguez, A. E., Verdejo, H. E., Ferreira, J., Iglewski, M., Chiong, M., Simmen, T., Zorzano, A., Hill, J. A., Rothermel, B. A., Szabadkai, G., & Lavandero, S. (2011). Increased ER–mitochondrial coupling promotes mitochondrial respiration and bioenergetics during early phases of ER stress. *Journal of Cell Science*, *124*(13), 2143–2152. https://doi.org/10.1242/jcs.080762

Caillat, C., Macheboeuf, P., Wu, Y., McCarthy, A. A., Boeri-Erba, E., Effantin, G., Göttlinger, H. G., Weissenhorn, W., & Renesto, P. (2015). Asymmetric ring structure of Vps4 required for ESCRT-III disassembly. *Nature Communications*, *6*(1), 8781. https://doi.org/10.1038/ncomms9781

Calcagno-Pizarelli, A. M., Hervás-Aguilar, A., Galindo, A., Abenza, J. F., Peñalva, M. A., & Arst, H. N. (2011). Rescue of *Aspergillus nidulans* severely debilitating null mutations in ESCRT-0, I, II and III genes by inactivation of a salt-tolerance pathway allows examination of ESCRT gene roles in pH signalling. *Journal of Cell Science*, *124*(23), 4064–4076. https://doi.org/10.1242/jcs.088344

Carlton, J. G., & Martin-Serrano, J. (2007). Parallels Between Cytokinesis and Retroviral Budding: A Role for the ESCRT Machinery. *Science*, *316*(5833), 1908–1912. https://doi.org/10.1126/science.1143422

Cashikar, A. G., Shim, S., Roth, R., Maldazys, M. R., Heuser, J. E., & Hanson, P. I. (2014). Structure of cellular ESCRT-III spirals and their relationship to HIV budding. *eLife*, *3*, e02184. https://doi.org/10.7554/eLife.02184

Castillon, G. A., Aguilera-Romero, A., Manzano-Lopez, J., Epstein, S., Kajiwara, K., Funato, K., Watanabe, R., Riezman, H., & Muñiz, M. (2011). The yeast p24 complex regulates GPI-anchored protein transport and quality control by monitoring anchor remodeling. *Molecular Biology of the Cell*, *22*(16), 2924–2936. https://doi.org/10.1091/mbc.e11-04-0294

Cheatham, A. M., Sharma, N. R., & Satpute-Krishnan, P. (2023). Competition for calnexin binding regulates secretion and turnover of misfolded GPI-anchored proteins. *Journal of Cell Biology*, *222*(10), e202108160. https://doi.org/10.1083/jcb.202108160

Chen, X., Shen, J., & Prywes, R. (2002). The Luminal Domain of ATF6 Senses Endoplasmic Reticulum (ER) Stress and Causes Translocation of ATF6 from the ER to the Golgi. *Journal of Biological Chemistry*, *277*(15), 13045–13052. https://doi.org/10.1074/jbc.M110636200

Chen, X., VanValkenburgh, C., Liang, H., Fang, H., & Green, N. (2001). Signal Peptidase and Oligosaccharyltransferase Interact in a Sequential and Dependent Manner within the Endoplasmic Reticulum. *Journal of Biological Chemistry*, *276*(4), 2411–2416. https://doi.org/10.1074/jbc.M007723200

Chiaruttini, N., Redondo-Morata, L., Colom, A., Humbert, F., Lenz, M., Scheuring, S., & Roux, A. (2015). Relaxation of Loaded ESCRT-III Spiral Springs Drives Membrane Deformation. *Cell*, *163*(4), 866–879. https://doi.org/10.1016/j.cell.2015.10.017

Cho, K. F., Branon, T. C., Rajeev, S., Svinkina, T., Udeshi, N. D., Thoudam, T., Kwak, C., Rhee, H.-W., Lee, I.-K., Carr, S. A., & Ting, A. Y. (2020). Split-TurboID enables contact-dependent proximity labeling in cells. *Proceedings of the National Academy of Sciences*, *117*(22), 12143–12154. https://doi.org/10.1073/pnas.1919528117

Choi-Rhee, E., Schulman, H., & Cronan, J. E. (2004). Promiscuous protein biotinylation by *Escherichia coli* biotin protein ligase. *Protein Science*, *13*(11), 3043–3050. https://doi.org/10.1110/ps.04911804

Christ, L., Wenzel, E. M., Liestøl, K., Raiborg, C., Campsteijn, C., & Stenmark, H. (2016). ALIX and ESCRT-I/II function as parallel ESCRT-III recruiters in cytokinetic abscission. *Journal of Cell Biology*, *212*(5), 499–513. https://doi.org/10.1083/jcb.201507009

Collado, J., Kalemanov, M., Campelo, F., Bourgoint, C., Thomas, F., Loewith, R., Martínez-Sánchez, A., Baumeister, W., Stefan, C. J., & Fernández-Busnadiego, R. (2019). Tricalbin-Mediated Contact Sites Control ER

Curvature to Maintain Plasma Membrane Integrity. *Developmental Cell*, *51*(4), 476-487.e7. https://doi.org/10.1016/j.devcel.2019.10.018

Costello, J. L., Castro, I. G., Hacker, C., Schrader, T. A., Metz, J., Zeuschner, D., Azadi, A. S., Godinho, L. F., Costina, V., Findeisen, P., Manner, A., Islinger, M., & Schrader, M. (2017). ACBD5 and VAPB mediate membrane associations between peroxisomes and the ER. *Journal of Cell Biology*, *216*(2), 331–342. https://doi.org/10.1083/jcb.201607055

Cox, J., & Mann, M. (2008). MaxQuant enables high peptide identification rates, individualized p.p.b.-range mass accuracies and proteome-wide protein quantification. *Nature Biotechnology*, *26*(12), 1367–1372. https://doi.org/10.1038/nbt.1511

Cox, J. S., Chapman, R. E., & Walter, P. (1997). The unfolded protein response coordinates the production of endoplasmic reticulum protein and endoplasmic reticulum membrane. *Molecular Biology of the Cell*, *8*(9), 1805–1814. https://doi.org/10.1091/mbc.8.9.1805

Cox, J. S., Shamu, C. E., & Walter, P. (1993). Transcriptional induction of genes encoding endoplasmic reticulum resident proteins requires a transmembrane protein kinase. *Cell*, *73*(6), 1197–1206. https://doi.org/10.1016/0092-8674(93)90648-A

Cox, J. S., & Walter, P. (1996). A Novel Mechanism for Regulating Activity of a Transcription Factor That Controls the Unfolded Protein Response. *Cell*, *87*(3), 391–404. https://doi.org/10.1016/S0092-8674(00)81360-4

Credle, J. J., Finer-Moore, J. S., Papa, F. R., Stroud, R. M., & Walter, P. (2005). On the mechanism of sensing unfolded protein in the endoplasmic reticulum. *Proceedings of the National Academy of Sciences*, *102*(52), 18773–18784. https://doi.org/10.1073/pnas.0509487102

D'Arcangelo, J. G., Crissman, J., Pagant, S., Čopič, A., Latham, C. F., Snapp, E. L., & Miller, E. A. (2015). Traffic of p24 Proteins and COPII Coat Composition Mutually Influence Membrane Scaffolding. *Current Biology*, *25*(10), 1296–1305. https://doi.org/10.1016/j.cub.2015.03.029

Dennis, E. A., & Kennedy, E. P. (1972). Intracellular sites of lipid synthesis and the biogenesis of mitochondria. *Journal of Lipid Research*, *13*(2), 263–267. https://doi.org/10.1016/S0022-2275(20)39421-9

Diaz, A., Zhang, J., Ollwerther, A., Wang, X., & Ahlquist, P. (2015). Host ESCRT proteins are required for bromovirus RNA replication compartment assembly and function. *PLoS Pathogens*, *11*(3), e1004742. https://doi.org/10.1371/journal.ppat.1004742

Eisenberg, T., & Büttner, S. (2014). Lipids and cell death in yeast. *FEMS Yeast Research*, *14*(1), 179–197. https://doi.org/10.1111/1567-1364.12105

Fawcett, D. W. (1981). *The cell* (2. ed). Saunders.

Federovitch, C. M., Ron, D., & Hampton, R. Y. (2005). The dynamic ER: Experimental approaches and current questions. *Current Opinion in Cell Biology*, *17*(4), 409–414. https://doi.org/10.1016/j.ceb.2005.06.010

Fresques, T., Niles, B., Aronova, S., Mogri, H., Rakhshandehroo, T., & Powers, T. (2015). Regulation of Ceramide Synthase by Casein Kinase 2-dependent Phosphorylation in Saccharomyces cerevisiae. *Journal of Biological Chemistry*, *290*(3), 1395–1403. https://doi.org/10.1074/jbc.M114.621086

Friedman, J. R., Lackner, L. L., West, M., DiBenedetto, J. R., Nunnari, J., & Voeltz, G. K. (2011). ER Tubules Mark Sites of Mitochondrial Division. *Science*, *334*(6054), 358–362. https://doi.org/10.1126/science.1207385

Funato, K., & Riezman, H. (2001). Vesicular and nonvesicular transport of ceramide from ER to the Golgi apparatus in yeast. *The Journal of Cell Biology*, *155*(6), 949–960. https://doi.org/10.1083/jcb.200105033

Gable, K., Slife, H., Bacikova, D., Monaghan, E., & Dunn, T. M. (2000). Tsc3p Is an 80-Amino Acid Protein Associated with Serine Palmitoyltransferase and Required for Optimal Enzyme Activity. *Journal of Biological Chemistry*, *275*(11), 7597–7603. https://doi.org/10.1074/jbc.275.11.7597

Galmozzi, C. V., Merker, D., Friedrich, U. A., Döring, K., & Kramer, G. (2019). Selective ribosome profiling to study interactions of translating ribosomes in yeast. *Nature Protocols*, *14*(8), 2279–2317. https://doi.org/10.1038/s41596-019-0185-z

Gardner, B. M., & Walter, P. (2011). Unfolded Proteins Are Ire1-Activating Ligands That Directly Induce the Unfolded Protein Response. *Science*, *333*(6051), 1891–1894. https://doi.org/10.1126/science.1209126

Garrus, J. E., Von Schwedler, U. K., Pornillos, O. W., Morham, S. G., Zavitz, K. H., Wang, H. E., Wettstein, D. A., Stray, K. M., Côté, M., Rich, R. L., Myszka, D. G., & Sundquist, W. I. (2001). Tsg101 and the Vacuolar Protein

Sorting Pathway Are Essential for HIV-1 Budding. *Cell*, *107*(1), 55–65. https://doi.org/10.1016/S0092-8674(01)00506-2

Giordano, F., Saheki, Y., Idevall-Hagren, O., Colombo, S. F., Pirruccello, M., Milosevic, I., Gracheva, E. O., Bagriantsev, S. N., Borgese, N., & De Camilli, P. (2013). PI(4,5)P(2)-dependent and Ca(2+)-regulated ER-PM interactions mediated by the extended synaptotagmins. *Cell*, *153*(7), 1494–1509. https://doi.org/10.1016/j.cell.2013.05.026

Hanada, K., Kumagai, K., Yasuda, S., Miura, Y., Kawano, M., Fukasawa, M., & Nishijima, M. (2003). Molecular machinery for non-vesicular trafficking of ceramide. *Nature*, *426*(6968), 803–809. https://doi.org/10.1038/nature02188

Hara-Kuge, S. (1994). En bloc incorporation of coatomer subunits during the assembly of COP- coated vesicles [published erratum appears in J Cell Biol 1994 Jul;126(2):589]. *The Journal of Cell Biology*, *124*(6), 883–892. https://doi.org/10.1083/jcb.124.6.883

Harding, H. P., Zhang, Y., & Ron, D. (1999). Protein translation and folding are coupled by an endoplasmic-reticulum-resident kinase. *Nature*, *397*(6716), 271–274. https://doi.org/10.1038/16729

Haze, K., Yoshida, H., Yanagi, H., Yura, T., & Mori, K. (1999). Mammalian Transcription Factor ATF6 Is Synthesized as a Transmembrane Protein and Activated by Proteolysis in Response to Endoplasmic Reticulum Stress. *Molecular Biology of the Cell*, *10*(11), 3787–3799. https://doi.org/10.1091/mbc.10.11.3787

Hierro, A., Sun, J., Rusnak, A. S., Kim, J., Prag, G., Emr, S. D., & Hurley, J. H. (2004). Structure of the ESCRT-II endosomal trafficking complex. *Nature*, *431*(7005), 221–225. https://doi.org/10.1038/nature02914

Ho, N., Yap, W. S., Xu, J., Wu, H., Koh, J. H., Goh, W. W. B., George, B., Chong, S. C., Taubert, S., & Thibault, G. (2020). Stress sensor Ire1 deploys a divergent transcriptional program in response to lipid bilayer stress. *Journal of Cell Biology*, *219*(7), e201909165. https://doi.org/10.1083/jcb.201909165

Hofmann, K., & Falquet, L. (2001). A ubiquitin-interacting motif conserved in components of the proteasomal and lysosomal protein degradation systems. *Trends in Biochemical Sciences*, *26*(6), 347–350. https://doi.org/10.1016/S0968-0004(01)01835-7

Hsu, J.-W., Tang, P.-H., Wang, I.-H., Liu, C.-L., Chen, W.-H., Tsai, P.-C., Chen, K.-Y., Chen, K.-J., Yu, C.-J., & Lee, F.-J. S. (2016). Unfolded protein response regulates yeast small GTPase Arl1p activation at late Golgi via phosphorylation of Arf GEF Syt1p. *Proceedings of the National Academy of Sciences*, *113*(12). https://doi.org/10.1073/pnas.1518260113

Hurley, J. H. (2015). ESCRTs are everywhere. *The EMBO Journal*, *34*(19), 2398–2407. https://doi.org/10.15252/embj.201592484

Hwang, J., Peterson, B. G., Knupp, J., & Baldridge, R. D. (2023). The ERAD system is restricted by elevated ceramides. *Science Advances*, *9*(2), eadd8579. https://doi.org/10.1126/sciadv.add8579

Ikeda, A., Schlarmann, P., Kurokawa, K., Nakano, A., Riezman, H., & Funato, K. (2020). Tricalbins Are Required for Non-vesicular Ceramide Transport at ER-Golgi Contacts and Modulate Lipid Droplet Biogenesis. *iScience*, *23*(10), 101603. https://doi.org/10.1016/j.isci.2020.101603

Ito, T., Chiba, T., Ozawa, R., Yoshida, M., Hattori, M., & Sakaki, Y. (2001). A comprehensive two-hybrid analysis to explore the yeast protein interactome. *Proceedings of the National Academy of Sciences*, *98*(8), 4569–4574. https://doi.org/10.1073/pnas.061034498

Jang, W., & Haucke, V. (2024). ER remodeling via lipid metabolism. *Trends in Cell Biology*, *34*(11), 942–954. https://doi.org/10.1016/j.tcb.2024.01.011

Janke, C., Magiera, M. M., Rathfelder, N., Taxis, C., Reber, S., Maekawa, H., Moreno-Borchart, A., Doenges, G., Schwob, E., Schiebel, E., & Knop, M. (2004). A versatile toolbox for PCR-based tagging of yeast genes: New fluorescent proteins, more markers and promoter substitution cassettes. *Yeast*, *21*(11), 947–962. https://doi.org/10.1002/yea.1142

Jeong, H., Park, J., Jun, Y., & Lee, C. (2017). Crystal structures of Mmm1 and Mdm12–Mmm1 reveal mechanistic insight into phospholipid trafficking at ER-mitochondria contact sites. *Proceedings of the National Academy of Sciences*, *114*(45). https://doi.org/10.1073/pnas.1715592114

Jimenez, A. J., Maiuri, P., Lafaurie-Janvore, J., Divoux, S., Piel, M., & Perez, F. (2014). ESCRT Machinery Is Required for Plasma Membrane Repair. *Science*, *343*(6174), 1247136. https://doi.org/10.1126/science.1247136

Katzmann, D. J., Babst, M., & Emr, S. D. (2001). Ubiquitin-Dependent Sorting into the Multivesicular Body Pathway Requires the Function of a Conserved Endosomal Protein Sorting Complex, ESCRT-I. *Cell*, *106*(2), 145–155. https://doi.org/10.1016/S0092-8674(01)00434-2

Kawano, M., Kumagai, K., Nishijima, M., & Hanada, K. (2006). Efficient Trafficking of Ceramide from the Endoplasmic Reticulum to the Golgi Apparatus Requires a VAMP-associated Protein-interacting FFAT Motif of CERT. *Journal of Biological Chemistry*, *281*(40), 30279–30288. https://doi.org/10.1074/jbc.M605032200

Kim, J., Sitaraman, S., Hierro, A., Beach, B. M., Odorizzi, G., & Hurley, J. H. (2005). Structural basis for endosomal targeting by the Bro1 domain. *Developmental Cell*, *8*(6), 937–947. https://doi.org/10.1016/j.devcel.2005.04.001

Kojima, R., Endo, T., & Tamura, Y. (2016). A phospholipid transfer function of ER-mitochondria encounter structure revealed in vitro. *Scientific Reports*, *6*(1), 30777. https://doi.org/10.1038/srep30777

Kornmann, B., Currie, E., Collins, S. R., Schuldiner, M., Nunnari, J., Weissman, J. S., & Walter, P. (2009). An ER-Mitochondria Tethering Complex Revealed by a Synthetic Biology Screen. *Science*, *325*(5939), 477–481. https://doi.org/10.1126/science.1175088

Kostelansky, M. S., Schluter, C., Tam, Y. Y. C., Lee, S., Ghirlando, R., Beach, B., Conibear, E., & Hurley, J. H. (2007). Molecular Architecture and Functional Model of the Complete Yeast ESCRT-I Heterotetramer. *Cell*, *129*(3), 485–498. https://doi.org/10.1016/j.cell.2007.03.016

Larochelle, M., Bergeron, D., Arcand, B., & Bachand, F. (2019). Proximity-dependent biotinylation mediated by TurboID to identify protein–protein interaction networks in yeast. *Journal of Cell Science*, *132*(11), jcs232249. https://doi.org/10.1242/jcs.232249

Larrañaga-SanMiguel, A., Bengoa-Vergniory, N., & Flores-Romero, H. (2025). Crosstalk between mitochondria–ER contact sites and the apoptotic machinery as a novel health meter. *Trends in Cell Biology*, *35*(1), 33–45. https://doi.org/10.1016/j.tcb.2024.08.007

Lee, S., Joshi, A., Nagashima, K., Freed, E. O., & Hurley, J. H. (2007). Structural basis for viral late-domain binding to Alix. *Nature Structural & Molecular Biology*, *14*(3), 194–199. https://doi.org/10.1038/nsmb1203

Letourneur, F., Gaynor, E. C., Hennecke, S., Démollière, C., Duden, R., Emr, S. D., Riezman, H., & Cosson, P. (1994). Coatomer is essential for retrieval of dilysine-tagged proteins to the endoplasmic reticulum. *Cell*, *79*(7), 1199–1207. https://doi.org/10.1016/0092-8674(94)90011-6

Levine, T. P., & Munro, S. (2002). Targeting of Golgi-Specific Pleckstrin Homology Domains Involves Both PtdIns 4-Kinase-Dependent and -Independent Components. *Current Biology*, *12*(9), 695–704. https://doi.org/10.1016/S0960-9822(02)00779-0

Levine, T. P., Wiggins, C. A. R., & Munro, S. (2000). Inositol Phosphorylceramide Synthase Is Located in the Golgi Apparatus of *Saccharomyces cerevisiae*. *Molecular Biology of the Cell*, *11*(7), 2267–2281. https://doi.org/10.1091/mbc.11.7.2267

Li, W., & Mitchell, A. P. (1997). Proteolytic activation of Rim1p, a positive regulator of yeast sporulation and invasive growth. *Genetics*, *145*(1), 63–73. https://doi.org/10.1093/genetics/145.1.63

Lima, D. C. A., Volpe Bossa, G., Ciancaglini, P., Ramos, A. P., & Soares, T. A. (2025). The Effect of Ceramide Ratio on the Membrane Curvature of Mimetic Models of Matrix Vesicles. *ACS Physical Chemistry Au*, acsphyschemau.5c00010. https://doi.org/10.1021/acsphyschemau.5c00010

Limar, S., Körner, C., Martínez-Montañés, F., Stancheva, V. G., Wolf, V. N., Walter, S., Miller, E. A., Ejsing, C. S., Galassi, V. V., & Fröhlich, F. (2023). Yeast Svf1 binds ceramides and contributes to sphingolipid metabolism at the ER cis-Golgi interface. *Journal of Cell Biology*, *222*(5), e202109162. https://doi.org/10.1083/jcb.202109162

Liu, C. Y., Schröder, M., & Kaufman, R. J. (2000). Ligand-independent Dimerization Activates the Stress Response Kinases IRE1 and PERK in the Lumen of the Endoplasmic Reticulum. *Journal of Biological Chemistry*, *275*(32), 24881–24885. https://doi.org/10.1074/jbc.M004454200

Liu, L.-K., Choudhary, V., Toulmay, A., & Prinz, W. A. (2017). An inducible ER-Golgi tether facilitates ceramide transport to alleviate lipotoxicity. *The Journal of Cell Biology*, *216*(1), 131–147. https://doi.org/10.1083/jcb.201606059

Loewen, C. J. R., Roy, A., & Levine, T. P. (2003). A conserved ER targeting motif in three families of lipid binding proteins and in Opi1p binds VAP. *The EMBO Journal*, *22*(9), 2025–2035. https://doi.org/10.1093/emboj/cdg201

Lomize, A. L., Pogozheva, I. D., Lomize, M. A., & Mosberg, H. I. (2007). The role of hydrophobic interactions in positioning of peripheral proteins in membranes. *BMC Structural Biology*, *7*(1), 44. https://doi.org/10.1186/1472-6807-7-44

Longtine, M. S., Mckenzie Iii, A., Demarini, D. J., Shah, N. G., Wach, A., Brachat, A., Philippsen, P., & Pringle, J. R. (1998). Additional modules for versatile and economical PCR-based gene deletion and modification in Saccharomyces cerevisiae. *Yeast*, *14*(10), 953–961. https://doi.org/10.1002/(SICI)1097-0061(199807)14:10<953::AID-YEA293>3.0.CO;2-U

Lopez, S., Rodriguez-Gallardo, S., Sabido-Bozo, S., & Muñiz, M. (2019). Endoplasmic Reticulum Export of GPI-Anchored Proteins. *International Journal of Molecular Sciences*, *20*(14), 3506. https://doi.org/10.3390/ijms20143506

Luhtala, N., & Odorizzi, G. (2004). Bro1 coordinates deubiquitination in the multivesicular body pathway by recruiting Doa4 to endosomes. *The Journal of Cell Biology*, *166*(5), 717–729. https://doi.org/10.1083/jcb.200403139

Makarova, K. S., Tobiasson, V., Wolf, Y. I., Lu, Z., Liu, Y., Zhang, S., Krupovic, M., Li, M., & Koonin, E. V. (2024). Diversity, origin, and evolution of the ESCRT systems. *mBio*, *15*(3), e00335-24. https://doi.org/10.1128/mbio.00335-24

Manford, A. G., Stefan, C. J., Yuan, H. L., MacGurn, J. A., & Emr, S. D. (2012). ER-to-Plasma Membrane Tethering Proteins Regulate Cell Signaling and ER Morphology. *Developmental Cell*, *23*(6), 1129–1140. https://doi.org/10.1016/j.devcel.2012.11.004

Mao, C., Xu, R., Bielawska, A., & Obeid, L. M. (2000). Cloning of an Alkaline Ceramidase from Saccharomyces cerevisiae. *Journal of Biological Chemistry*, *275*(10), 6876–6884. https://doi.org/10.1074/jbc.275.10.6876

Mao, C., Xu, R., Bielawska, A., Szulc, Z. M., & Obeid, L. M. (2000). Cloning and Characterization of a Saccharomyces cerevisiae Alkaline Ceramidase with Specificity for Dihydroceramide. *Journal of Biological Chemistry*, *275*(40), 31369–31378. https://doi.org/10.1074/jbc.M003683200

Mast, F. D., Herricks, T., Strehler, K. M., Miller, L. R., Saleem, R. A., Rachubinski, R. A., & Aitchison, J. D. (2018). ESCRT-III is required for scissioning new peroxisomes from the endoplasmic reticulum. *The Journal of Cell Biology*, *217*(6), 2087–2102. https://doi.org/10.1083/jcb.201706044

Matsuo, H., Chevallier, J., Mayran, N., Le Blanc, I., Ferguson, C., Fauré, J., Blanc, N. S., Matile, S., Dubochet, J., Sadoul, R., Parton, R. G., Vilbois, F., & Gruenberg, J. (2004). Role of LBPA and Alix in Multivesicular Liposome Formation and Endosome Organization. *Science*, *303*(5657), 531–534. https://doi.org/10.1126/science.1092425

Matsuoka, K., Morimitsu, Y., Uchida, K., & Schekman, R. (1998). Coat Assembly Directs v-SNARE Concentration into Synthetic COPII Vesicles. *Molecular Cell*, *2*(5), 703–708. https://doi.org/10.1016/s1097-2765(00)80168-9

Mayers, J. R., Fyfe, I., Schuh, A. L., Chapman, E. R., Edwardson, J. M., & Audhya, A. (2011). ESCRT-0 Assembles as a Heterotetrameric Complex on Membranes and Binds Multiple Ubiquitinylated Cargoes Simultaneously. *Journal of Biological Chemistry*, *286*(11), 9636–9645. https://doi.org/10.1074/jbc.M110.185363

Melero, A., Boulanger, J., Kukulski, W., & Miller, E. A. (2022). Ultrastructure of COPII vesicle formation in yeast characterized by correlative light and electron microscopy. *Molecular Biology of the Cell*, *33*(13), ar122. https://doi.org/10.1091/mbc.E22-03-0103

Mesmin, B., Bigay, J., Moser von Filseck, J., Lacas-Gervais, S., Drin, G., & Antonny, B. (2013). A Four-Step Cycle Driven by PI(4)P Hydrolysis Directs Sterol/PI(4)P Exchange by the ER-Golgi Tether OSBP. *Cell*, *155*(4), 830–843. https://doi.org/10.1016/j.cell.2013.09.056

Miller, E., Antonny, B., Hamamoto, S., & Schekman, R. (2002). Cargo selection into COPII vesicles is driven by the Sec24p subunit. *The EMBO Journal*, *21*(22), 6105–6113. https://doi.org/10.1093/emboj/cdf605

Milstein, C., Brownlee, G. G., Harrison, T. M., & Mathews, M. B. (1972). A Possible Precursor of Immunoglobulin Light Chains. *Nature New Biology*, *239*(91), 117–120. https://doi.org/10.1038/newbio239117a0

Mori, K., Kawahara, T., Yoshida, H., Yanagi, H., & Yura, T. (1996). Signalling from endoplasmic reticulum to nucleus: Transcription factor with a basic-leucine zipper motif is required for the unfolded protein-response pathway. *Genes to Cells*, *1*(9), 803–817. https://doi.org/10.1046/j.1365-2443.1996.d01-274.x

Morita, E., Sandrin, V., Chung, H.-Y., Morham, S. G., Gygi, S. P., Rodesch, C. K., & Sundquist, W. I. (2007). Human ESCRT and ALIX proteins interact with proteins of the midbody and function in cytokinesis. *The EMBO Journal*, *26*(19), 4215–4227. https://doi.org/10.1038/sj.emboj.7601850

Mouchlis, V. D., Bucher, D., McCammon, J. A., & Dennis, E. A. (2015). Membranes serve as allosteric activators of phospholipase A_2 , enabling it to extract, bind, and hydrolyze phospholipid substrates. *Proceedings of the National Academy of Sciences*, *112*(6). https://doi.org/10.1073/pnas.1424651112

Muñiz, M., Morsomme, P., & Riezman, H. (2001). Protein Sorting upon Exit from the Endoplasmic Reticulum. *Cell*, *104*(2), 313–320. https://doi.org/10.1016/S0092-8674(01)00215-X

Muñiz, M., Nuoffer, C., Hauri, H. P., & Riezman, H. (2000). The Emp24 complex recruits a specific cargo molecule into endoplasmic reticulum-derived vesicles. *The Journal of Cell Biology*, *148*(5), 925–930. https://doi.org/10.1083/jcb.148.5.925

Nair, A., Nair, A., Stock, P., Jain, A., Somerville, E., Sanyal, A., & Kirchhausen, T. (2025). *Close-Up of vesicular ER Exit Sites by Volume Electron Imaging using FIB-SEM*. Cell Biology. https://doi.org/10.1101/2025.04.23.650353

Nakano, A., & Muramatsu, M. (1989). A novel GTP-binding protein, Sar1p, is involved in transport from the endoplasmic reticulum to the Golgi apparatus. *The Journal of Cell Biology*, *109*(6), 2677–2691. https://doi.org/10.1083/jcb.109.6.2677

Nixon-Abell, J., Obara, C. J., Weigel, A. V., Li, D., Legant, W. R., Xu, C. S., Pasolli, H. A., Harvey, K., Hess, H. F., Betzig, E., Blackstone, C., & Lippincott-Schwartz, J. (2016). Increased spatiotemporal resolution reveals highly dynamic dense tubular matrices in the peripheral ER. *Science (New York, N.Y.)*, *354*(6311), aaf3928. https://doi.org/10.1126/science.aaf3928

Obita, T., Saksena, S., Ghazi-Tabatabai, S., Gill, D. J., Perisic, O., Emr, S. D., & Williams, R. L. (2007). Structural basis for selective recognition of ESCRT-III by the AAA ATPase Vps4. *Nature*, *449*(7163), 735–739. https://doi.org/10.1038/nature06171

Odorizzi, G., Katzmann, D. J., Babst, M., Audhya, A., & Emr, S. D. (2003). Bro1 is an endosome-associated protein that functions in the MVB pathway in Saccharomyces cerevisiae. *Journal of Cell Science*, *116*(10), 1893–1903. https://doi.org/10.1242/jcs.00395

Ogata, M., Hino, S., Saito, A., Morikawa, K., Kondo, S., Kanemoto, S., Murakami, T., Taniguchi, M., Tanii, I., Yoshinaga, K., Shiosaka, S., Hammarback, J. A., Urano, F., & Imaizumi, K. (2006). Autophagy Is Activated for Cell Survival after Endoplasmic ReticulumStress. *Molecular and Cellular Biology*, *26*(24), 9220–9231. https://doi.org/10.1128/MCB.01453-06

Okamura, K., Kimata, Y., Higashio, H., Tsuru, A., & Kohno, K. (2000). Dissociation of Kar2p/BiP from an ER Sensory Molecule, Ire1p, Triggers the Unfolded Protein Response in Yeast. *Biochemical and Biophysical Research Communications*, *279*(2), 445–450. https://doi.org/10.1006/bbrc.2000.3987

Osman, C., Voelker, D. R., & Langer, T. (2011). Making heads or tails of phospholipids in mitochondria. *Journal of Cell Biology*, *192*(1), 7–16. https://doi.org/10.1083/jcb.201006159

Palade, G. (1975). Intracellular aspects of the process of protein synthesis. *Science (New York, N.Y.)*, *189*(4200), 347–358. https://doi.org/10.1126/science.1096303

Palade, G. E. (1956). The endoplasmic reticulum. *The Journal of Biophysical and Biochemical Cytology*, *2*(4 Suppl), 85–98. https://doi.org/10.1083/jcb.2.4.85

Palade, G. E., & Porter, K. R. (1954). STUDIES ON THE ENDOPLASMIC RETICULUM. *Journal of Experimental Medicine*, *100*(6), 641–656. https://doi.org/10.1084/jem.100.6.641

Pan, X., Roberts, P., Chen, Y., Kvam, E., Shulga, N., Huang, K., Lemmon, S., & Goldfarb, D. S. (2000). Nucleus–Vacuole Junctions in *Saccharomyces cerevisiae* Are Formed Through the Direct Interaction of Vac8p with Nvj1p. *Molecular Biology of the Cell*, *11*(7), 2445–2457. https://doi.org/10.1091/mbc.11.7.2445

Papagiannidis, D., Bircham, P. W., Lüchtenborg, C., Pajonk, O., Ruffini, G., Brügger, B., & Schuck, S. (2021). Ice2 promotes ER membrane biogenesis in yeast by inhibiting the conserved lipin phosphatase complex. *The EMBO Journal*, *40*(22), e107958. https://doi.org/10.15252/embj.2021107958

Papanikou, E., Day, K. J., Austin, J., & Glick, B. S. (2015). COPI selectively drives maturation of the early Golgi. *eLife*, *4*, e13232. https://doi.org/10.7554/eLife.13232

Papanikou, E., & Glick, B. S. (2014). Golgi compartmentation and identity. *Current Opinion in Cell Biology*, *29*, 74–81. https://doi.org/10.1016/j.ceb.2014.04.010

Pashkova, N., Gakhar, L., Winistorfer, S. C., Sunshine, A. B., Rich, M., Dunham, M. J., Yu, L., & Piper, R. C. (2013). The yeast Alix homolog Bro1 functions as a ubiquitin receptor for protein sorting into multivesicular endosomes. *Developmental Cell*, *25*(5), 520–533. https://doi.org/10.1016/j.devcel.2013.04.007

Peñalva, M. A., Lucena-Agell, D., & Arst, H. N. (2014). Liaison alcaline: Pals entice non-endosomal ESCRTs to the plasma membrane for pH signaling. *Current Opinion in Microbiology*, *22*, 49–59. https://doi.org/10.1016/j.mib.2014.09.005

Peter, B. J., Kent, H. M., Mills, I. G., Vallis, Y., Butler, P. J. G., Evans, P. R., & McMahon, H. T. (2004). BAR Domains as Sensors of Membrane Curvature: The Amphiphysin BAR Structure. *Science*, *303*(5657), 495–499. https://doi.org/10.1126/science.1092586

Pfitzner, A.-K., Mercier, V., Jiang, X., Moser von Filseck, J., Baum, B., Šarić, A., & Roux, A. (2020). An ESCRT-III Polymerization Sequence Drives Membrane Deformation and Fission. *Cell*, *182*(5), 1140-1155.e18. https://doi.org/10.1016/j.cell.2020.07.021

Pfitzner, A.-K., Zivkovic, H., Bernat-Silvestre, C., West, M., Peltier, T., Humbert, F., Odorizzi, G., & Roux, A. (2023). Vps60 initiates alternative ESCRT-III filaments. *Journal of Cell Biology*, *222*(11), e202206028. https://doi.org/10.1083/jcb.202206028

Phillips, M. J., & Voeltz, G. K. (2016). Structure and function of ER membrane contact sites with other organelles. *Nature Reviews. Molecular Cell Biology*, *17*(2), 69–82. https://doi.org/10.1038/nrm.2015.8

Pincus, D., Chevalier, M. W., Aragón, T., Van Anken, E., Vidal, S. E., El-Samad, H., & Walter, P. (2010). BiP Binding to the ER-Stress Sensor Ire1 Tunes the Homeostatic Behavior of the Unfolded Protein Response. *PLoS Biology*, *8*(7), e1000415. https://doi.org/10.1371/journal.pbio.1000415

Pires, R., Hartlieb, B., Signor, L., Schoehn, G., Lata, S., Roessle, M., Moriscot, C., Popov, S., Hinz, A., Jamin, M., Boyer, V., Sadoul, R., Forest, E., Svergun, D. I., Göttlinger, H. G., & Weissenhorn, W. (2009). A Crescent-Shaped ALIX Dimer Targets ESCRT-III CHMP4 Filaments. *Structure*, *17*(6), 843–856. https://doi.org/10.1016/j.str.2009.04.007

Platzek, A., Schessner, J. P., Odehnalová, K., Borner, G. H. H., & Schuck, S. (2025). *Dynamic Organellar Mapping in yeast reveals extensive protein localization changes during ER stress*. Cold Spring Harbor Laboratory. https://doi.org/10.1101/2025.02.21.639471

Porter, K. R., & Palade, G. E. (1957). STUDIES ON THE ENDOPLASMIC RETICULUM. *The Journal of Cell Biology*, *3*(2), 269–300. https://doi.org/10.1083/jcb.3.2.269

Prasad, R., Sliwa-Gonzalez, A., & Barral, Y. (2020). Mapping bilayer thickness in the ER membrane. *Science Advances*, *6*(46), eaba5130. https://doi.org/10.1126/sciadv.aba5130

Preuss, D., Mulholland, J., Franzusoff, A., Segev, N., & Botstein, D. (1992). Characterization of the Saccharomyces Golgi complex through the cell cycle by immunoelectron microscopy. *Molecular Biology of the Cell*, *3*(7), 789–803. https://doi.org/10.1091/mbc.3.7.789

Prinz, W. A., Toulmay, A., & Balla, T. (2020). The functional universe of membrane contact sites. *Nature Reviews Molecular Cell Biology*, *21*(1), 7–24. https://doi.org/10.1038/s41580-019-0180-9

Prosser, D. C., Wrasman, K., Woodard, T. K., O'Donnell, A. F., & Wendland, B. (2016). Applications of pHluorin for Quantitative, Kinetic and High-throughput Analysis of Endocytosis in Budding Yeast. *Journal of Visualized Experiments*, *116*, 54587. https://doi.org/10.3791/54587

Radanović, T., & Ernst, R. (2021). The Unfolded Protein Response as a Guardian of the Secretory Pathway. *Cells*, *10*(11), 2965. https://doi.org/10.3390/cells10112965

Raiborg, C., Bremnes, B., Mehlum, A., Gillooly, D. J., D'Arrigo, A., Stang, E., & Stenmark, H. (2001). FYVE and coiled-coil domains determine the specific localisation of Hrs to early endosomes. *Journal of Cell Science*, *114*(12), 2255–2263. https://doi.org/10.1242/jcs.114.12.2255

Raiborg, C., & Stenmark, H. (2009). The ESCRT machinery in endosomal sorting of ubiquitylated membrane proteins. *Nature*, *458*(7237), 445–452. https://doi.org/10.1038/nature07961

Raote, I., Chabanon, M., Walani, N., Arroyo, M., Garcia-Parajo, M. F., Malhotra, V., & Campelo, F. (2020). A physical mechanism of TANGO1-mediated bulky cargo export. *eLife*, *9*, e59426. https://doi.org/10.7554/eLife.59426

Rapoport, T. A., Li, L., & Park, E. (2017). Structural and Mechanistic Insights into Protein Translocation. *Annual Review of Cell and Developmental Biology*, *33*(1), 369–390. https://doi.org/10.1146/annurev-cellbio-100616-060439

Rego, N. B., Xi, E., & Patel, A. J. (2021). Identifying hydrophobic protein patches to inform protein interaction interfaces. *Proceedings of the National Academy of Sciences*, *118*(6), e2018234118. https://doi.org/10.1073/pnas.2018234118

Rodriguez-Gallardo, S., Kurokawa, K., Sabido-Bozo, S., Cortes-Gomez, A., Ikeda, A., Zoni, V., Aguilera-Romero, A., Perez-Linero, A. M., Lopez, S., Waga, M., Araki, M., Nakano, M., Riezman, H., Funato, K., Vanni, S., Nakano, A., & Muñiz, M. (2020). Ceramide chain length–dependent protein sorting into selective endoplasmic reticulum exit sites. *Science Advances*, *6*(50), eaba8237. https://doi.org/10.1126/sciadv.aba8237

Roux, K. J., Kim, D. I., Raida, M., & Burke, B. (2012). A promiscuous biotin ligase fusion protein identifies proximal and interacting proteins in mammalian cells. *Journal of Cell Biology*, *196*(6), 801–810. https://doi.org/10.1083/jcb.201112098

Roy Chowdhury, S., Bhattacharjee, C., Casler, J. C., Jain, B. K., Glick, B. S., & Bhattacharyya, D. (2020). ER arrival sites associate with ER exit sites to create bidirectional transport portals. *Journal of Cell Biology*, *219*(4), e201902114. https://doi.org/10.1083/jcb.201902114

Rue, S. M., Mattei, S., Saksena, S., & Emr, S. D. (2008). Novel Ist1-Did2 Complex Functions at a Late Step in Multivesicular Body Sorting. *Molecular Biology of the Cell*, *19*(2), 475–484. https://doi.org/10.1091/mbc.e07-07-0694

Rueden, C. T., Schindelin, J., Hiner, M. C., DeZonia, B. E., Walter, A. E., Arena, E. T., & Eliceiri, K. W. (2017). ImageJ2: ImageJ for the next generation of scientific image data. *BMC Bioinformatics*, *18*(1), 529. https://doi.org/10.1186/s12859-017-1934-z

Sadeqi, F., Dong, D., Stroh, K., Vache, M., Metz, J., Riedel, D., Janshoff, A., Risselada, H. J., Kolenda, C., & Meinecke, M. (2025). *Membrane curvature regulates Ups1 dependent phosphatidic acid transfer across lipid bilayers*. https://doi.org/10.7554/eLife.106979.1

Saito, K., Chen, M., Bard, F., Chen, S., Zhou, H., Woodley, D., Polischuk, R., Schekman, R., & Malhotra, V. (2009). TANGO1 Facilitates Cargo Loading at Endoplasmic Reticulum Exit Sites. *Cell*, *136*(5), 891–902. https://doi.org/10.1016/j.cell.2008.12.025

Satpute-Krishnan, P., Ajinkya, M., Bhat, S., Itakura, E., Hegde, R. S., & Lippincott-Schwartz, J. (2014). ER Stress-Induced Clearance of Misfolded GPI-Anchored Proteins via the Secretory Pathway. *Cell*, *158*(3), 522–533. https://doi.org/10.1016/j.cell.2014.06.026

Sawyer, E. M., Jensen, L. E., Meehl, J. B., Larsen, K. P., Petito, D. A., Hurley, J. H., & Voeltz, G. K. (2024). SigmaR1 shapes rough endoplasmic reticulum membrane sheets. *Developmental Cell*, *59*(19), 2566-2577.e7. https://doi.org/10.1016/j.devcel.2024.06.005

Schäfer, J. A., Schessner, J. P., Bircham, P. W., Tsuji, T., Funaya, C., Pajonk, O., Schaeff, K., Ruffini, G., Papagiannidis, D., Knop, M., Fujimoto, T., & Schuck, S. (2020). ESCRT machinery mediates selective microautophagy of endoplasmic reticulum in yeast. *The EMBO Journal*, *39*(2). https://doi.org/10.15252/embj.2019102586

Schauder, C. M., Wu, X., Saheki, Y., Narayanaswamy, P., Torta, F., Wenk, M. R., De Camilli, P., & Reinisch, K. M. (2014). Structure of a lipid-bound extended synaptotagmin indicates a role in lipid transfer. *Nature*, *510*(7506), 552–555. https://doi.org/10.1038/nature13269

Scheffer, L. L., Sreetama, S. C., Sharma, N., Medikayala, S., Brown, K. J., Defour, A., & Jaiswal, J. K. (2014). Mechanism of Ca2+-triggered ESCRT assembly and regulation of cell membrane repair. *Nature Communications*, *5*(1), 5646. https://doi.org/10.1038/ncomms6646

Schindelin, J., Arganda-Carreras, I., Frise, E., Kaynig, V., Longair, M., Pietzsch, T., Preibisch, S., Rueden, C., Saalfeld, S., Schmid, B., Tinevez, J.-Y., White, D. J., Hartenstein, V., Eliceiri, K., Tomancak, P., & Cardona, A. (2012). Fiji: An open-source platform for biological-image analysis. *Nature Methods*, *9*(7), 676–682. https://doi.org/10.1038/nmeth.2019

Schindler, A. J., & Schekman, R. (2009). In vitro reconstitution of ER-stress induced ATF6 transport in COPII vesicles. *Proceedings of the National Academy of Sciences*, *106*(42), 17775–17780. https://doi.org/10.1073/pnas.0910342106

Schlösser, L., Sachse, C., Low, H. H., & Schneider, D. (2023). Conserved structures of ESCRT-III superfamily members across domains of life. *Trends in Biochemical Sciences*, *48*(11), 993–1004. https://doi.org/10.1016/j.tibs.2023.08.009

Schöneberg, J., Lee, I.-H., Iwasa, J. H., & Hurley, J. H. (2017). Reverse-topology membrane scission by the ESCRT proteins. *Nature Reviews Molecular Cell Biology*, *18*(1), 5–17. https://doi.org/10.1038/nrm.2016.121

Schopp, I. M., & Béthune, J. (2018). Split-BioID — Proteomic Analysis of Context-specific Protein Complexes in Their Native Cellular Environment. *Journal of Visualized Experiments*, *134*, 57479. https://doi.org/10.3791/57479

Schroeder, L. K., Barentine, A. E. S., Merta, H., Schweighofer, S., Zhang, Y., Baddeley, D., Bewersdorf, J., & Bahmanyar, S. (2019). Dynamic nanoscale morphology of the ER surveyed by STED microscopy. *Journal of Cell Biology*, *218*(1), 83–96. https://doi.org/10.1083/jcb.201809107

Schröter, S., Beckmann, S., & Schmitt, H. D. (2016). ER arrival sites for COPI vesicles localize to hotspots of membrane trafficking. *The EMBO Journal*, *35*(17), 1935–1955. https://doi.org/10.15252/embj.201592873

Schuck, S., Gallagher, C. M., & Walter, P. (2014). ER-phagy mediates selective degradation of endoplasmic reticulum independently of the core autophagy machinery. *Journal of Cell Science*, jcs.154716. https://doi.org/10.1242/jcs.154716

Schuck, S., Prinz, W. A., Thorn, K. S., Voss, C., & Walter, P. (2009). Membrane expansion alleviates endoplasmic reticulum stress independently of the unfolded protein response. *The Journal of Cell Biology*, *187*(4), 525–536. https://doi.org/10.1083/jcb.200907074

Shamu, C. E., & Walter, P. (1996). Oligomerization and phosphorylation of the Ire1p kinase during intracellular signaling from the endoplasmic reticulum to the nucleus. *The EMBO Journal*, *15*(12), 3028–3039.

Shen, Q.-T., Schuh, A. L., Zheng, Y., Quinney, K., Wang, L., Hanna, M., Mitchell, J. C., Otegui, M. S., Ahlquist, P., Cui, Q., & Audhya, A. (2014). Structural analysis and modeling reveals new mechanisms governing ESCRT-III spiral filament assembly. *Journal of Cell Biology*, *206*(6), 763–777. https://doi.org/10.1083/jcb.201403108

Shibata, Y., Shemesh, T., Prinz, W. A., Palazzo, A. F., Kozlov, M. M., & Rapoport, T. A. (2010). Mechanisms Determining the Morphology of the Peripheral ER. *Cell*, *143*(5), 774–788. https://doi.org/10.1016/j.cell.2010.11.007

Shomron, O., Nevo-Yassaf, I., Aviad, T., Yaffe, Y., Zahavi, E. E., Dukhovny, A., Perlson, E., Brodsky, I., Yeheskel, A., Pasmanik-Chor, M., Mironov, A., Beznoussenko, G. V., Mironov, A. A., Sklan, E. H., Patterson, G. H., Yonemura, Y., Sannai, M., Kaether, C., & Hirschberg, K. (2021). COPII collar defines the boundary between ER and ER exit site and does not coat cargo containers. *Journal of Cell Biology*, *220*(6), e201907224. https://doi.org/10.1083/jcb.201907224

Sidrauski, C., Cox, J. S., & Walter, P. (1996). tRNA Ligase Is Required for Regulated mRNA Splicing in the Unfolded Protein Response. *Cell*, *87*(3), 405–413. https://doi.org/10.1016/S0092-8674(00)81361-6

Sidrauski, C., & Walter, P. (1997). The Transmembrane Kinase Ire1p Is a Site-Specific Endonuclease That Initiates mRNA Splicing in the Unfolded Protein Response. *Cell*, *90*(6), 1031–1039. https://doi.org/10.1016/S0092-8674(00)80369-4

Skowyra, M. L., Schlesinger, P. H., Naismith, T. V., & Hanson, P. I. (2018). Triggered recruitment of ESCRT machinery promotes endolysosomal repair. *Science*, *360*(6384), eaar5078. https://doi.org/10.1126/science.aar5078

Slagsvold, T., Aasland, R., Hirano, S., Bache, K. G., Raiborg, C., Trambaiolo, D., Wakatsuki, S., & Stenmark, H. (2005). Eap45 in Mammalian ESCRT-II Binds Ubiquitin via a Phosphoinositide-interacting GLUE Domain. *Journal of Biological Chemistry*, *280*(20), 19600–19606. https://doi.org/10.1074/jbc.M501510200

Souza, D. P., Espadas, J., Chaaban, S., Moody, E. R. R., Hatano, T., Balasubramanian, M., Williams, T. A., Roux, A., & Baum, B. (2025). Asgard archaea reveal the conserved principles of ESCRT-III membrane remodeling. *Science Advances*, *11*(6), eads5255. https://doi.org/10.1126/sciadv.ads5255

Stefan, C. J., Manford, A. G., Baird, D., Yamada-Hanff, J., Mao, Y., & Emr, S. D. (2011). Osh Proteins Regulate Phosphoinositide Metabolism at ER-Plasma Membrane Contact Sites. *Cell*, *144*(3), 389–401. https://doi.org/10.1016/j.cell.2010.12.034

Strack, B., Calistri, A., Craig, S., Popova, E., & Göttlinger, H. G. (2003). AIP1/ALIX Is a Binding Partner for HIV-1 p6 and EIAV p9 Functioning in Virus Budding. *Cell*, *114*(6), 689–699. https://doi.org/10.1016/S0092-8674(03)00653-6

Stuchell-Brereton, M. D., Skalicky, J. J., Kieffer, C., Karren, M. A., Ghaffarian, S., & Sundquist, W. I. (2007). ESCRT-III recognition by VPS4 ATPases. *Nature*, *449*(7163), 740–744. https://doi.org/10.1038/nature06172

Tang, S., Buchkovich, N. J., Henne, W. M., Banjade, S., Kim, Y. J., & Emr, S. D. (2016). ESCRT-III activation by parallel action of ESCRT-I/II and ESCRT-0/Bro1 during MVB biogenesis. *eLife*, *5*, e15507. https://doi.org/10.7554/eLife.15507

Tang, S., Henne, W. M., Borbat, P. P., Buchkovich, N. J., Freed, J. H., Mao, Y., Fromme, J. C., & Emr, S. D. (2015). Structural basis for activation, assembly and membrane binding of ESCRT-III Snf7 filaments. *eLife*, *4*, e12548. https://doi.org/10.7554/eLife.12548

Teis, D., Saksena, S., & Emr, S. D. (2008). Ordered Assembly of the ESCRT-III Complex on Endosomes Is Required to Sequester Cargo during MVB Formation. *Developmental Cell*, *15*(4), 578–589. https://doi.org/10.1016/j.devcel.2008.08.013

Teo, H., Gill, D. J., Sun, J., Perisic, O., Veprintsev, D. B., Vallis, Y., Emr, S. D., & Williams, R. L. (2006). ESCRT-I Core and ESCRT-II GLUE Domain Structures Reveal Role for GLUE in Linking to ESCRT-I and Membranes. *Cell*, *125*(1), 99–111. https://doi.org/10.1016/j.cell.2006.01.047

Thomas, F. B., Omnus, D. J., Bader, J. M., Chung, G. H., Kono, N., & Stefan, C. J. (2022). Tricalbin proteins regulate plasma membrane phospholipid homeostasis. *Life Science Alliance*, *5*(8), e202201430. https://doi.org/10.26508/lsa.202201430

Tkacz, J. S., & Lampen, J. O. (1975). Tunicamycin inhibition of polyisoprenyl N-acetylglucosaminyl pyrophosphate formation in calf-liver microsomes. *Biochemical and Biophysical Research Communications*, *65*(1), 248–257. https://doi.org/10.1016/S0006-291X(75)80086-6

Tojima, T., Suda, Y., Jin, N., Kurokawa, K., & Nakano, A. (2024). Spatiotemporal dissection of the Golgi apparatus and the ER-Golgi intermediate compartment in budding yeast. *eLife*, *13*, e92900. https://doi.org/10.7554/eLife.92900

Toulmay, A., & Prinz, W. A. (2012). A conserved membrane-binding domain targets proteins to organelle contact sites. *Journal of Cell Science*, *125*(1), 49–58. https://doi.org/10.1242/jcs.085118

Travers, K. J., Patil, C. K., Wodicka, L., Lockhart, D. J., Weissman, J. S., & Walter, P. (2000). Functional and Genomic Analyses Reveal an Essential Coordination between the Unfolded Protein Response and ER-Associated Degradation. *Cell*, *101*(3), 249–258. https://doi.org/10.1016/S0092-8674(00)80835-1

Tseng, C.-C., Dean, S., Davies, B. A., Azmi, I. F., Pashkova, N., Payne, J. A., Staffenhagen, J., West, M., Piper, R. C., Odorizzi, G., & Katzmann, D. J. (2021). Bro1 stimulates Vps4 to promote intralumenal vesicle formation during multivesicular body biogenesis. *Journal of Cell Biology*, *220*(8), e202102070. https://doi.org/10.1083/jcb.202102070

Tyanova, S., Temu, T., Sinitcyn, P., Carlson, A., Hein, M. Y., Geiger, T., Mann, M., & Cox, J. (2016). The Perseus computational platform for comprehensive analysis of (prote)omics data. *Nature Methods*, *13*(9), 731–740. https://doi.org/10.1038/nmeth.3901

Venditti, R., Rega, L. R., Masone, M. C., Santoro, M., Polishchuk, E., Sarnataro, D., Paladino, S., D'Auria, S., Varriale, A., Olkkonen, V. M., Di Tullio, G., Polishchuk, R., & De Matteis, M. A. (2019). Molecular determinants of ER–Golgi contacts identified through a new FRET–FLIM system. *Journal of Cell Biology*, *218*(3), 1055–1065. https://doi.org/10.1083/jcb.201812020

VerPlank, L., Bouamr, F., LaGrassa, T. J., Agresta, B., Kikonyogo, A., Leis, J., & Carter, C. A. (2001). Tsg101, a homologue of ubiquitin-conjugating (E2) enzymes, binds the L domain in HIV type 1 $Pr55^{Gag}$. *Proceedings of the National Academy of Sciences*, *98*(14), 7724–7729. https://doi.org/10.1073/pnas.131059198

Vietri, M., Radulovic, M., & Stenmark, H. (2020). The many functions of ESCRTs. *Nature Reviews Molecular Cell Biology*, *21*(1), 25–42. https://doi.org/10.1038/s41580-019-0177-4

Voeltz, G. K., Prinz, W. A., Shibata, Y., Rist, J. M., & Rapoport, T. A. (2006). A Class of Membrane Proteins Shaping the Tubular Endoplasmic Reticulum. *Cell*, *124*(3), 573–586. https://doi.org/10.1016/j.cell.2005.11.047

Volmer, R., Van Der Ploeg, K., & Ron, D. (2013). Membrane lipid saturation activates endoplasmic reticulum unfolded protein response transducers through their transmembrane domains. *Proceedings of the National Academy of Sciences*, *110*(12), 4628–4633. https://doi.org/10.1073/pnas.1217611110

Voynova, N. S., Vionnet, C., Ejsing, C. S., & Conzelmann, A. (2012). A novel pathway of ceramide metabolism in *Saccharomyces cerevisiae*. *Biochemical Journal*, *447*(1), 103–114. https://doi.org/10.1042/BJ20120712

Walter, P., & Ron, D. (2011). The unfolded protein response: From stress pathway to homeostatic regulation. *Science (New York, N.Y.)*, *334*(6059), 1081–1086. https://doi.org/10.1126/science.1209038

Wang, E., Norred, W. P., Bacon, C. W., Riley, R. T., & Merrill, A. H. (1991). Inhibition of sphingolipid biosynthesis by fumonisins. Implications for diseases associated with Fusarium moniliforme. *Journal of Biological Chemistry*, *266*(22), 14486–14490. https://doi.org/10.1016/S0021-9258(18)98712-0

Webster, B. M., Thaller, D. J., Jäger, J., Ochmann, S. E., Borah, S., & Lusk, C. P. (2016). Chm7 and Heh1 collaborate to link nuclear pore complex quality control with nuclear envelope sealing. *The EMBO Journal*, *35*(22), 2447–2467. https://doi.org/10.15252/embj.201694574

Weigel, A. V., Chang, C.-L., Shtengel, G., Xu, C. S., Hoffman, D. P., Freeman, M., Iyer, N., Aaron, J., Khuon, S., Bogovic, J., Qiu, W., Hess, H. F., & Lippincott-Schwartz, J. (2021). ER-to-Golgi protein delivery through an interwoven, tubular network extending from ER. *Cell*, *184*(9), 2412-2429.e16. https://doi.org/10.1016/j.cell.2021.03.035

Welihinda, A. A., & Kaufman, R. J. (1996). The Unfolded Protein Response Pathway in. *Journal of Biological Chemistry*, *271*(30), 18181–18187. https://doi.org/10.1074/jbc.271.30.18181

Wemmer, M., Azmi, I., West, M., Davies, B., Katzmann, D., & Odorizzi, G. (2011). Bro1 binding to Snf7 regulates ESCRT-III membrane scission activity in yeast. *Journal of Cell Biology*, *192*(2), 295–306. https://doi.org/10.1083/jcb.201007018

Wu, H., Carvalho, P., & Voeltz, G. K. (2018). Here, there, and everywhere: The importance of ER membrane contact sites. *Science*, *361*(6401), eaan5835. https://doi.org/10.1126/science.aan5835

Wyles, J. P., McMaster, C. R., & Ridgway, N. D. (2002). Vesicle-associated Membrane Protein-associated Protein-A (VAP-A) Interacts with the Oxysterol-binding Protein to Modify Export from the Endoplasmic Reticulum. *Journal of Biological Chemistry*, *277*(33), 29908–29918. https://doi.org/10.1074/jbc.M201191200

Xu, W., & Mitchell, A. P. (2001). Yeast PalA/AIP1/Alix Homolog Rim20p Associates with a PEST-Like Region and Is Required for Its Proteolytic Cleavage. *Journal of Bacteriology*, *183*(23), 6917–6923. https://doi.org/10.1128/JB.183.23.6917-6923.2001

Xu, W., Smith, F. J., Subaran, R., & Mitchell, A. P. (2004). Multivesicular Body-ESCRT Components Function in pH Response Regulation in *Saccharomyces cerevisiae* and *Candida albicans*. *Molecular Biology of the Cell*, *15*(12), 5528–5537. https://doi.org/10.1091/mbc.e04-08-0666

Yan, Q., & Lennarz, W. J. (1999). Oligosaccharyltransferase: A Complex Multisubunit Enzyme of the Endoplasmic Reticulum. *Biochemical and Biophysical Research Communications*, *266*(3), 684–689. https://doi.org/10.1006/bbrc.1999.1886

Yang, B., Stjepanovic, G., Shen, Q., Martin, A., & Hurley, J. H. (2015). Vps4 disassembles an ESCRT-III filament by global unfolding and processive translocation. *Nature Structural & Molecular Biology*, *22*(6), 492–498. https://doi.org/10.1038/nsmb.3015

Zelnik, I. D., Ventura, A. E., Kim, J. L., Silva, L. C., & Futerman, A. H. (2020). The role of ceramide in regulating endoplasmic reticulum function. *Biochimica et Biophysica Acta (BBA) - Molecular and Cell Biology of Lipids*, *1865*(1), 158489. https://doi.org/10.1016/j.bbalip.2019.06.015

8. ACKNOWLEDGEMENTS

First of all, I want to thank Sebastian for giving me the opportunity to explore the mysteries of the ESCRT machinery at the ER for my Master Thesis and for encouraging me to further pursue them throughout my PhD. Thank you for all your scientific guidance, for sharing your expertise and always being open for discussions. Thank you for supporting Oli and me to present our project at international conferences, as well as to learn new methods in the lab of Liz Miller at the LMB in Cambridge and the lab of Friedrich Förster at the University of Utrecht. These opportunities greatly contributed to my development as a scientist and my understanding of the research community.

I further want to thank the members of my committee. Thank you, Axel, for accompanying me as an examiner and supporting my academic journey from the Bachelor studies to the Master studies to the PhD. Thank you, Joachim, for your support and the scientific input for our project as representative of the ESCRT field. Thank you, Axel and Joachim, for all the valuable discussions during TAC meetings. Thank you, Walter for taking the time to chair my defense.

I am grateful to the Fonds National de la Recherche in Luxembourg for funding my PhD project for four years and for providing me with resources for courses and conferences.

I also want to thank everyone who contributed to this project: Jasmin for discovering the exciting phenotype that started this project. Sabine Merker, Thomas Ruppert and Marcin Luzarowski from the ZMBH Mass Spectrometry Facility for their advice, support and the execution of the mass spectrometry for the PDB-MS experiment. Georg Borner for the MaxQuant analysis of the mass spectrometry data, as well as his support for the subsequent data analysis. Carlos, Natalie and Fay for their significant contributions during lab rotations and Master theses.

Moreover, I want to thank Liz Miller and Friedrich Förster for the opportunity to join their respective labs for a week to learn new techniques. Also, thank you, Imogen, for showing us around the LMB, for teaching us hot lab work and contributing to our great time in Cambridge! A big thanks also to Leanne for providing us with amazing cryo-EM structures of the ER clusters, for many fruitful scientific discussions and chats about life, for taking us along on the lab run and for making our stay in Utrecht, as well as our collaboration, a lot of fun!

Our research would not be possible without the many people working behind the scenes and making sure that the everyday life in the lab runs smoothly. A huge thank you to the staff at ZMBH and BZH including the scullery and media kitchen services (thank you, Melanie, Linda and Selene!), the cleaning personnel and the EDV team (thank you, Lutz!). Not to forget the people in administration that help us navigate the jungle of German bureaucracy; thank you, Olga and Anke! Moreover, I want to thank the Mensa Team for providing us with the nutrients necessary to handle our busy days in the lab.

Furthermore, I want to thank the research communities I got to be part of during this time, in particular the ER field and the protein trafficking and secretion field. Thanks to everyone who supported our project, asked questions and gave input at poster sessions! The conferences I attended emphasized the value of collaboration and communication for science, and showed that quite simply put – teamwork makes the dream work. Having witnessed this sense of community and mutual support makes me hopeful, especially in the light of the difficulties that scientific research is currently facing.

Along the same line, I want to thank my fellow members of the PhD board for promoting the scientific community at BZH. I enjoyed my two years on the board and had fun organizing our retreat and other events with you! Thanks as well to everyone at BZH, especially the 3rd floor people, for exchanging ideas and advice, both scientific and personal. Special shoutout also to the 5th floor coffee crew, Matteo, Merlin and Florestan for keeping us entertained with stories about their lab adventures.

And now to my fellow Schookees (past and present), what can I say…THANK YOU for this amazing time together! We've certainly been through a lot together, from pandemic shift systems to several moves, to setting up our "new home" at BZH, to the many highs and lows that the PhD and research bring, to hat-making marathons, actual (half-)marathons and fun retreats together. Thank you for creating such a supportive and positive work environment. Thank you for all the input at lab meetings, the scientific as well as the personal advice, all the support, the shared laughter and tears, lots of cakes, coffee walks, lunches at 11:30, lab runs, beer brewing sessions, and so much more. There are so many great moments to look back on! This journey certainly has not always been easy, but you always gave me a reason to look forward to coming to the lab. To quote my favorite writer, John Green: "Surround yourself with people who you like and make cool stuff with them. In the end, what you do isn't going to be nearly as interesting or important as who you do it with. "

Thank you, Dimitris, for introducing me to this lab and for sparking my interest in yeast cell biology. Thank you for all the bouldering sessions, for taking me climbing, for getting me out of my comfort zone and for all the advice, be it science-related or personal. Thank you, Carlos, for all your work as part of the ESCRT team, for your positivity and the Spanish lessons. Thank you, Aye, for the joy you brought to the lab, the fascinating dream stories and for all the times we could not stop laughing. Thank you for inspiring us with your art and for supporting me in my science communications endeavors! Thank you, Inge, for welcoming us so openly when we started at BZH. Thank you, Rolf, for the fun jam sessions and bouldering sessions, and the shared fascination of mind-blowing space photos. Thank you, Klára, for all your bioinformatic expertise, for creating the most amazing PhD defense posters and for entertaining us with stories about camp/Theodor/burning ovens/… Thank you, Sneha, for your enthusiasm for science and for introducing us to delicious food and snacks from India.

Thank you, Heike, for joining our lab and contributing to the typical Schookee group atmosphere right from the start. Thank you, Anna(nananana), my fellow 3rd generation Schookee, for your sense of humor, your endless optimism (aka. Optimismus, aka. Sumsi mit Po), your excitement for tiny plants and trampolining and surfing and autophagy, and for introducing me to Udo and Opuntia. Thank you, Petra for everything you do for the lab, for sparking our creativity and for the yummy brunches/Kaffee und Kuchen sessions. Thank you, (Sch)Niklas, for all the bouldering sessions and lab runs together, for organizing the yearly lab BBQ, for the occasional refreshing sound of a Frische Brise being opened, for the constant Spongebob references and the funny goodbye puns. Thank you, Natalie, for bringing your cool cassis energy to the lab, for sharing your bubblegum supply and teaching us the slang of the young people. Thank you for being an amazing first labrotation student and for our shared adventure of making GFP-binder beads. It was inspiring to see you grow from an already talented Master student to the scientist you are now. Thank you, Giulia, for all your support, our chats about science and life and for sharing good and bad moments. Starting from our shared shifts, to becoming desk neighbors, to trying to make it as influencers, to making music on the street together, to being “not that close” to cheering each other on, … we’ve been through it all. And the thing is…I am so glad to have had you as a labmate during all this time. Thank you, Sibi, aka Schniebi, for the biking and hiking tours, for the wining and whining, the (almost) daily podcasts, the occasional funny sounds and for just being yourself. Thank you for all the cheer-ups and for always being there for me, inside and outside the lab. Team Ostrich and Lizard ftw!

Thank you, Oli, for being the best team partner one could wish for. Your supervision during my Master thesis and your excitement for the ESCRT project added to the reasons I wanted to stay on this project for my PhD. Little did I know that this would turn into incredible teamwork and a close friendship. Thank you for your advice on experiments, our project discussions and for enduring my typical panic 10 min before a poster presentation. Thank you for the shared conference visits and workations and all the fun memories and moments connected to these. Thank you for all the jam sessions, the Sunday runs, the Rosinis, for sparking my interest in good coffee and for the chats about life. This PhD would have been way harder without having you as a constant support and cheerleader beside me. Thank you for always believing in me, especially when I didn’t.

Moreover, I want to thank the Monday Bouldering Crew for providing a weekly ritual and way to unwind after a busy day in the lab. I always enjoy our shared bouldering sessions and sitting down with drinks and Flammkuchen afterwards!

Another big thank you goes to Giulia, Rolf and Oli for all the jam sessions, which were another welcome distraction. Thank you for taking me in and supporting my singing and playing! You made me rediscover the joy in making music. I would not have believed it if someone had told me a few years ago that I

would play music and sing on Hauptstraße, so thank you for getting me out of my comfort zone and letting me be a part of this experience!

I also want to thank everyone else who supported me during this time, including Jasi, Itamar, Nic, Nils, Hanna and Sophie.

A big thank you goes to Annalena, Anna-Lena, Katha and Laura for being my family away from home during my Bachelor and Master studies and for being a constant source of support during my PhD journey, even from afar. Thank you for all the hiking or cycling tours, the phone call walks, the Kürbis-Gnocchi-Auflauf gatherings and our reunions! Und danke vor allem, dass ihr mich ständig dran erinnert habt, dass ich dem Ziel noch nie so nah war!

Furthermore, I want to thank Charlotte, Cathy and Anne. E grousse merci u meng Miseler Meedecher! Thank you for getting me out of the science bubble once in while, for the vacations together, the wine festival weekends, the late-night chats at Scheierbierg, the phone calls, and, and, and… We've grown so much together and even though we pursue different endeavors, we keep supporting each other and I am very grateful for that.

Finally, I want to thank my entire family for their support, especially my mum, my dad, my brother and my grandparents. Merci, Mama, Papa a Pit, fir äer Ënnerstetzung wärend der ganzer Zäit, am Klengen an am Groussen. Merci fir d'Nolauschteren, fir d'Oflenken, fir d'Opmonteren an dat der ëmmer u mech gegleeft huet! Oni eech hätt ech dat net esou hikréit.